# Chapter 5
# Vibrations of Laminated Structures Composed of Smart Materials

**Abstract** In this chapter, we consider thin-walled laminated beams, plates and shells containing layers made of viscoelastic smart materials (VSMs). Generally, from all variety of these materials, the magnetorheological elastomer MRE-1 with properties specified in Chapt. 2 will be used for damping layers or core. To compare the damping capabilities of this material with others, we will study also vibrations of thin-walled laminates assembled from other smart materials (MREs, MRFs and ERCs) described in Chapt. 2.

The basic purpose of this chapter is to analyze free and forced vibrations of thin-walled laminated structures with adaptive physical properties and to show that the application of VSMs embedded between elastic layers allows changing not only the total rigidity, as detected in Chapt. 3, but more the total damping capability of the structure when subjected to the action of an external magnetic or electric field. In particular, it will be shown that the application of a magnetic field may result in significant enhance of the damping capacity of a MRE-based laminated structure and as a consequence, in effective damping of both free and forced vibrations.

The chapter begins with a brief review of the state of the art of research on vibration of MR/ER-based laminated structures (Sect. 5.1). In Sect. 5.2, free and forced vibrations of sandwich beams with MRF or MRE cores are examined. In Sect. 5.3, free and forced vibrations of MRE-based rectangular plates are shortly discussed. Section 5.4 is the main one, it is devoted to free and forced vibrations of laminated and sandwich MRE/ERC-based panels and shells affected by stationary magnetic fields. The detailed analysis of damping capability of different VSMs materials (MREs and ERCs with properties specified in Chapt. 2) incorporated with sandwich panels is given. Finally, in Sects. 5.5 and 5.6, the impact of magnetic field on localized modes and non-stationary vibrations in medium-length MRE-based cylindrical shells is studied. In particular, the effect of soft suppression of travelling localized waves under slowly varying magnetic field is demonstrated.


G. I. Mikhasev and H. Altenbach, *Thin-walled Laminated Structures*,
Advanced Structured Materials 106, https://doi.org/10.1007/978-3-030-12761-9_5

## 5.1 Brief Review of the State of the Art

One of the main issues of any thin-walled structure are undesirable vibrations. The control of structural vibrations may be implemented by passive, semi-active or active manner. The passive damping of vibrations is provided by utilizing viscoelastic materials with fixed physical properties. A passive damped thin-walled structure is formed as a rule by placing viscoelastic damping material between elastic layers. The problems of free and forced vibrations of similar laminated structures assembled with traditional viscoelastic materials are well studied (we do not discuss here investigations arising to the earliest papers of DiTaranto (1965); Mead and Markus (1970) and refer only to the review article by Qatu et al, 2010).

The semi-active or active control of structural vibrations is attained as a rule by modifying the total stiffness and damping ratio (viscosity). A number of active materials such as piezoelectric, electromagnetotstrictive materials, electro- and magnetorheological fluids and elastomers, etc., may be used to vary the total viscoelastic characteristics of thin-walled smart structures (Gandhi et al, 1989; Gandhi and Thompson, 1992).

During the last two decades, electrorheological (ER) and magnetrheological (MR) fluids as well as magnetorheological elastomers (MREs) became to attract a heightened attention of researchers studying controllable damping vibrations of thin-walled laminated structures (Li et al, 2014). Gandhi et al (1989) reported on the first experimental investigation focussed on evaluating the electro-elastodynamic response of cantilevered multi-layered beams containing ER fluids. The results of this pioneering paper have clearly demonstrated for the first time the feasibility of actively controlling in real-time the dynamic characteristics (natural frequencies, amplitudes and damping ratio) of laminated structures fabricated upon ultra-advanced smart composite materials. Afterwards, numerous theoretical and experimental studies on the behavior of a sandwich beam with ER fluid were carried out (among many others, s. Choi et al, 1990; Lee, 1995; Berg et al, 1996; Oyadiji, 1996; Yalcintas and Coulter, 1995, 1998; Yalcintas and Dai, 1999; Shaw, 2000; Kang et al, 2001; Phani and Venkatraman, 2003; Allahverdizadeh et al, 2013). In particular, detailed investigations of the influence of ER materials on the composite structural vibration and damping have been carried out by Yalcintas and Coulter (1995, 1998); Yalcintas and Dai (1999). They and afterwards Kang et al (2001) have discussed variations of the modal loss factors with different designed parameters and showed that the possible damping capacity of ER based sandwich beams can be maximized by the proper choice of geometrical parameters and electric field. It has been also revealed that the adaptive nature of sandwich beams with ER liquid core was achieved by controlling the pre-yield rheology of ER smart materials in response to varying applied electric field levels. An important outcome of all aforementioned theoretical studies are analytical models of sandwich (three-layered) beams with a liquid ER core. The principle assumptions of these models are the following:

- ER liquid core exhibits linear shear behavior at small strain levels, corresponding to the pre-yield regime;

- the shear modulus of a viscoelastic core is a complex magnitude dependent of the electrical field level;
- no normal stresses in the ER layer;
- all three layers experience the same transverse displacement;
- no slipping between the elastic layers and ER layer.

All studies based on these models have reported that the definite increase in electric field across ER fluid, corresponding to the pre-yield regime, results in the increase of the loss factor of the ER layer and ultimately the equivalent damping ratio for a smart beam.

As for MR materials, they have demonstrated very quick time response, in the order of milliseconds, to an applied magnetic field (s. Chapt. 2), and thus become potentially applicable to smart tunable laminated structures (Sun et al, 2003). The available experimental studies (Yalcintas and Dai, 2004; Wei et al, 2008; Lara-Prieto et al, 2010; Chikh et al, 2016; Kozlowska et al, 2016; Irazu and Elejabarrieta, 2017) and numerous theoretical papers (Yalcintas and Dai, 1999; Sun et al, 2003; Zhou and Wang, 2005, 2006a,b,c; Hu et al, 2006; Mikhasev et al, 2010; Nayak et al, 2011, 2012; Korobko et al, 2012) have shown that the application of an external magnetic field results in very quick increasing of the stiffness and damping properties of sandwich beams containing MR fluids or elastomers. This effect may be efficiently used to tune the dynamic characteristics such as natural frequencies, vibration amplitudes, mode shapes and loss factors. As shown in Korobko et al (2012), for assumed and fixed geometrical and physical parameters of a MRE based beam, there is an optimal intensity of the magnetic field providing the maximum loss factor for a smart beam. In contrast to earlier papers on the ER fluid based sandwich beams, the theoretical investigations by Zhou and Wang (2006a,b,c); Choi et al (2010) containing mathematical models were based on the higher-order shear deformation theory for a soft MRE core, some of approaches (Zhou and Wang, 2006b,c) accounting the normal stresses in the MRE layer. The effect of non-homogeneous magnetic field on MRE sandwich beams fabricated from a MRE between two aluminum layers was examined by Hu et al (2011, 2012); Long et al (2013). Whereas the majority of investigations showed that the application of a uniform magnetic field results in increasing the total stiffness of a MRE based sandwich beam and leads to right shifting natural frequencies, the experimental tests performed by Hu et al (2011, 2012) have revealed unlooked-for result: the first natural frequency of the cantilever MRE beam decreased as the magnetic field applied to the beam was moved from the clamped edge to the free one. The left shift trend of the first natural frequency has been also confirmed by finite element simulations performed by Megha et al (2016). The nonlinear mechanical behavior of sandwich beams with a MRE core subjected to a permanent magnetic field was recently analyzed by Zeerouni et al (2018). They showed that MRE beams may exhibit a non-linear behavior even at small deformations due to the rheological properties of a MRE.

The vibration analysis becomes very important when the applied load is not constant and induces unstable modes or resonance. The advantages of using MR liquids or elastomers to active control the forced vibration of sandwich beams were illustrated in Dwivedy et al (2009); Rajamohan et al (2010); Nayak et al (2014);

Aguib et al (2016); Megha et al (2016); Yildirim et al (2016). Using finite element and Ritz' methods, Rajamohan et al (2010) have demonstrated the efficiency of utilizing MR fluid to suppress forced vibrations of a sandwich beam under harmonic force excitation. Dwivedy et al (2009) have examined parametric instability of a MRE based sandwich beam subjected to a periodic axial load. Aguib et al (2016) have experimentally and numerically studied the vibrational response of a MRE sandwich beam subjected to harmonic excitation by magnetic force applied at the free end. The nonlinear dynamic response of a clamped-clamped geometrically imperfect MRE sandwich beam with a concentrated mass at the centre under a point excitation has been investigated by Yildirim et al (2016). The numerical calculations and experimental tests on free and forced vibrations of sandwich beams and panels with carbon/epoxy composite skins and a honeycomb core filled with MRE were performed recently by de Souza Eloy et al (2018, 2019). Free and forced vibration tests conducted under several magnetic field intensities were performed to evaluate dynamic properties of the sandwich beams. The experiments showed the noticable reduction of mechanical vibrations, especially on the fundamental mode of the sandwich structure. It was also revealed shifting the natural frequencies to the right due to the increase of an induced magnetic field.

Contrary to laminated smart beams, the dynamics of sandwich plates and shells with embedded ER or MR cores remains less studied. The vibration analysis of isotropic and orthotropic sandwich rectangular plates with MRE core has been performed by Yeh (2013, 2014). In Aguib et al (2014) numerical and experimental studies of the dynamic behavior of sandwich plates consisting of two aluminum skins and a polarized MRE core (elaborated under the action of a magnetic field) have been performed. Eshaghi et al (2015) considered two sandwich plates consisting of polyethylene terephthalate face layers with two different magnetorheological fluids as core layers. At first, the dynamic responses of the cantilever sandwich plate were experimentally characterized; then, using a finite element model based on the classical plate theory, they showed enhanced vibration suppression properties of the magnetorheological sandwich plate over a wide frequency range. The dynamic performance of tapered laminated MRE sandwich plates has been analyzed in recent papers by Vemuluri and Rajamohan (2016); Vemuluri et al (2018). Applying FEM and carrying out experiments on the various prototypes of tapered composite silicon based MRE sandwich plates, they have investigated the effects of magnetic field, taper angle of the top and bottom layers and various end conditions on the dynamic properties of sandwich plates. Further, the transverse vibration responses of tapered sandwich plates under harmonic force excitation have been also analyzed at various levels of applied magnetic field. The nonlinear vibration analysis of a MRE sandwich plate was conducted experimentally by Zhang et al (2018). They have constructed the frequency-response curves in the vicinity of the fundamental natural frequency of a MRE sandwich plate in either the absence or presence of a localized external magnetic field at different geometrical locations. It was observed that all the MRE plates displayed strong hardening-type nonlinear behaviour, however, this behaviour transitioned to a weak hardening-type nonlinearity with increasing magnetic field.

As concerns shells, there are only a few investigations on the dynamic analysis of thin-walled structures containing ER or MR cores (Yeh, 2011; Mohammadi and Sedaghati, 2012; Mikhasev et al, 2011, 2014, 2016; Mikhasev, 2018). In Yeh (2011) vibrations of orthotropic cylindrical sandwich shells composed of ER core and constraining layers have been studied by utilizing the discrete layer FEM. The author has computed the natural frequencies and modal loss factors of an orthotropic cylindrical sandwich shell and concluded that by applying different electric fields, the natural frequencies and modal loss factors of the smart shell can be controlled and changed immediately. In Mohammadi and Sedaghati (2012) a nonlinear finite element model of a sandwich shell with an ER fluid in the core has been developed to perform nonlinear vibration analysis and examine the effect of small and large displacements, core thickness ratio and electric field intensity on the nonlinear damping behavior of the shell. The equivalent single-layer model for multi-layered cylindrical shells containing MRE cores has been proposed by Mikhasev et al (2011). Later, this model has been used to study the effect of an external magnetic field on the natural modes of a medium-length thin sandwich cylindrical shell containing a highly polarized MR core (Mikhasev et al, 2014). It has been revealed that applying a constant magnetic field may result in strong distortion of eigenmodes corresponding to the lowest eigenfrequencies. In Mikhasev et al (2016) the response of the MRE-based sandwich medium-length cylindrical shell to the initial localized perturbations and an applied time-dependent magnetic field has been studied. It has been shown that the time dependent magnetic field may result in soft suppression of running localized bending waves. Finally, the analysis of different problems considered in Mikhasev (2017, 2018) has clearly demonstrated that MREs may be successfully used in designing smart thin-walled laminated structures of variable and predictable mechanical properties. Some problems on free and forced vibrations of MRE based cylindrical shells studied in Mikhasev et al (2011, 2014); Mikhasev (2017, 2018) will be in detail considered in the subsequent sections of this chapter. Concluding the section, we refer readers to the review by Eshaghi et al (2016).

## 5.2 Sandwich and Multi-layered Beams with Magnetorheological Core

Consider a sandwich beam of the length $L$ and the rectangular cross section with the sides $h$ and $b$ as shown in Fig. 5.1. The face sheets of the thickness $h_1, h_3$ are made of an elastic material, and the viscoelastic core of the thickness $h_2$ is fabricated from a magnetorheological composite (MRC). From all variations of smart composite materials, we consider here only the magnetorheological fluids (MRFs) and the magnetorheological elastomer (MRE-1) with properties given in Chapt. 2. Obviously, the choice of a mathematical model for the sandwich MR beam depends on whether the core is a liquid or an elastomer.

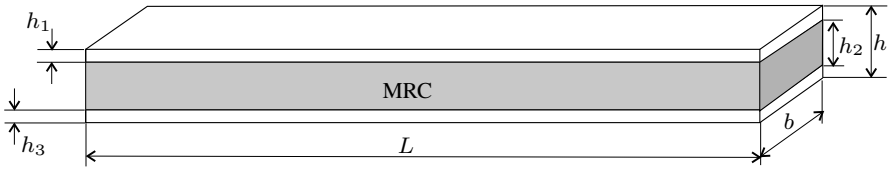


**Fig. 5.1** Sandwich beam with MRC core.

### *5.2.1 Sandwich Beam with Magnetorheological Fluid Core*

Let the core be a smart magnetorheological fluid, MRF. The ESL model for laminated beams presented in Chapt. 2 and based on the generalized hypotheses of Timoshenko can not be used here, because it presupposes the same order of stiffness for all layers composing a beam. We shall take here the simplest model proposed by Yalcintas and Dai (2004) and based on the assumptions stated in Sect. 5.1. According to this model for a sandwich beam with the same thicknesses for all layers ($h_1 = h_2 = h_3 = a$), the governing equations accounting tranverse shear in the liquid MR core are the following

$$\begin{aligned} \rho\frac{\partial^2 w}{\partial t^2} + 2EI\frac{\partial^4 w}{\partial x^4} - 4G_{\mathrm{v}}ab\left(\frac{\partial^2 w}{\partial x^2} - \frac{\partial\phi}{\partial x}\right) &= f, \\ J\frac{\partial^2\phi}{\partial t^2} - 2Ea^2b\frac{\partial^2\phi}{\partial x^2} - 4G_{\mathrm{v}}ab\left(\frac{\partial w}{\partial x} - \phi\right) &= 0, \end{aligned} \tag{5.1}$$

where $w$ is the normal deflection of the beam (the medium line of the core), $\phi$ is the cross-sectional rotation, $x$ is a coordinate at the core medium line, $f$ is the external force per unit length, $t$ is time, $E$ is the Young's modulus of the surface layers, $G_{\mathrm{v}}$ is the complex shear modulus for the one of MRFs with properties given in Tables 2.8-2.10, $\rho$ is the reduced density of the sandwich per unit length, $I$ is the geometric moment of area 2nd order of the cross-section, and $J$ is the moment of inertia per unit length. The magnitudes $\rho, I, J$ are introduced as

$$\begin{aligned} \rho &= 2\rho_1 + \rho_2, \\ I &= \frac{9}{4}ba^3, \\ J &= a^2\left(\frac{13\rho_1}{6} + \frac{\rho_2}{12}\right), \end{aligned} \tag{5.2}$$

where $\rho_1$ and $\rho_2$ are densities per unit length of the face sheets and MRF, respectively. Let the edges be simply supported. The appropriate boundary conditions read

$$w = \frac{\partial^2 w}{\partial x^2} = \frac{\partial\phi}{\partial x} = 0 \quad \text{at} \quad x = 0, L. \tag{5.3}$$

#### 5.2.1.1 Free Vibrations

Let $f = 0$. Then the natural modes corresponding to conditions (5.3) are given by functions

$$w = w_n(x,t) = \sin \lambda_n x \, \mathrm{e}^{\mathrm{i}\Omega t}, \quad \phi = \phi_n(x,t) = C_n \cos \lambda_n x \, \mathrm{e}^{\mathrm{i}\Omega t}, \quad n = 1, 2, \ldots \tag{5.4}$$

where

$$\lambda_n = \frac{\pi n}{L}, \quad C_n = \frac{2\lambda_n G_{\mathrm{v}}}{\lambda^2 a^2 E + 2G} \tag{5.5}$$

and

$$\Omega = \Omega_n = \lambda_n^2 \sqrt{\frac{E}{\rho}\left[2I + \frac{4G_{\mathrm{v}}ab}{E\lambda_n^2}\left(1 + \frac{2G_{\mathrm{v}}}{\lambda_n^2 a^2 E + 2G_{\mathrm{v}}}\right)\right]} \tag{5.6}$$

is the complex eigenvalue. Deriving Eq. (5.6), we neglected the rotation inertia of the cross-section. Separating in (5.6) the real and imaginary parts, one obtains the required natural frequency $\omega = \Re\Omega$ and the associated damping ratio $\alpha = \Im\Omega > 0$ of damped vibrations.

**Remark 5.1.** In addition to the complex eigenvalue $\Omega = \omega + \mathrm{i}\alpha$ defined by (5.6), the boundary-value problem (5.1), (5.3) has another eigenvalue $\Omega = -\omega - \mathrm{i}\alpha$. It is obvious that the second one does not satisfy the condition of damped vibrations, and so will not be taking into consideration in what follows.

To analyse the effect of magnetic field and the type of MRF chosen on damped vibrations, we consider the following example.

**Example 5.1.** Let the sandwich beam of the length $L = 390$ mm with the sides $a = 0.7$ mm, $b = 25$ mm in the cross-section be assembled from aluminum face sheets and MRF placed between these sheets. We consider three types of MRFs: MRF-1, MRF-2 and MRF-3, with properties given in Tables 2.8-2.10. Figures 5.2-5.4 demonstrate the effect of magnetic field on the natural frequencies $\omega = \Re\Omega$ corresponding to three modes with numbers of semi-waves $n = 1, 3, 5$ for the beams with different MRFs. As can be seen from the figures, the natural frequencies shift right as the applied magnetic field increases from 0 to 350 mT, these variations being observed more dominantly for the MRF-1, which contains iron particles of large size.

An important parameter characterizing the rate of vibration damping is the logarithmic decrement

$$D_{\mathrm{l}} = \frac{2\pi\alpha}{\sqrt{\omega^2 - \alpha^2}}. \tag{5.7}$$

Figures 5.5-5.7 show the behavior of scaled logarithmic decrement $d_{\mathrm{l}} = 50 D_{\mathrm{l}}/\pi$ under varying the magnetic induction $B$ for three types of MRFs. Calculations have been performed for $n = 1, 3, 5$. It is seen that the effect of magnetic field on the logarithmic decrement is very complicated due to complicated behavior of the loss factor $\eta_{\mathrm{v}}$ for all the MR liquids (s. Tables 2.8-2.10). The general conclusion related to all MRFs under consideration is that the logarithmic decrement decreases

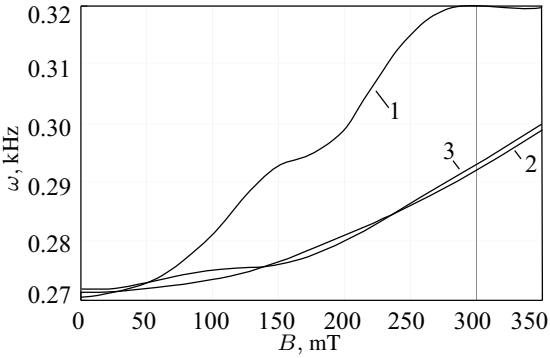


**Fig. 5.2** First natural frequency $\omega_1 = \Re\Omega_1$ for sandwich beams with different MRF cores vs. induction $B$:
1 - MRF-1; 2 - MRF-2;
3 - MRF-3.

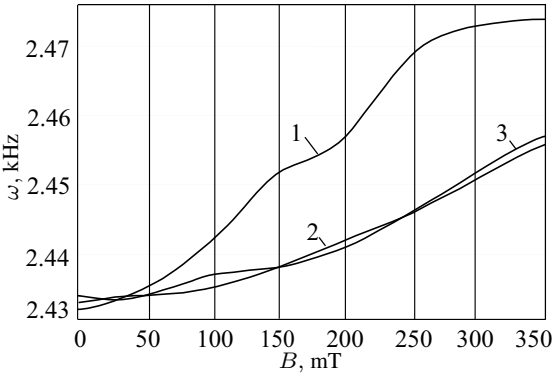


**Fig. 5.3** Third natural frequency $\omega_3 = \Re\Omega_3$ for sandwich beams with different MRF cores vs. induction $B$:
1 - MRF-1; 2 - MRF-2;
3 - MRF-3.

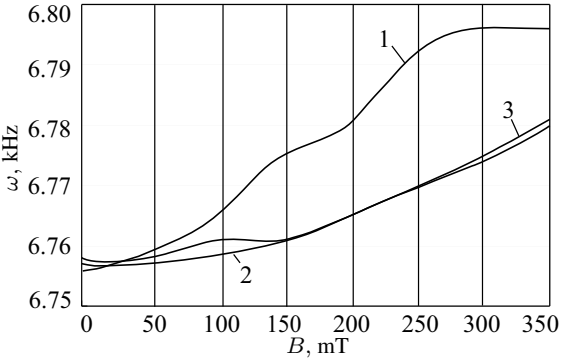


**Fig. 5.4** Fifth natural frequency $\omega_5 = \Re\Omega_5$ for sandwich beams with different MRF cores vs. induction $B$:
1 - MRF-1; 2 - MRF-2;
3 - MRF-3.

with growing the mode number. Thus, the mathematical model for a sandwich used here shows that MRFs are most effective for damping low-frequency vibrations of three-layered beams with the MRF core.

Figures 5.8 and 5.9 allow us to compare the damping capabilities of different smart fluids on the first and third modes, respectively, at different levels of applied magnetic field. It is seen that the MRF-2 and MRF-3 possess the best damping

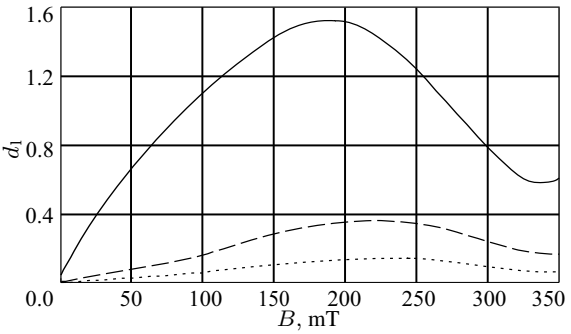


**Fig. 5.5** Scaled logarithmic decrement $d_1$ for the sandwich beam with the MRF-1 core corresponding to different modes vs. induction $B$: solid line - $n = 1$, dashed line - $n = 3$, dotted line - $n = 5$.

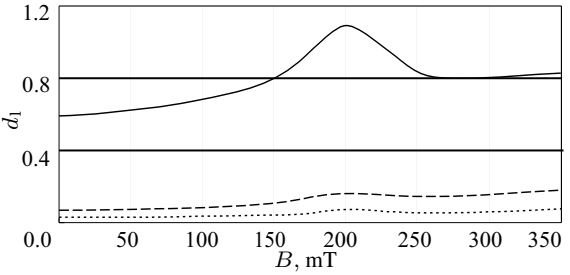


**Fig. 5.6** Scaled logarithmic decrement $d_1$ for the sandwich beam with the MRF-2 core corresponding to different modes vs. induction $B$: solid line - $n = 1$, dashed line - $n = 3$, dotted line - $n = 5$.

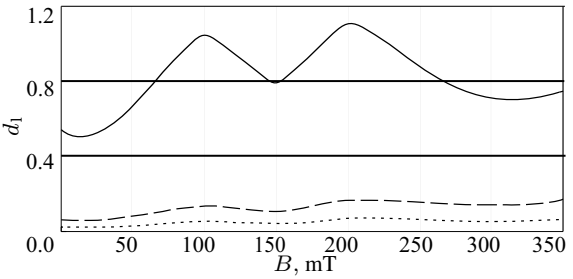


**Fig. 5.7** Scaled logarithmic decrement $d_1$ for the sandwich beam with the MRF-3 core corresponding to different modes vs. induction $B$: solid line - $n = 1$, dashed line - $n = 3$, dotted line - $n = 5$.

capability at a weak magnetic field ($B < 50$ mT), while the MRF-1 demonstrates the highest damping effect for $B$ varying from 50 to 300 mT.

#### 5.2.1.2 Forced Stationary Vibrations

Now we consider forced vibrations under the external normal harmonic force

$$f = \rho F_0(x)\, \mathrm{e}^{\mathrm{i}\omega_\mathrm{e} t}, \tag{5.8}$$

where $\omega_\mathrm{e}$ is the excitation frequency. The magnetic field, if applied, is constant and homogeneous (independent of time $t$ and coordinate $x$).

A solution of Eqs. (5.1) with the boundary conditions (5.3) may be found in the form of series

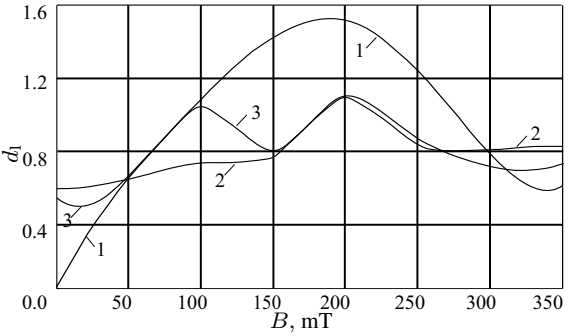


**Fig. 5.8** Scaled logarithmic decrement $d_1$ for the sandwich beam with different MRFs cores corresponding to the first mode ($n = 1$) vs. induction $B$: 1 - MRF-1; 2 - MRF-1; 3 - MRF-3.

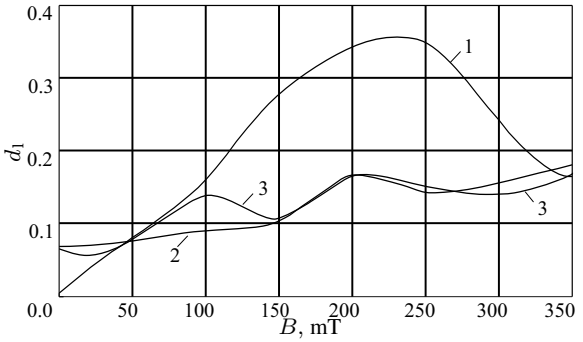


**Fig. 5.9** Scaled logarithmic decrement $d_1$ for the sandwich beam with different MRFs cores corresponding to the third mode ($n = 3$) vs. induction $B$: 1 - MRF-1; 2 - MRF-1; 3 - MRF-3.

$$w(x,t) = \sum_{n=1}^{\infty} \sin(\lambda_n x)\, q_{\rm n}(t), \quad \phi(x,t) = \sum_{n=1}^{\infty} C_n \cos(\lambda_n x)\, q_{\rm n}(t), \tag{5.9}$$

where $q_{\rm n}(t)$ is the so-called generalized coordinates of the vibrating system. Substituting Eqs. (5.9) into (5.1), then multiplying them by $\sin(\lambda_n x)$ and integrating over the beam length, we obtain the following equation

$$\ddot{q}_n(t) + \Omega_n^2 q_{\rm n}(t) = F_n {\rm e}^{{\rm i}\omega_{\rm e} t}, \tag{5.10}$$

where

$$F_n = \int_0^L F_0(x) \sin(\lambda_n x) dx \tag{5.11}$$

is the generalized force corresponding to $q_{\rm n}(t)$. The partial solution of Eq. (5.10) is

$$q_{\rm n}(t) = F_n \frac{{\rm e}^{{\rm i}\omega_{\rm e} t}}{\Omega_n^2 - \omega_{\rm e}^2}. \tag{5.12}$$

Then the amplitude of forced stationary vibrations at any point of the beam will be defined by

$$w(x,t)=\sum_{n=1}^{\infty}\frac{F_n}{\Omega_n^2-\omega_{\rm e}^2}\sin(\lambda_n x)\mathrm{e}^{\mathrm{i}\omega_{\rm e}t}=\sum_{n=1}^{\infty}\frac{F_n\sin(\lambda_n x)\mathrm{e}^{\mathrm{i}\omega_{\rm e}t}}{\omega_n^2-\alpha_n^2-\omega_{\rm e}^2+2\mathrm{i}\omega_n\alpha_n}. \quad (5.13)$$

Since the complex eigenfrequency $\Omega_n$ depend on the complex shear modulus $G_{\rm v}$ being the function of induction $B$, the amplitude of sustained forced vibrations becomes to some extent a controllable quantity.

#### 5.2.1.3 Equivalent Model with External Friction for Prediction of Unsteady Vibrations

We note that the homogeneous equation corresponding to Eq. (5.10) has the two partial solutions, $\mathrm{e}^{-\alpha+\mathrm{i}\omega t}$ and $\mathrm{e}^{\alpha-\mathrm{i}\omega t}$, of which the second one does not satisfy the damping condition (s. Remark 5.1). Thus, the general solution of Eq. (5.10) based on the assumed above model for viscoelastic MRF with internal friction can not be used to describe unsteady forced vibrations of the MRF-based sandwich beam.

In order to give an approximate analysis of unsteady vibrations, we shall replace the initial model by an *equivalent model* with external friction. The idea of this substitution is the following. The dynamic unsteady response of the beam to the external harmonic excitation can be represented by the superposition of the damped eigenmodes and undamped forced modes (5.13). Each of the damped eigenmodes is characterized by the natural frequency $\omega_n=\Re\Omega_n$ and the associated damping ratio $\alpha_n=\Im\Omega_n$. We consider the series of viscoelastic $n$-oscillators

$$\ddot{y}_n+2\alpha_n\dot{y}_n+(\omega_n^2+\alpha_n^2)y_n=0 \quad (5.14)$$

with the external friction and having the same natural frequencies $\omega_n$ and damping ratio $\alpha_n$. Then Eq. (5.10) may be replaced by the following equation

$$\ddot{\tilde{q}}_n(t)+2\alpha_n\dot{\tilde{q}}_n+(\omega_n^2+\alpha_n^2)\tilde{q}_{\rm n}=F_n\mathrm{e}^{\mathrm{i}\omega_{\rm e}t}, \quad (5.15)$$

where $\tilde{q}_{\rm n}$ is the generalized coordinate of the *equivalent viscoelastic system* with damping ratio depending on the wave number $n$.

The general solution of Eq. (5.15) is

$$\tilde{q}_{\rm n}=\frac{F_n\mathrm{e}^{\mathrm{i}\omega_{\rm e}t}}{\omega_n^2-\omega_{\rm e}^2+\alpha_n^2+2\mathrm{i}\alpha_n\omega_{\rm e}}. \quad (5.16)$$

Then the amplitude of forced unsteady vibrations for the *equivalent smart beam* will be as follows

$$w(x,t)=\sum_{n=1}^{\infty}\left[\mathrm{e}^{-\alpha_n t}\left(c_n^{(s)}\sin\omega_n t+c_n^{(c)}\cos\omega_n t\right)+\frac{F_n\mathrm{e}^{\mathrm{i}\omega_{\rm e}t}}{\omega_n^2-\omega_{\rm e}^2+\alpha_n^2+2\mathrm{i}\alpha_n\omega_{\rm e}}\right]\sin(\lambda_n x). \quad (5.17)$$

We note that the component in Eq. (5.17) corresponding to the amplitude of forced unsteady vibrations does not coincide with the amplitude of forced stationary vibrations (5.13). However, the real parts of these components become the same for the resonance excitation, i.e. for $\omega_{\rm e} = \omega_n$. Equation (5.17) derived for the *equivalent beam* can be used only to estimate approximately unsteady vibrations of the smart beam under consideration. To make that, we shall consider the following example.

**Example 5.2.** Let the motionless sandwich MR beam with parameters specified in Example 5.1 be subjected to the periodic concentrated force

$$f = \rho\delta(x - x^*)\sin\omega_{\rm e}t$$

applied in the point $x = x^* \in (0, L)$ at $t \geq 0$, where $\delta(x)$ is the delta function. Then the generalized force

$$F_n = \frac{2}{L}\sin\lambda_n x^*.$$

We consider the case when the frequency of excitation is very close to the first natural frequency $\omega_{\rm e} \approx \omega_1 = \Re\Omega_1$ of the beam when a magnetic field is absent. In Fig. 5.10, curve 1 shows the scaled amplitude $A = w_{\max} \times 10^5$ of the *resonance* vibrations of the *equivalent beam* without magnetic field, and the curve marked by 2 corresponds to vibrations of the same beam when the magnetic field of the constant induction $B = 250$ mT is applied. Here, $w_{\max}$ is the maximum amplitude. The calculations were performed for $x^* = L/7$ and $\omega_{\rm e} = 271$ Hz. It is clearly seen, that due to viscosity of the MRF-1 the small oscillations generated by the initial conditions quickly decay with and without magnetic field, while the amplitude of forced vibrations is the growing function which converges to some limited value at $t \to \infty$, if a magnetic field is absent. The application of magnetic field leads to slight shifting all natural frequencies, including the first one (s. again Fig. 5.2), to right and in that way prevents resonance vibrations.

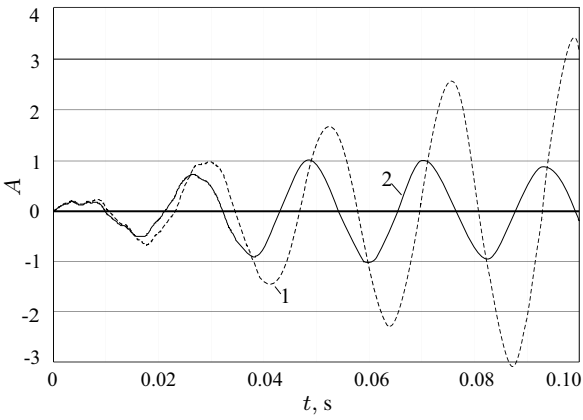


**Fig. 5.10** Scaled maximum amplitude $A$ of forced vibrations of the sandwich beam with the MRF-1 core vs. time $t$ without magnetic field (curve 1) and under magnetic field of the induction $B = 250$ mT (curve 2).

#### 5.2.1.4 Suppression of Forced Vibrations in Thin-walled Structures via Magnetic/Electric Fields

The basic principles of damping forced vibrations of MR/ER-based beams, plates and shells are to give a time signal of the magnetic/electric field and also to determine its optimal intensity. The criteria of selecting the signal time of an external physical field may be different. The simplest criterion is monitoring of the maximum amplitude of vibrations: the magnetic/electric field signal is fed, if the maximum amplitude (in some point) achieves a certain critical magnitude. Another criterion is based on the estimation of the total mechanical energy of the structure. For instance, for the sandwich beam considered in this section this energy is defined as

$$\mathbb{E}_{\rm s} = T + \Pi_1 + \Pi_2 + \Pi_3, \tag{5.18}$$

where

$$T = \frac{1}{2}\int\limits_0^L \left(\frac{\partial w}{\partial t}^2\right) \rho \,\mathrm{d}x + \frac{1}{2}\int\limits_0^L \left(\frac{\partial \phi}{\partial t}^2\right) J \,\mathrm{d}x,$$

$$\Pi_1 = ba^3 E \int\limits_0^L \left(\frac{\partial \phi}{\partial t}^2\right) \mathrm{d}x, \quad \Pi_2 = EI \int\limits_0^L \left(\frac{\partial w}{\partial t}^2\right) \mathrm{d}x,$$

$$\Pi_3 = \frac{1}{2} G'_{\rm v} ab \int\limits_0^L \gamma^2 \rho \mathrm{d}x.$$

In Eq. (5.18), $T$ is the kinetic energy of the beam, $\Pi_1, \Pi_2$ are the potential energy of tangential and bending deformations, and $\Pi_3$ is the potential energy of the transversal shears in the MR/ER core. We note that the energy (5.18) does not contain the work that goes to the heating the whole system, including the work on heating the MR/ER core, which depends on the loss modulus $G''_{\rm v}$ of the smart viscoelastic material.

The problem is to minimize the maximum amplitude of excited vibrations, the mechanical energy $\mathbb{E}_{\rm s}$ or the rate of its growth $\dot{\mathbb{E}}_{\rm s}$ (Lai and Wang, 1996). For instance, if at $t = t_{\rm cr}$ the energy achieves some critical value $\mathbb{E}_{\rm s}^{(\rm cr)}$, a magnetic/electric field signal is applied, leading to a sudden or gradual change in the physical characteristics of a smart core.

**Example 5.3.** In this example, we study the response of the beam considered in the previous example when the magnetic field of the intensity $B = 270$ mT is suddenly applied at $t = t_{\rm cr} = 0.1$ s. Let $w^{(1)}(x,t)$ be the beam response to the resonance excitation at the interval $0 < t \le t_{\rm cr} = 0.1$ s (see the dotted line in Fig. 5.10). Consider the following initial conditions

$$w(x,t)|_{t_{\rm cr}} = w^{(1)}(x,t_{\rm cr}), \quad \dot{w}(x,t)|_{t=t_{\rm cr}} = \dot{w}^{(1)}(x,t_{\rm cr}) \tag{5.19}$$

for Eqs. (5.1). Let $w^{(2)}(x,t)$ be a solution of the initial boundary-value problem (5.1), (5.3), (5.19) for $t \ge t_{\rm cr}$ when the magnetic field signal is fed. We assume

that after applying the magnetic field at $t = t_{\rm cr}$ the viscoelastic properties of the beam is changed in a moment. So, to use formulae (5.17) at $t \geq t_{\rm cr}$, one needs to recalculate at first all natural frequencies for the sandwich at $B = 270$ mT. Figure 5.11 shows the response of the equivalent MRF-1 sandwich at two time gaps, for $0 \leq t < t_{\rm cr}$ (the dotted line) and $t \geq t_{\rm cr}$ (the solid line). It is seen that the application of a magnetic field results in some high-frequency oscillations generated by the initial displacements and velocities (5.19), these oscillations being rapidly suppressed during the time. However, the basic effect of the applied magnetic field is a quick withdrawal of the beam from a regime of the resonance vibrations and stabilization of forced vibrations with more low amplitude.

**Remark 5.2.** It should be noted that the response of a smart material to a signal of magnetic/electric field depends on the ratio of timescales of controlling signal and the reaction of the very MR/ER medium (Korobko et al, 2012). So, at sudden application of a magnetic field, the time of reaction of MRF or MRE is about $10^{-3} - 10^{-2}$ $s$. An abrupt impact of an external physical field is the kind of a *parametric blow* for the adaptable mechanical system and can excite additional high-frequency modes.

Solution (5.17) found above for the *equivalent smart beam* as well as Examples 5.2, 5.3 relate to the case when the applied magnetic field is stationary. It is obvious that these solutions do not take into account the aforementioned parametric impact. In the next item, we shall construct high-frequency modes accounting for the real time response of a smart MR material to a signal of an external magnetic field.

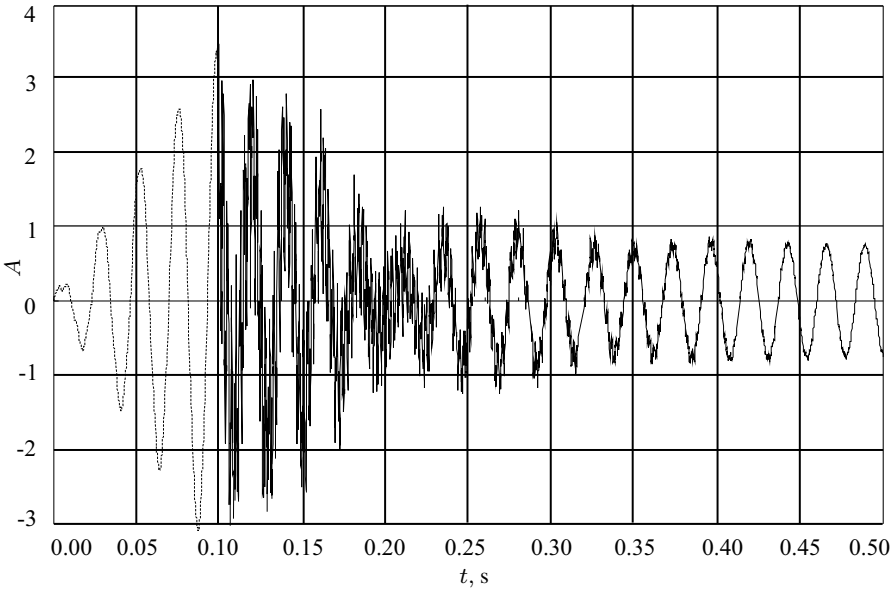


**Fig. 5.11** Response of the MRF-1 based sandwich beam to the resonance harmonic force and magnetic field applied at $t = t_{\rm cr} = 0.1$ s.

#### 5.2.1.5 High-frequency Response of Magnetorheological Beam on the Rapid Signal of a Magnetic Field

Let the complex shear modulus $G_\mathrm{v} = G_\mathrm{v}(v_r t)$ of the MRF be a function of time, where $v_\mathrm{r} = 1/t_\mathrm{r}$ is the speed of the liquid reaction on the signal of a magnetic field. For a majority of MRFs, $v_\mathrm{r}$ varies from $10^{-3}$ to $10^{-2}$ $s^{-1}$. Let $t_\mathrm{r} = 10^{-2}$ s be the characteristic time.

We introduce the dimensionless magnitudes

$$\begin{aligned} &w = LW^*, \quad t = t_\mathrm{r}\tau, \qquad\qquad g(\tau) = \frac{2G_\mathrm{v}(t_\mathrm{r}\tau)L^2}{\varepsilon^{1/2}Ea^2} \\ &\varepsilon = \frac{t_\mathrm{r}}{T_\mathrm{p}}, \qquad T_\mathrm{p} = \frac{1}{3}\sqrt{\frac{2\rho a}{Eb}}\,\frac{L^2}{a^2}, \end{aligned} \tag{5.20}$$

where $T_\mathrm{p}$ is the period of low-frequency vibrations of the beam without the MRF core. Furthermore, it is assumed that $\varepsilon$ is a small parameter.

The dimensionless deflection and angle of rotation satisfying the boundary conditions (5.3) are sought in the form

$$W^* = W(\tau)\sin\frac{\pi n x}{L}, \quad \phi = \Phi(\tau)\cos\frac{\pi n x}{L}, \quad n = \varepsilon^{-1/2}p,\ p \sim 1, \tag{5.21}$$

where $n$ is an integer. Then Eqs. (5.1) can be rewritten as

$$\begin{aligned} \varepsilon\frac{\mathrm{d}^2 W}{\mathrm{d}\tau^2} + \delta^4 W + \frac{4}{9}\varepsilon^{1/2}\delta^2 g(\tau)W + \frac{4}{9}\varepsilon\delta g(\tau)\Phi = 0, \\ \varepsilon\varsigma^2\frac{\mathrm{d}^2\Phi}{\mathrm{d}\tau^2} + \delta^2\Phi + \delta g(\tau)W - \varepsilon^{1/2}g(\tau)\Phi = 0, \end{aligned} \tag{5.22}$$

where

$$\delta = \pi p, \quad \varsigma^2 = \frac{9\rho_J a^2}{2\rho L^2}, \quad \rho_J = \frac{13}{6}\rho_1 + \frac{1}{12}\rho_2, \quad g(\tau) = g_1(\tau) + \mathrm{i}g_2(\tau). \tag{5.23}$$

Here, $g_1$ and $g_2$ are the real and imaginary parts of the complex function $g(\tau)$, $g_2$ being positive.

To solve Eqs. (5.21), we apply to the multiple scale method. Let

$$\tau_0 = \varepsilon^{-1/2}\tau, \qquad \tau_1 = \tau, \qquad \tau_2 = \varepsilon^{1/2}\tau, \quad \ldots \tag{5.24}$$

be independent variables. The asymptotic solution of Eqs. (5.22) can be found in the form of series

$$W = W_0 + \varepsilon^{1/2}W_1 + \varepsilon W_2 + \ldots, \qquad \Phi = \Phi_0 + \varepsilon^{1/2}\Phi_1 + \varepsilon\Phi_2 + \ldots \tag{5.25}$$

where $W_k$ and $\Phi_k$ are functions of independent arguments $\tau_j$ defined by (5.24).

Substitution of (5.25) into Eqs. (5.22) results in the sequence of differential equations with respect to required $W_k, \Phi_k$. Consider these equations step-by-step. In the zeroth-order approximation, one has the homogeneous equations

$$\frac{\partial^2 W_0}{\partial \tau_0^2} + \delta^4 W_0 = 0, \qquad \frac{\partial^2 \Phi_0}{\partial \tau_0^2} + \frac{\delta^2}{\varsigma^2}\Phi_0 + \frac{\delta}{\varsigma^2} g(\tau_1) W_0 = 0. \tag{5.26}$$

Their solution are

$$\begin{aligned} W_0 &= A_0(\tau_1, \ldots)\mathrm{e}^{\mathrm{i}\delta^2\tau_0} + \bar{A}_0(\tau_1, \ldots)\mathrm{e}^{-\mathrm{i}\delta^2\tau_0}, \\ \Phi_0 &= B_0(\tau_1, \ldots)\mathrm{e}^{\mathrm{i}\frac{\delta}{\varsigma}\tau_0} + \bar{B}_0(\tau_1, \ldots)\mathrm{e}^{-\mathrm{i}\frac{\delta}{\varsigma}\tau_0} \\ &\quad + \frac{g(\tau_1)}{\delta(1-\delta^2\varsigma^2)}\left[A_0\mathrm{e}^{\mathrm{i}\delta^2\tau_0} + \bar{A}_0\mathrm{e}^{-\mathrm{i}\delta^2\tau_0}\right], \end{aligned} \tag{5.27}$$

where $A_0(\tau_1, \tau_2, \ldots), B_0(\tau_1, \tau_2, \ldots)$ are required complex functions. In the first-order approximation, one obtains the nonhomogeneous system of differential equations

$$\begin{aligned} \frac{\partial^2 W_1}{\partial \tau_0^2} + \delta^4 W_1 &= -2\frac{\partial^2 W_0}{\partial \tau_0 \partial \tau_1} - \frac{4}{9}\delta^2 g(\tau_1) W_0, \\ \frac{\partial^2 \Phi_1}{\partial \tau_0^2} + \frac{\delta^2}{\varsigma^2}\Phi_1 + \frac{\delta}{\varsigma^2} g(\tau_1) W_1 &= -2\frac{\partial^2 \Phi_0}{\partial \tau_0 \partial \tau_1} - \frac{g(\tau_1)}{\varsigma^2}\Phi_0. \end{aligned} \tag{5.28}$$

In above equations, the right-hand members generate secular partial solutions. Eliminating these solutions, one arrives at the differential equations

$$\mathrm{i}\frac{\partial A_0}{\partial \tau_1} + \frac{2}{9} g(\tau_1) A_0 = 0, \quad 2\mathrm{i}\delta\varsigma\frac{\partial B_0}{\partial \tau_1} - g(\tau_1) B_0 = 0. \tag{5.29}$$

These equations have the solutions

$$\begin{aligned} A_0(\tau_1, \tau_2, \ldots) &= A_{01}(\tau_2, \ldots)\exp\left\{\frac{2\mathrm{i}}{9}\int\limits_0^{\tau_1} g(\tau)\mathrm{d}\tau\right\}, \\ B_0(\tau_1, \tau_2, \ldots) &= B_{01}(\tau_2, \ldots)\exp\left\{\frac{\mathrm{i}}{2\delta\varsigma}\int\limits_0^{\tau_1} g(\tau)\mathrm{d}\tau\right\}. \end{aligned} \tag{5.30}$$

When taking into account (5.30), the general solution of the system (5.28) becomes as follows

$$\begin{aligned} W_1 &= A_1(\tau_1, \ldots)\mathrm{e}^{\mathrm{i}\delta^2\tau_0} + \bar{A}_1(\tau_1, \ldots)\mathrm{e}^{-\mathrm{i}\delta^2\tau_0}, \\ \Phi_1 &= B_1(\tau_1, \ldots)\mathrm{e}^{\mathrm{i}\frac{\delta}{\varsigma}\tau_0} + \bar{B}_1(\tau_1, \ldots)\mathrm{e}^{-\mathrm{i}\frac{\delta}{\varsigma}\tau_0} \\ &\quad + C_1(\tau_1, \ldots)\mathrm{e}^{\mathrm{i}\delta^2\tau_0} + \tilde{C}_1(\tau_1, \ldots)\mathrm{e}^{-\mathrm{i}\delta^2\tau_0}, \end{aligned} \tag{5.31}$$

where

$$C_1 = -\frac{g}{\delta(1-\delta^2\varsigma^2)}A_1 + \frac{4\varsigma^2\delta^2 g^2 - 9\mathrm{i}\delta^2 g' + 9g^2}{9\delta(1-\delta^2\varsigma^2)^2}\,A_0,$$
$$\tilde{C}_1 = -\frac{g}{\delta(1-\delta^2\varsigma^2)}\bar{A}_1 + \frac{4\varsigma^2\delta^2 g^2 + 9\mathrm{i}\delta^2 g' + 9g^2}{9\delta(1-\delta^2\varsigma^2)^2}\,\bar{A}_0. \tag{5.32}$$

The unknown functions $A_{01}, B_{01}, A_1, B_1$ are found from the next approximation.

We limit ourselves to the first two approximations. Then the approximate formulae for the deflection and the angle of rotation become as follows

$$w = L\sin\left(\frac{\pi ps}{\varepsilon^{1/2}}\right)\exp\left[-\frac{2}{9}\int\limits_0^\tau g_2(\tau)\mathrm{d}\tau\right]\left\{A_{01}\exp\left[\mathrm{i}\left(\frac{\delta^2\tau}{\varepsilon^{1/2}} + \frac{2}{9}\int\limits_0^\tau g_1(\tau)\mathrm{d}\tau\right)\right]\right.$$
$$\left. +\ \bar{A}_{01}\exp\left[-\mathrm{i}\left(\frac{\delta^2\tau}{\varepsilon^{1/2}} + \frac{2}{9}\int\limits_0^\tau g_1(\tau)\mathrm{d}\tau\right)\right]\right\} + O\left(\varepsilon^{1/2}\right), \tag{5.33}$$

$$\phi = \cos\left(\frac{\pi ps}{\varepsilon^{1/2}}\right)\exp\left[-\frac{1}{2\delta\varsigma}\int\limits_0^\tau g_2(\tau)\mathrm{d}\tau\right]\left\{B_{01}\exp\left[\mathrm{i}\left(\frac{\delta\tau}{\varsigma\varepsilon^{1/2}} + \frac{1}{2\delta\varsigma}\int\limits_0^\tau g_1(\tau)\mathrm{d}\tau\right)\right]\right.$$
$$\left. +\ \bar{B}_{01}\exp\left[-\mathrm{i}\left(\frac{\delta\tau}{\varsigma\varepsilon^{1/2}} + \frac{1}{2\delta\varsigma}\int\limits_0^\tau g_1(\tau)\mathrm{d}\tau\right)\right]\right\} + O\left(\varepsilon^{1/2}\right), \tag{5.34}$$

where $A_{01}$ and $B_{01}$ are found from the initial conditions.

Equations (5.33) and (5.34) give the leading terms in the asymptotic series predicting high-frequency unsteady damping vibrations. It is seen that these terms are asymptotically independent. Equation (5.33) describes bending vibrations with the current frequency

$$\omega_\mathrm{b} = \frac{\delta^2\tau}{\varepsilon^{1/2}} + \frac{2}{9}\int\limits_0^\tau g_1(\tau)\mathrm{d}\tau \tag{5.35}$$

and the damping ratio

$$\alpha_\mathrm{b} = \frac{2}{9}\int\limits_0^\tau g_2(\tau)\mathrm{d}\tau, \tag{5.36}$$

and Eq. (5.34) predicts torsional vibrations with the frequency

$$\omega_\mathrm{r} = \frac{\delta\tau}{\varsigma\varepsilon^{1/2}} + \frac{1}{2\delta\varsigma}\int\limits_0^\tau g_1(\tau)\mathrm{d}\tau \tag{5.37}$$

and the damping ratio

$$\alpha_{\mathrm{r}} = \frac{1}{2\delta_{\varsigma}} \int_0^{\tau} g_2(\tau)\mathrm{d}\tau. \tag{5.38}$$

Thus, high-frequency vibrations are asymptotically decomposed into bending and torsional ones. The second terms in Eqs. (5.35) and (5.37) give nonstationary corrections for frequencies, these corrections are induced by the rapid variation of the storage modulus of the MRF under the impulse signal of the magnetic field. The time-dependent damping ratios (5.36) and (5.38) reflect the variation of the loss modulus of the smart viscoelastic core. If we take into account the next approximations, it would be detected that the bending vibrations defined by Eq. (5.33) generate torsional vibrations with amplitudes of order $O\left(\varepsilon^{1/2}\right)$ and vice versa, the high-frequency rotations of the beam cross-sections (5.34) cause small bending oscillations. Thus, the bending and torsional vibrations are coupled.

The above mentioned methods of vibration damping belong to semi-active methods. Obviously, they have both advantages and disadvantages. One of the advantages of these approaches, based on the application of MR/ER smart materials, is that without the use of any special damping devices it is possible to change reversibly the elastic and viscous properties of the entire mechanical system to withdraw it from the regime of resonance vibrations. In addition, these methods allow suppressing efficiently any free oscillations generated by the initial conditions. Their common drawback is that their implementation results in partial suppression of the forced vibrations only due to some increasing all natural frequencies.

### *5.2.2 Laminated Beams with Magnetorhelogical Elastomer Layers*

In this subsection, we consider both sandwich and multi-layered beams with one ore several layers made of a MRE. To predict the dynamic response of the MRE-based laminated beams, we use the ESL theory stated in Chapt. 2. The differential equation governing forced vibrations of the beam represented in Fig. 5.1 is the following (2.153)

$$EI\eta_3 \left(1 - \frac{\theta h^2}{\beta}\frac{\partial^2}{\partial x^2}\right)\frac{\partial^4 \chi}{\partial x^4} + \rho_{\mathrm{l}} \left(1 - \frac{h^2}{\beta}\frac{\partial^2}{\partial x^2}\right)\frac{\partial^2 \chi}{\partial t^2} = q_{\mathrm{l}}, \tag{5.39}$$

where $q_{\mathrm{l}}(x,t)$ is the external normal force per unit length of the beam, $\rho_{\mathrm{l}}$ is the linear mass introduced in Sect. 2.1, $\chi$ is the displacement function coupled with the normal displacement $w$ by

$$w = \left(1 - \frac{h^2}{\beta}\frac{\partial^2}{\partial x^2}\right)\chi. \tag{5.40}$$

In contrast to the cases considered in Chapt. 4, the reduced Young's modulus $E$ and parameters $\eta_3, \theta, \beta$ are here complex magnitudes dependent on the induction $B$ of the external magnetic field. The complex values of these parameters are calculated by Eqs. (2.18), (2.25), (2.84) and (2.89).

Consider here only one variant of boundary conditions

$$\chi = \frac{\mathrm{d}^2\chi}{\mathrm{d}x^2} = \frac{\mathrm{d}^4\chi}{\mathrm{d}x^4} = 0, \tag{5.41}$$

corresponding to the simply supported edges $\alpha_1 = 0, L$. We remind that for a laminated beam represented by the ESL model, boundary conditions for the simply supported edges with and without diaphragm are identical (s. Subsect. 3.1.1).

#### 5.2.2.1 Free Vibrations

At first, we consider free vibrations ($q_l = 0$). The eigenmodes satisfying conditions (5.40) are written down

$$\chi = \chi_0 \sin\frac{\pi n x}{L}\,\mathrm{e}^{\mathrm{i}\Omega t}, \tag{5.42}$$

where $n$ is the number of semi-waves, and $\Omega$ is the *complex natural frequency*. Then $\omega = \Re\Omega$ is the natural frequency and $\alpha = \Im\Omega$ is the damping ratio.

The substitution of Eq. (5.42) in Eq. (5.39) gives the formula for the complex eigenvalues

$$\Omega = \Omega_n = \frac{1}{\sqrt{\rho_1}}\sqrt{\frac{EI\eta_3\pi^4 n^4(1+\theta K n^2)}{L^4(1+Kn^2)}}, \tag{5.43}$$

where $K = \pi^2 h^2/\beta L^2$ is the complex shear parameter. The variation of induction $B$ allows changing the complex parameters $\eta_3, \theta, K$ and ultimately the natural frequencies $\omega = \Re\Omega$ and corresponding damping ratios $\alpha = \Im\Omega > 0$. To estimated this effect, we consider the following example.

**Example 5.4.** Let $L = 0.3$ m, $b = 15$ mm and $h_1 = h_3 = 1$ mm. The face sheets are made of aluminum. The smart core is the MRE-1 (see its properties in Chapt. 2). Figure 5.12 shows the influence of the magnetic field on the lowest frequency $\omega$ ($n = 1$) for different thicknesses $h_2$ of the smart material. Figure 5.13 gives the frequencies $\omega$ at $n = 9$ versus the induction $B$ when the core thickness $h_2 = 12$ mm. It is clearly seen that the eigenfrequencies increase at the interval of varying of the induction $B$ from 0 to 210 mT, however this influence is very weak for the first modes and thin core; it becomes noticeable with growing of the smart core layer thickness $h_2$ for a large number of mode (compare Figs. 5.12 and 5.13).

Figure 5.14 shows the scaled logarithmic decrement $d_1 = 500\, D_1/\pi$, where $D_1$ is calculated by (5.7), as a function of the increasing magnetic field. For the first and ninth modes and different thicknesses of the MRE core, the best damping takes place at about 280 mT, this effect becoming stronger with growing the MRE layer. Comparing outcomes presented on Fig. 5.14 with similar results for the sandwich beam with MRF core (s. Figs. from 5.5 to 5.9), one can conclude: MR liquids display the best damping capability at the lowest frequencies, while the MRE-1 does it for modes with large number $n$ of semi-waves.

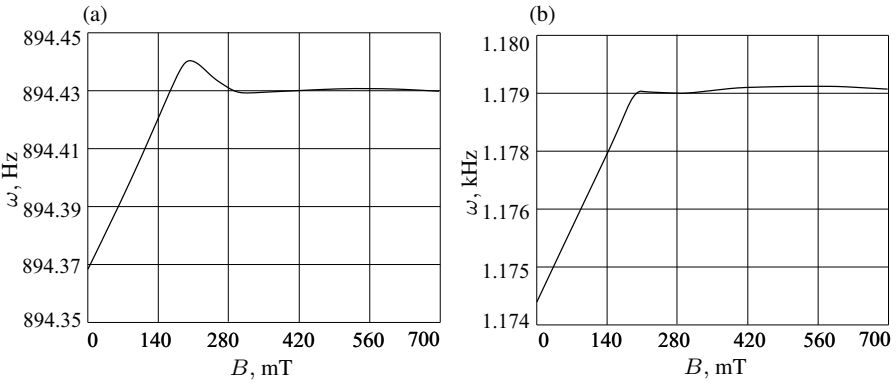


**Fig. 5.12** Natural frequency $\omega$ at $n = 1$ vs. induction $B$ for different values of thickness $h_2$. (a) $h_2 = 5$ mm; (b) $h_2 = 12$ mm.

**Fig. 5.13** Natural frequency $\omega$ at $n = 9$ vs. induction $B$ for $h_2 = 12$ mm.

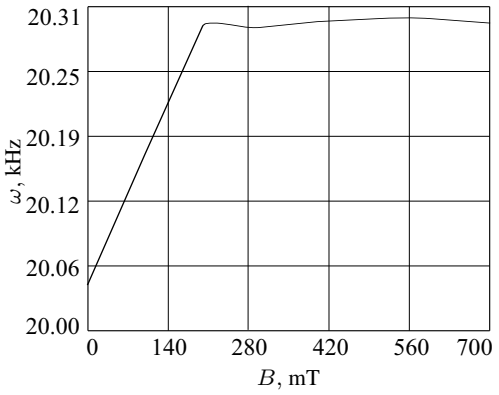


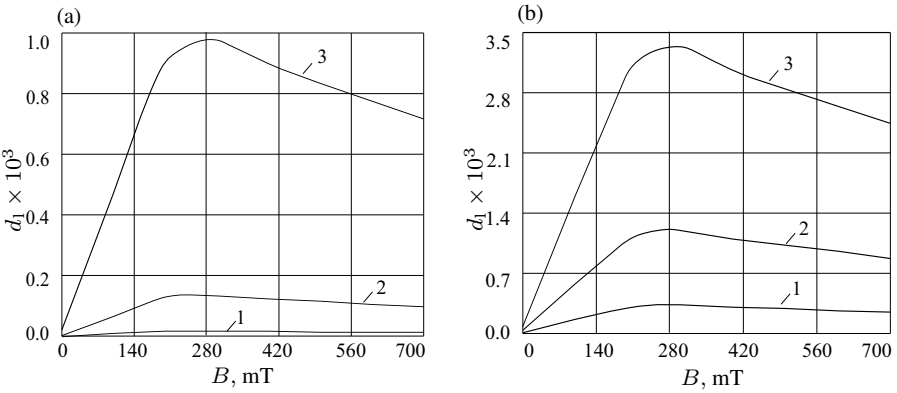


**Fig. 5.14** Scaled logarithmic decrement $d_1$ vs. induction $B$ at (a) $n = 1$ and (b) $n = 9$ for different values of thickness $h_2$: 1- $h_2 = 5$ mm; 2-$h_2 = 9$ mm; 3- $h_2 = 12$ mm.

It is of interesting to study the effect of a MRE uniformly distributed between different elastic layers on natural frequencies and decrement for multi-layered beams.

**Example 5.5.** We consider different beams of the same geometrical parameters as in Example 5.4, but consisting of three, five, seven and nine layers. The total thickness $h_{\mathrm{Al}}$ of sheets made of aluminum is equal to 2 mm, and the total thickness $h_{\mathrm{MRE}}$ of the MRE-1 laminaes is 12 mm. It is assumed that the elastic material (aluminum) and the MRE-1 are uniformly distributed between layers so that the thicknesses of laminas with odd and even numbers are as follows:

- for the sandwich ($N = 3$),

$$h_1 = h_3 = \frac{h_{\mathrm{Al}}}{2}, \quad h_2 = h_{\mathrm{MRE}};$$

- for the five-layer beam ($N = 5$),

$$h_1 = h_3 = h_5 = \frac{h_{\mathrm{Al}}}{3}, \quad h_2 = h_4 = \frac{h_{\mathrm{MRE}}}{2};$$

- for the seven-layer beam ($N = 7$),

$$h_1 = h_3 = h_5 = h_7 = \frac{h_{\mathrm{Al}}}{4}, \quad h_2 = h_4 = h_6 = \frac{h_{\mathrm{MRE}}}{3},$$

- for the nine-layer beam ($N = 9$)

$$h_1 = h_3 = h_5 = h_7 = h_9 = \frac{h_{\mathrm{Al}}}{5}, \quad h_2 = h_4 = h_6 = h_8 = \frac{h_{\mathrm{MRE}}}{4}.$$

Regardless of a number of layers, the quantity of elastic and smart viscoelastic materials is fixed. The outcomes for the sandwich beam ($N = 3$) are presented in Figs. 5.12 (b), 5.13 and 5.14.

The first and ninth frequencies and the corresponding logarithmic decrements for multi-layered beams are displayed in Figs. 5.15 and 5.16. As seen, the impact of magnetic field on eigenfrequencies and damping ratio becomes more weak with increasing number of layers. However, at the fixed induction $B$, the number of layers greatly influences on all the spectrum of natural frequencies and corresponding damping ratios. When comparing Figs. 5.12 (b) and 5.15 (a), then one concludes that increasing number of layers results in some decreasing the lowest natural frequency at all range of varying $B$. As for modes with a large number of semi-waves (for instance, compare Figs. 5.13 and 5.15 (b)), the corresponding natural frequencies unevenly increase when the beam is subjected to the partition into five, seven and more number of layers. So, for the ninth mode ($n = 9$) and $B \geq 200$ mT, the natural frequency jumps from 20.30 kHz (for the sandwich beam) up to about 63.60 kHz (for the five-ply beam) and then slightly decreases when the number of layers is increasing. The comparison of Figs. 5.14 and 5.16 shows that the increase of the number of layers leads to a dramatic decreasing of the logarithmic decrement for each mode at the fixed level of applied magnetic field, this reduction being more

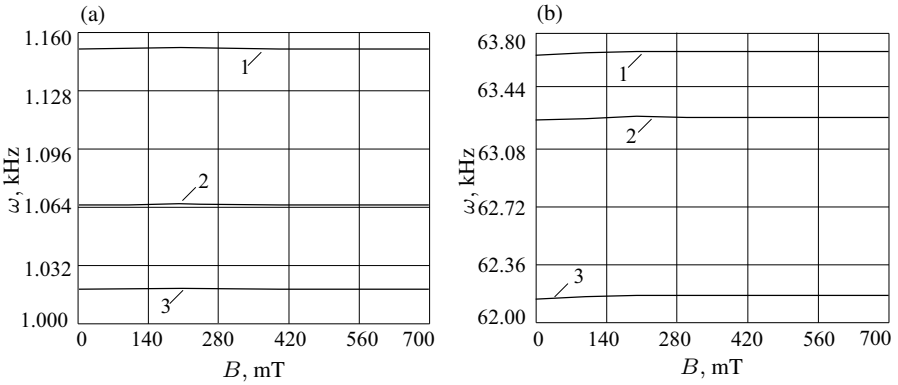


**Fig. 5.15** First (a) and ninth (b) natural frequencies $\omega$ vs. induction $B$ for different number of layers: 1 - $N = 5$; 2 - $N = 7$; 3 - $N = 9$.

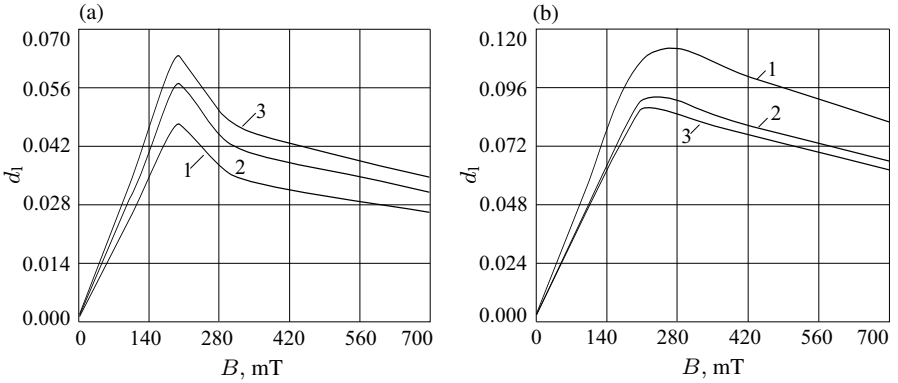


**Fig. 5.16** Scaled logarithmic decrement for the first (a) and ninth (b) modes $\omega$ vs. induction $B$ for different number of layers: 1 - $N = 5$; 2 - $N = 7$; 3 - $N = 9$.

noticeable for the highest modes. It is of interest to note the behavior of the scaled logarithmic decrement $d_1$ corresponding to the first mode versus the number of layers: under increasing $N$ from 3 to 5, the maximum value of $d_1$ (at $B = 200$ mT) drops from about 1 to 0.046, and then it grows together with the number $N$ of layers.

This example allows us to conclude: splitting the sandwich beam with the MRE core into a large number of layers under fixed quantity of elastic and viscoelastic smart materials results in the reduction of damping properties of the beam, however permits to change significantly the spectrum of natural frequencies (especially its part corresponding to highest modes) removing it to right. Obviously, this property may be used in designing smart laminated beam with adjustable elastic and damping properties.

#### 5.2.2.2 Forced Stationary Vibrations and Their Suppression

Let the beam be under the external periodic force

$$q_{\rm l} = \rho_{\rm l} F_0(x)\, {\rm e}^{{\rm i}\omega_{\rm e} t}, \tag{5.44}$$

where $\omega_{\rm e}$ is the excitation frequency. A solution of Eq. (5.39) with the boundary conditions (5.41) can be presented in the form of the series

$$\chi(x,t) = \sum_{n=1}^{\infty} \sin(\lambda_n x) q_{\rm n}(t). \tag{5.45}$$

Substituting (5.45) into Eq. (5.39), we obtain the series of equations

$$\ddot{q}_n + \Omega_n^2 q_{\rm n} = \frac{2F_n}{L(1+Kn^2)} {\rm e}^{{\rm i}\omega_{\rm e} t}, \quad n = 1, 2, \ldots, \tag{5.46}$$

where the generalized forces $F_n$ are defined by Eq. (5.11). The partial solution of (5.46) is

$$q_{\rm n}(t) = \frac{2F_n}{L(1+Kn^2)(\Omega_n^2 - \omega_{\rm e}^2)}\, {\rm e}^{{\rm i}\omega_{\rm e} t}. \tag{5.47}$$

Then the amplitude of forced stationary vibrations will be given by

$$\chi = \sum_{n=1}^{\infty} \frac{2F_n\, {\rm e}^{{\rm i}\omega_{\rm e} t}}{L(1+Kn^2)(\Omega_n^2 - \omega_{\rm e}^2)} \sin(\lambda_n x). \tag{5.48}$$

**Example 5.6.** Consider the sandwich beam with parameters specified in Example 5.5. The thickness of the MRE core is equal to $h_2 = 12$ mm. We assume the following distribution of the normal periodic force

$$F_0(x) = 4\frac{x}{L}\left(1 - \frac{x}{L}\right). \tag{5.49}$$

Figures 5.17 and 5.18 demonstrate the amplitude-frequency characteristics for the sandwich beam subjected to the periodic force (5.44) with (5.49) in the frequency interval $\omega_{\rm e}$ from 1.10 to 10.10 kHz, the dotted line showing the scaled amplitude $A_{\rm s}$ versus $\omega_{\rm e}$ if the magnetic field is absent and the solid curve corresponds to the case, when the beam is in the magnetic field of the induction $B = 200$ mT. It is clearly seen that the applied magnetic field shifts the resonance regions to right, this shifting being slight for the lowest resonance frequencies and growing together with the mode number $n$. The relative reduction of the maximum amplitude $A_{\rm s}^B / A_{\rm s}^0$, where $A_{\rm s}^B$ and $A_{\rm s}^0$ are the scaled amplitude calculated at $B = 200$ mT and $B = 0$ mT, respectively, depends also on $n$. So, it is equal to approximately 2, 16, 14 for $n = 1, 2, 3$, respectively. Thus, our conclusion made above on the basis of the modal analysis (see the previous example) is confirmed: MREs used as smart cores in sandwich beams reveal the best damping capability at the highest modes and so,

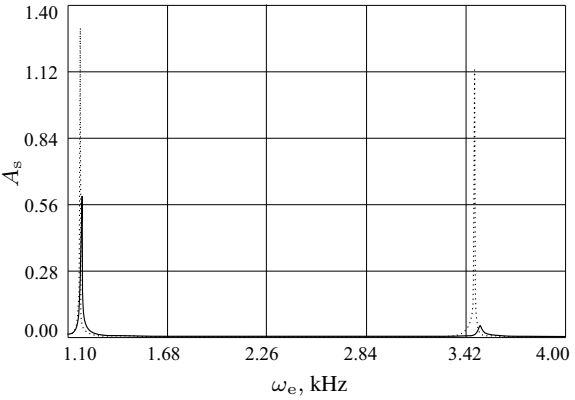


**Fig. 5.17** Amplitude-frequency characteristics for the MRE-1 sandwich beam at the interval $\omega_e$ from 1.10 to 4.00 kHz for two different cases: dotted line - magnetic field is absent, solid line - magnetic field of the induction $B = 200$ mT is applied.

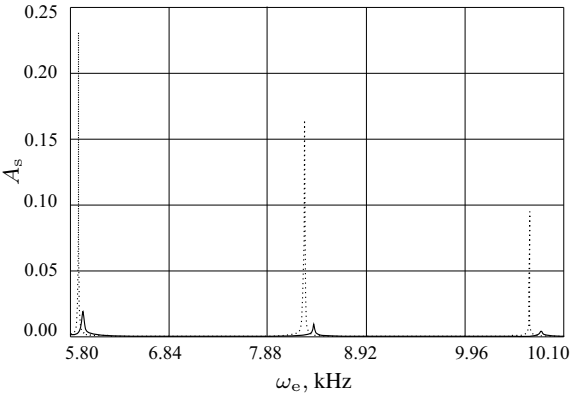


**Fig. 5.18** Amplitude-frequency characteristics for the MRE-1 sandwich beam at the interval $\omega_e$ from 5.80 to 10.10 kHz for two different cases: dotted line - magnetic field is absent, solid line - magnetic field of the induction $B = 200$ mT is applied.

their application turns out to be more effective for suppression of high-frequency vibrations.

The next example illustrates the resonance response of the beam without magnetic field and after its application.

**Example 5.7.** Let the beam considered in the previous example be subjected to the resonance periodic force (5.44) applied in the point $x = x^* = L/7$, where the excitation frequency $\omega_e = 3.46$ kHz is close to the second natural frequency of the beam. In Fig. 5.19, the scaled maximum amplitude for the so-called *equivalent beam* with external friction is plotted at $0 \le t < t_{cr}$, when the magnetic field is absent, and for $t \ge t_{cr}$ as well, where $t_{cr} = 0.2$ is the time of turning on the magnetic field of the induction $B = 300$ mT. In the initial moment the beam is motionless. Computations at $t \ge t_{cr}$ were performed by the approach applied in Example 5.2 in accordance to which the natural frequencies, damping ratio and modes were recalculated after applying the magnetic field. The high-frequency excited oscillations due to the impact action of magnetic field were disregarded. Figure 5.19 shows that the application of magnetic field *removed* the beam from the regime of resonance vibrations and resulted in about fourfold reduction of the amplitude of forced vibrations.

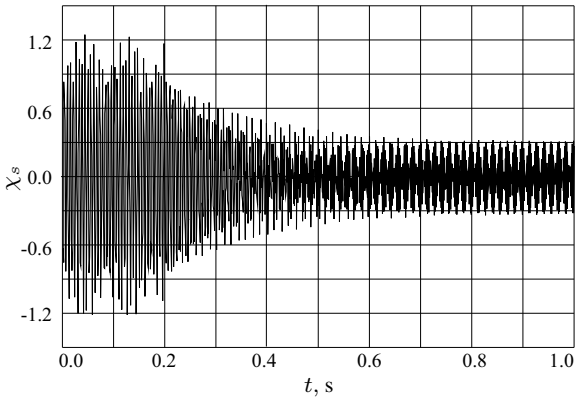


**Fig. 5.19** Response of the *equivalent MRE-1 based sandwich beam* to resonance harmonic force and the magnetic field of induction $B = 300$ mT applied at $t = t_{\rm cr} = 0.2$ s.

## 5.3 Magnetorheological Sandwich and Multi-Layered Plates

In this section, we consider laminated plates consisting of $N$ transversally isotropic laminas. The sides in the plate plane are equal to $L_1$ and $L_2$. Each layer with the number $k (k = 1, 2, \ldots, N)$ is characterized by the thickness $h_k$, Young's modulus $E_k$, shear modulus $G_k$ and Poisson's ratio $\nu_k$. If a plate is three-layered (sandwich), as shown in Fig. 5.1, then the face sheets are elastic and the core is a MRE. For multi-layered plate, elastic and smart viscoelastic laminas alternate, odd laminas being made of an elastic material, and even ones being MREs.

Assuming the ESL theory for laminated plate stated in Chapt. 2, we use here the following equations

$$\begin{aligned} &D\left(1-\frac{\theta h^2}{\beta}\triangle\right)\triangle^2\chi+\rho_0 h\frac{\partial^2 w}{\partial t^2}=q_{\rm ex},\quad w=\left(1-\frac{h^2}{\beta}\triangle\right)\chi,\\ &\frac{(1-\nu)h^2}{2\beta}\triangle\phi=\phi, \end{aligned} \tag{5.50}$$

where $\triangle$ is the Laplace operator in a Cartesian coordinate system $\alpha_1, \alpha_2$, $(0 \le \alpha_1 \le L_1,\ 0 \le \alpha_2 \le L_2)$, $w$ is the deflection of the plate, $\phi$ is the shear function, s. its introduction in Chapt. 2, Eq. (2.78), $q_{\rm ex}(\alpha_1, \alpha_2, t)$ is the normal load, $t$ is time. All other notations appearing in Eq. (5.50) are the same as in Chapt. 2. We only note that the reduced bending stiffness $D$ and the shear parameter $\beta$ depend on the intensity of the applied magnetic field.

We consider here only one variant of boundary conditions. Let all the edges be simply supported and provided by diaphragm preventing edge shear

$$\chi = \triangle\chi = \frac{\partial\phi}{\partial\alpha_k} = 0 \quad \text{at} \quad \alpha_k = 0,\ L_k; \quad k = 1, 2. \tag{5.51}$$

Then, one can set $\phi = 0$.

### 5.3.1 Free Vibrations

At first, we analyse free vibrations ($q_{\rm ex} = 0$). The solution of the boundary-value problem (5.50), (5.51) can be found as

$$\chi = \chi_0 \sin\frac{\pi n\alpha_1}{L_1} \sin\frac{\pi m\alpha_2}{L_2} \mathrm{e}^{\mathrm{i}\Omega t}, \tag{5.52}$$

where $n, m$ are numbers of semi-waves in the $\alpha_1-$ and $\alpha_2-$ directions, respectively, and $\Omega$ is the complex natural frequency.

Substituting Eq. (5.52) into Eqs. (5.50) gives a simple formula for the required complex eigenvalue

$$\Omega = \Omega_{nm} = \sqrt{\frac{\pi^2 D}{\rho_0 h L_1^4}}\, \Lambda^{1/2}, \tag{5.53}$$

where

$$\Lambda = \Lambda_{nm} = \frac{\delta_{nm}^2(1+\theta K\delta_{nm})}{1+K\delta_{nm}}, \quad K = \frac{\pi^2 h^2}{\beta L_2^2}, \quad \delta_{nm} = n^2 + e^2 m^2, \quad e = \frac{L_1}{L_2}. \tag{5.54}$$

Equation (5.53) gives two complex eigenvalues. We need to chose only one value with the positive imaginary part.

If some of the edges is free of a diaphragm, then a solution of Eqs. (5.50) with corresponding boundary conditions (4.38) may be constructed by the asymptotic approach developed in Subsect. 4.2.2 for an elastic laminated plate. According to this approach, the solution is constructed in the form of superposition of functions corresponding to the main stress-strain state and edge effect integrals in the neighborhood of an edge which is free of diaphragm.

In Eqs. (5.53), (5.54), parameters $D, K$ depend on the induction $B$, the shear parameter $K$ being the principal one. Just as for a layered beam, a magnetic field and, as consequence, a parameter $K$ have a weak effect on the lowest frequencies and the corresponding decrements. The effect of magnetic field and shears manifests itself on modes for which the number of waves is large in at least one direction. This conclusion is clearly confirmed by the following example.

**Example 5.8.** Let us consider a square sandwich plate with $L_1 = L_2 = 1$ m. The outer layers (thicknesses $h_1 = h_3 = 0.5$ mm) are made of ABS-plastic SD-0170 with parameters $E_1 = E_3 = 1.5 \cdot 10^3$ MPa, $\nu_1 = \nu_3 = 0.4$, $\rho_1 = \rho_3 = 1.4 \cdot 10^3$ kg/m$^3$. The core of thickness $h_2 = 10$ mm is MRE-1 with properties given in Chapt. 2 (s. Fig. 2.9). Figures 5.20 and 5.21 show the influence of the magnetic field induction on the natural frequencies $\omega = \Re\Omega$ and decrements $\alpha = \Im\Omega$ for modes with $n = 10$ waves in the $\alpha_1$-direction and different number of waves in the other direction. It is seen, the larger the wave numbers $m$ and/or $n$, the stronger the effect of the magnetic field on the characteristics of eigenmodes for the sandwich plate.

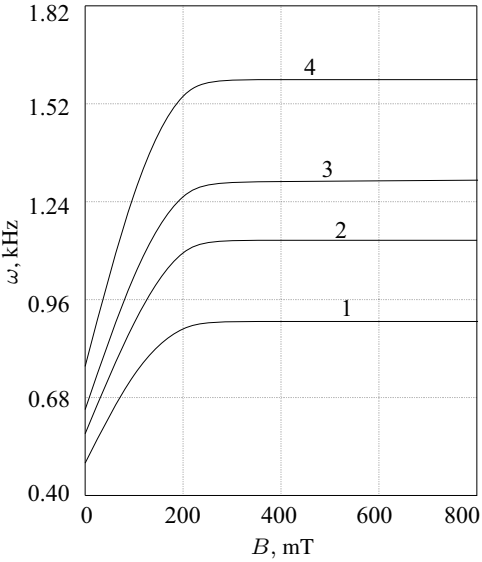


**Fig. 5.20** Natural frequency $\omega$ vs. induction $B$ for modes with $n = 10$ and different values of $m$: 1 - $m = 1$, 2 - $m = 5$, 3 - $m = 7$, 4 - $m = 10$.

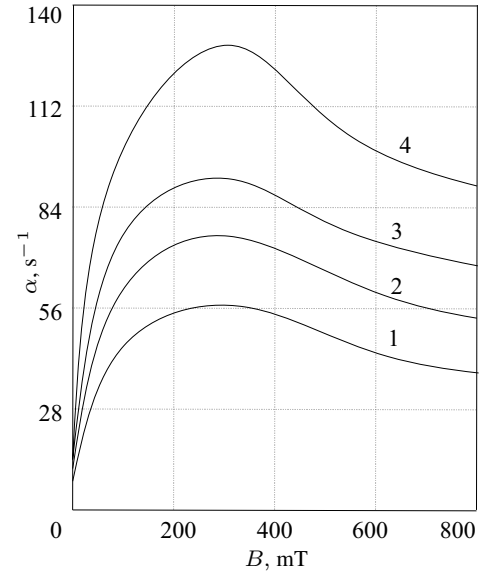


**Fig. 5.21** Decrement $\alpha$ vs. induction $B$ for modes with $n = 10$ and different values of $m$: 1 - $m = 1$, 2 - $m = 5$, 3 - $m = 7$, 4 - $m = 10$.

## *5.3.2 Forced Stationary Vibrations*

Let the plate be under action of the periodic normal force

$$q_{\rm ex}(\alpha_1, \alpha_2, t) = F_0(\alpha_1, \alpha_2)\mathrm{e}^{\mathrm{i}\omega_{\rm e} t} \tag{5.55}$$

with the frequency $\omega_{\rm e}$. Here, a solution of Eq. (5.50) with boundary conditions (5.51) is found in the form of the double series

$$\chi(\alpha_1,\alpha_2,t)=\sum_{n=1}^{\infty}\sum_{m=1}^{\infty}\sin\frac{\pi n\alpha_1}{L_1}\sin\frac{\pi mn\alpha_1}{L_2}q_{nm}(t), \tag{5.56}$$

where $q_{nm}(t)$ is generalized coordinates of the system. We substitute (5.56) into Eq. (5.50) and expand function (5.56) into Fourier series. Then, we arrive at the series of differential equations

$$\ddot{q}_{nm}+\Omega_{nm}^2\,q_{nm}=\frac{F_{nm}}{\rho h(1+K\delta_{nm})},\quad n,m=1,2,\ldots, \tag{5.57}$$

where

$$F_{nm}=\frac{4}{L_1L_2}\int_0^{L_1}\int_0^{L_2}F_0(\alpha_1,\alpha_2)\sin\frac{\pi n\alpha_1}{L_1}\sin\frac{\pi n\alpha_2}{L_2} \tag{5.58}$$

are the generalized forces corresponding to the generalized coordinates $q_{nm}(t)$ and the $\Omega_{nm}$ are the complex eigenfrequencies defined by (5.54).

The partial solutions of Eqs. (5.58) are the functions

$$q_{nm}(t)=\frac{F_{nm}\mathrm{e}^{\mathrm{i}\omega_e t}}{\rho h(1+K\delta_{nm})(\Omega_{nm}^2-\omega_{\mathrm{e}}^2)},\quad n,m=1,2,\ldots \tag{5.59}$$

Then, the amplitude of forced steady-state vibrations will be as follows

$$\chi(\alpha_1,\alpha_2,t)=\sum_{n=1}^{\infty}\sum_{m=1}^{\infty}\frac{F_{nm}\mathrm{e}^{\mathrm{i}\omega_e t}}{\rho h(1+K\delta_{nm})(\Omega_{nm}^2-\omega_e^2)}\sin\frac{\pi n\alpha_1}{L_1}\sin\frac{\pi n\alpha_2}{L_2}. \tag{5.60}$$

Equation (5.60) serves to predict the dynamic stationary response of the plate to the periodic force (5.55) arbitrary distributed along the surface. We note that $D, K, \theta, \Omega_{nm}$ are complex magnitudes depending on the magnetic field induction. Thus, applying a magnetic field one can affect the modes and the damping capability of a MRE embedded in the plate and reduce the response of the plate to external forces. We do not give here any examples because the mechanism of suppression of forced vibrations in MRE-based laminated plates is the same as for smart beams considered above.

## 5.4 Shells with Magneto- and Electrorhelogical Layers Affected by Magnetic/Electric Fields

In this section, we study free and steady-state forced vibrations of laminated MRE- and ERC-based cylindrical panels and shells affected by a constant magnetic or electric field. The main attention will be paid to sandwich panels with a core made of different smart materials whose elastic and rheological properties were given in Chapt. 2.

Let us consider a laminated cylindrical panel (cylinder not closed in the circumferential direction) of the radius $R$. The length of the straight side is equal to $L_1$ and the panel width is $L_2 = R\varphi_2$, where $[0, 2\pi) \ni \varphi_2$ is the apex angle of the panel. If $\varphi_2 = 2\pi$, one has a shell closed in the circumferential direction. The choice of the governing equations depends on the geometric dimensions of the panel as well as the expected vibration shape. So, to predict vibrations with formation of very long waves, one has to use the full system of differential equations (2.61)-(2.63) written in terms of displacements $\hat{u}_i, \psi_i, w$, while for studying vibrations accompanied by formation of a large number of short waves, equations of the technical shell theory (2.85) and (2.90) can be used.

### *5.4.1 Governing Equations and Boundary Conditions*

At first, we apply to the full system of differential equations (2.61)-(2.63) which are universal and may be used to examine any type of vibrations for any geometrical dimensions. Omitting non-linear terms, one obtains the system of linear differential equations governing small vibrations of a laminated cylindrical shell

$$
\begin{aligned}
\frac{\partial^2 \hat{u}_1}{\partial \alpha_1^2} + \frac{1-\nu}{2}\frac{\partial^2 \hat{u}_1}{\partial \alpha_2^2} + \frac{1+\nu}{2}\frac{\partial^2 \hat{u}_2}{\partial \alpha_1 \partial \alpha_2} + \frac{\nu}{R}\frac{\partial w}{\partial \alpha_1} + \frac{1-\nu^2}{Eh}\left(q_1 - \rho_0 \frac{\partial^2 \hat{u}_1}{\partial t^2}\right) &= 0,\\
\frac{1+\nu}{2}\frac{\partial^2 \hat{u}_1}{\partial \alpha_1 \partial \alpha_2} + \frac{1-\nu}{2}\frac{\partial^2 \hat{u}_2}{\partial \alpha_1^2} + \frac{\partial^2 \hat{u}_2}{\partial \alpha_2^2} + \frac{\partial}{\alpha_2}\left(\frac{w}{R}\right) + \frac{1-\nu^2}{Eh}\left(q_2 - \rho_0 \frac{\partial^2 \hat{u}_2}{\partial t^2}\right) &= 0,\\
\eta_2 \frac{\partial \triangle w}{\partial \alpha_1} - \eta_1 \left(\frac{\partial^2 \psi_1}{\partial \alpha_1^2} + \frac{1+\nu}{2}\frac{\partial^2 \psi_2}{\partial \alpha_1 \partial \alpha_2} + \frac{1-\nu}{2}\frac{\partial^2 \psi_1}{\partial \alpha_2^2}\right)&\\
+ \frac{12(1-\nu^2)}{Eh^3}\left(q_{44}\psi_1 + \frac{1}{2}hc_{12}q_1\right) &= 0,\\
\eta_2 \frac{\partial \triangle w}{\partial \alpha_2} - \eta_1 \left(\frac{\partial^2 \psi_2}{\partial \alpha_2^2} + \frac{1+\nu}{2}\frac{\partial^2 \psi_1}{\partial \alpha_1 \partial \alpha_2} + \frac{1-\nu}{2}\frac{\partial^2 \psi_2}{\partial \alpha_1^2}\right)&\\
+ \frac{12(1-\nu^2)}{Eh^3}\left(q_{44}\psi_2 + \frac{1}{2}hc_{12}q_2\right) &= 0,\\
\frac{h^2}{12(1-\nu^2)}\triangle\left[\eta_3 \triangle w - \eta_2\left(\frac{\partial \psi_1}{\partial \alpha_1} + \frac{\partial \psi_2}{\partial \alpha_2}\right)\right] + \frac{1}{R(1-\nu^2)}\left(\nu\frac{\partial \hat{u}_1}{\partial \alpha_1} + \frac{w}{R}\right)&\\
= \frac{1}{Eh}\left(q_{\rm n} - \frac{1}{2}hc_{13}\sum_{i=1}^{2}\frac{\partial q_i}{\partial \alpha_i} - \rho_0\frac{\partial^2 w}{\partial t^2}\right),&
\end{aligned}
\tag{5.61}
$$

where $\hat{u}_i$ are the generalized tangential displacements coupled with the corresponding tangential displacements $u_i$, deflection $w$ and shear displacements $\psi_i$ by Eq. (2.26), $q_i, q_{\rm n} (i = 1, 2)$ are components of the surface load, and parameters $c_{12}, c_{13}$, $q_{44}$ and $\rho_0$ are calculated by Eqs. (2.25), (2.59) and (2.68), respectively.

Let the straight and curvilinear edges $\alpha_1 = 0, L_1$ and $\alpha_2 = 0, L_2$ be simply supported and provided by diaphragm. The appropriate boundary conditions are written as

$$w = \hat{u}_j = \psi_j = 0, \tag{5.62}$$

$$\hat{M}_{ii} = T_{ii} = \hat{L}_{ii} = 0 \tag{5.63}$$

for $\alpha_i = 0, L_i$, where $i, j = 1, 2$ and $i \neq j$. Taking into account Eqs. (2.60), the second set of boundary conditions (5.63) may be rewritten in terms of displacements

$$\begin{gathered} \eta_3 \left( \frac{\partial^2 w}{\partial \alpha_i^2} + \nu \frac{\partial^2 w}{\partial \alpha_j^2} \right) - \eta_2 \left( \frac{\partial \psi_i}{\partial \alpha_i} + \nu \frac{\partial \psi_j}{\partial \alpha_j} \right) = 0, \\ \frac{\partial \hat{u}_i}{\partial \alpha_i} + \nu \frac{\partial \hat{u}_j}{\partial \alpha_j} + \frac{\nu w}{R} = 0, \\ \eta_2 \left( \frac{\partial^2 w}{\partial \alpha_i^2} + \nu \frac{\partial^2 w}{\partial \alpha_j^2} \right) - \eta_1 \left( \frac{\partial \psi_i}{\partial \alpha_i} + \nu \frac{\partial \psi_j}{\partial \alpha_j} \right) = 0. \end{gathered} \tag{5.64}$$

The linearized dynamic equations (2.85) and (2.90) of the technical shell theory are written as follows

$$\begin{gathered} D \left( 1 - \frac{\theta h^2}{\beta} \triangle \right) \triangle^2 \chi + \frac{1}{R} \frac{\partial^2 F}{\partial \alpha_1^2} + \rho_0 h \frac{\partial^2 w}{\partial t^2} = q_{\mathrm{n}}, \\ w = \left( 1 - \frac{h^2}{\beta} \triangle \right) \chi, \qquad \triangle^2 F - \frac{Eh}{R} \frac{\partial^2 w}{\partial \alpha_1^2} = 0, \\ \frac{1 - \nu}{2} \frac{h^2}{\beta} \triangle \phi = \phi. \end{gathered} \tag{5.65}$$

where $\chi, F$ are the displacement and the force functions, respectively, $\phi$ is the additional shear functions, s. Eqs. (2.78) and (2.83), $\beta$ and $D$ are the shear parameter and the reduced bending stiffness, respectively, introduced by Eqs. (2.84) and (2.88), respectively. The appropriate boundary conditions in terms of displacement, stress and shear functions for the straight and curvilinear edges are the following

$$\chi = \Delta\chi = \Delta^2 \chi = \frac{\partial \phi}{\partial \alpha_i} = 0, \quad \frac{\partial^2 F}{\partial \alpha_2^2} = 0, \quad \frac{\partial^2 F}{\partial \alpha_1^2} = 0 \quad \text{at} \quad \alpha_i = 0, L_i, \tag{5.66}$$

where $i = 1, 2$. We note that all coefficients $D, E, \nu, \beta, \eta_k, c_{12}, c_{13}, q_{44}$, appearing in the above equations and boundary conditions, are complex quantities depending on the magnitude of the magnetic or electric field depending on whether the shell contains MRE or ERE layers.

### 5.4.2 Free Vibrations

Let $q_i = q_{\rm n} = 0$. Then the natural modes for a shell governed by Eqs. (5.61) with the boundary conditions (5.66) can be represented by the following functions

$$\begin{aligned}
\hat{u}_1 &= u_1^\circ \cos\frac{\pi n\alpha_1}{L_1}\sin\frac{\pi m\alpha_2}{L_2}\exp(\mathrm{i}\Omega t),\\
\hat{u}_2 &= u_2^\circ \sin\frac{\pi n\alpha_1}{L_1}\cos\frac{\pi m\alpha_2}{L_2}\exp(\mathrm{i}\Omega t),\\
w &= w^\circ \sin\frac{\pi n\alpha_1}{L_1}\sin\frac{\pi m\alpha_2}{L_2}\exp(\mathrm{i}\Omega t),\\
\psi_1 &= \psi_1^\circ \cos\frac{\pi n\alpha_1}{L_1}\sin\frac{\pi m\alpha_2}{L_2}\exp(\mathrm{i}\Omega t),\\
\psi_2 &= \psi_2^\circ \sin\frac{\pi n\alpha_1}{L_1}\cos\frac{\pi m\alpha_2}{L_2}\exp(\mathrm{i}\Omega t),
\end{aligned} \tag{5.67}$$

where $\Omega = \omega + \mathrm{i}\alpha$, $\omega = \Re\Omega$ is the required natural frequency, $\alpha = \Im\Omega > 0$ is the associated damping ratio, $n, m$ are numbers of semi-waves in the axial and circumferential directions, respectively, and $u_i^\circ, w^\circ, \psi_i^\circ$ are constants. If the shell is closed in the circumferential direction, then $m$ is an even number.

Substituting (5.67) into Eqs. (5.61), we arrive at the linear system of five algebraic equations

$$\mathbf{A}\mathbf{X}^{\rm T} = 0, \tag{5.68}$$

where $\mathbf{X} = (u_1^\circ, u_2^\circ, w^\circ, \psi_1^\circ, \psi_2^\circ)$ is the amplitude vector and $\mathbf{A}$ is the matrix with complex elements

$$\begin{aligned}
&a_{11} = -\delta_n^2 - \frac{1-\nu}{2}\delta_m^2 + \frac{\rho_0 R^2(1-\nu^2)}{E}\Omega^2, \quad a_{12} = \frac{1+\nu}{2}\delta_n\delta_m,\\
&a_{13} = \nu\delta_n, \quad a_{14} = a_{15} = 0, \quad a_{21} = \frac{1+\nu}{2}\delta_n\delta_m,\\
&a_{22} = -\frac{1-\nu}{2}\delta_n^2 - \delta_m^2 + \frac{\rho_0 R^2(1-\nu^2)}{E}\Omega^2, \quad a_{23} = -\delta_m, \quad a_{24} = a_{25} = 0,\\
&a_{31} = a_{32} = 0,\ a_{33} = -\eta_2\delta_n(\delta_n^2+\delta_m^2),\ a_{34} = \eta_1\left(\delta_n^2 + \frac{1-\nu}{2}\delta_m^2\right) + \frac{q_{44}R^2\eta_3}{D},\\
&a_{35} = -\frac{\eta_1(1+\nu)}{2}\delta_n\delta_m, \quad a_{41} = a_{42} = 0, \quad a_{43} = -\eta_2\delta_m(\delta_n^2+\delta_m^2),\\
&a_{44} = -\frac{\eta_1(1+\nu)}{2}\delta_n\delta_m, \quad a_{45} = \eta_1\left(\delta_m^2 + \frac{1-\nu}{2}\delta_n^2\right) + \frac{q_{44}R^2\eta_3}{D},\\
&a_{51} = -\frac{\nu}{1-\nu^2}\delta_n, \quad a_{52} = \frac{1}{1-\nu^2}\delta_m,\\
&a_{53} = \frac{h^2\eta_3}{12(1-\nu^2)R^2}(\delta_n^2+\delta_m^2)^2 + \frac{1}{1-\nu^2} - \frac{\rho_0 R^2}{E}\Omega^2,\\
&a_{54} = -\frac{h^2\eta_2}{12(1-\nu^2)R^2}\delta_n(\delta_n^2+\delta_m^2), \quad a_{55} = \frac{h^2\eta_2}{12(1-\nu^2)R^2}\delta_m(\delta_n^2+\delta_m^2),
\end{aligned} \tag{5.69}$$

where

$$\delta_n = \frac{\pi n R}{L_1}, \quad \delta_m = \frac{\pi m R}{L_2} = \frac{\pi m}{\varphi_2}. \tag{5.70}$$

Although, the structure of the matrix $\mathbf{A}$ with elements (4.81) and (5.71) is the same, but there are differences: all elements (4.81) are real, while the quantities $\eta_k, \nu, E, D$ in (5.71) are complex magnitudes; in (4.81), $m$ is the number of waves in the circumferential direction for a cylinder closed in the circumferential direction and $m$ appearing in Eqs. (5.71) denotes the number of semi-waves in this direction for a panel.

The condition for the existence of a nontrivial solution of Eqs. (5.70) leads to the equation

$$\det \mathbf{A} = 0 \tag{5.71}$$

which serves to find the complex eigenvalue $\Omega$. For any fixed numbers $n, m$, this equation gives six complex roots

$$\begin{aligned} \Omega_{nm}^{(j)} &= \omega_{nm}^{(j)} + \mathrm{i}\alpha_{nm}^{(j)}, \quad \alpha_{nm}^{(j)} > 0, \\ \Omega_{nm}^{(j+3)} &= -(\omega_{nm}^{(j)} + \mathrm{i}\alpha_{nm}^{(j)}), \quad j = 1, 2, 3. \end{aligned} \tag{5.72}$$

It is obvious that the eigenvalues $\Omega_{nm}^{(4)}, \Omega_{nm}^{(5)}, \Omega_{nm}^{(6)}$ do not satisfy to the damping conditions and are not taken into consideration in what follows.

In the general case, the first three roots in (5.72) correspond to the coupled bending (out-of-plane) and tangential (in-plane) vibrations accounting for shears (we note that the inertia of shear deformations is here not taking into account). To study predominately bending vibrations, the terms containing $\Omega$ in the elements $a_{11}, a_{22}$ of the matrix $\mathbf{A}$ might be omitted. Then Eq. (5.71) will give only the one root $\Omega_{nm}^{(1)}$ with the positive imaginary part $\alpha_{nm}^{(1)} > 0$.

Regardless of the mode type, the amplitudes of tangential and shear displacements are coupled with the normal displacement as follows

$$\begin{aligned} u_1^\circ &= b_1(n,m)w^\circ, \quad u_2^\circ = b_2(n,m)w^\circ, \\ \psi_1^\circ &= d_1(n,m)w^\circ, \quad \psi_2^\circ = d_2(n,m)w^\circ, \\ b_1(n,m) &= \frac{a_{13}a_{22} - a_{12}a_{23}}{a_{12}a_{21} - a_{22}a_{11}}, \quad b_2(n,m) = \frac{a_{23}a_{11} - a_{13}a_{21}}{a_{12}a_{21} - a_{22}a_{11}}, \\ d_1(n,m) &= \frac{a_{33}a_{45} - a_{35}a_{43}}{a_{44}a_{35} - a_{34}a_{45}}, \quad d_2(n,m) = \frac{a_{43}a_{34} - a_{44}a_{33}}{a_{44}a_{35} - a_{34}a_{45}}, \end{aligned} \tag{5.73}$$

where $b_j, d_j$ are the functions of the number of semi-waves $n$ and $m$ in the axial and circumferential directions.

Consider a cylindrical shell closed in the circumferential direction. For axisymmetric modes ($m = 0$), Eq. (5.71) results in four complex roots calculated by the formula

$$\Omega = \Omega_{n0} = \pm\sqrt{\frac{E\Lambda_{n0}^{(j)}}{\rho_0 R^2(1-\nu^2)}}, \quad j = 1, 2, \tag{5.74}$$

where the complex $\Lambda_{n0}^{(j)}$ are found by (4.86)

$$\Lambda_{n0}^{(j)} = \frac{1}{2}\left[1 + \delta_n^2 + \mu_1\delta_n^4 r_n - (-1)^j\sqrt{(1-\delta_n^2+\mu_1\delta_n^4 r_n)^2 + 4\nu^2\delta_n^2}\right]. \tag{5.75}$$

Here,

$$\mu_1 = (1-\nu^2)\varepsilon^8, \quad r_n = \frac{\pi^2 + \theta K\delta_n^2}{\pi^2 + K\delta_n^2}, \quad K = \frac{\pi^2 h^2}{\beta R^2}, \quad \theta = 1 - \frac{\eta_2^2}{\eta_1\eta_3}. \tag{5.76}$$

Obviously, from four complex eigenmodes (5.74), one needs to choose only two ones, $\Omega_{n0}^{(j)} = \omega_{n0}^{(j)} + \mathrm{i}\alpha_{n0}^{(j)}$, with $\alpha_{n0}^{(j)} > 0$ for $j = 1, 2$.

Now we consider Eqs. (5.65) corresponding to the technical shell theory. Their solution satisfying to the boundary conditions (5.68) at all edges is readily written down:

$$\begin{aligned} \chi &= \chi^\circ \sin\frac{\pi n\alpha_1}{L_1}\sin\frac{\pi m\alpha_2}{L_2}\exp(\mathrm{i}\Omega t) \\ F &= F^\circ \sin\frac{\pi n\alpha_1}{L_1}\sin\frac{\pi m\alpha_2}{L_2}\exp(\mathrm{i}\Omega t), \end{aligned} \tag{5.77}$$

where $\chi^\circ, F^\circ$ are constant amplitudes of flexural vibrations. The substitution of (5.77) into Eqs. (5.67) results in the required complex eigenfrequency

$$\Omega = \Omega_{nm} = \sqrt{\frac{E}{\rho_0 R^2}}\left[\frac{\eta h^2}{12R^2}\frac{\delta_{nm}^2(1+\theta K\delta_{nm})}{1+K\delta_{nm}} + \frac{n^4}{l_1^4\delta_{nm}^2}\right]^{1/2}, \tag{5.78}$$

where

$$\eta = \frac{\pi^4\eta_3}{1-\nu^2}, \quad \delta_{nm} = \frac{1}{\pi^2}(\delta_n^2 + \delta_m^2) = \frac{n^2}{l_1^2} + \frac{m^2}{\varphi_2^2}, \quad l_1 = \frac{L_1}{R},$$

and the magnitudes $\beta, \theta$ are calculated by Eqs. (2.84) and (2.89), respectively.

The frequency equation (5.71) with (5.69) may be used to predict the frequency and damping response of the smart viscoelastic laminated panel of arbitrary length $L_1$ and apex angle $\varphi_2$. If $L_2 \sim R$ and the angle $\varphi_2$ is large (close to $2\pi$), then to predict low-frequency vibrations with a large number of semi-waves in the circumferential direction, one can apply to more simple formula (5.78).

#### 5.4.2.1 Main Tunable Complex Parameters[1]

Coefficients of Eq. (5.71) depend on the following six complex parameters

[1] This subsection is written in cooperation with S.S. Maevskaya (Vitebsk State University, Belarus, Vitebsk, e-mail: svetlanamaevskaya@ya.ru).

$$\eta_1,\ \eta_2,\ \eta_3,\ E,\ q_{44}\,(\text{or } K),\ \nu, \tag{5.79}$$

which are functions of the magnitude of the applied magnetic/electric field. In the framework of the ESL theory, they can be considered as independent integral characteristics of variable viscoelastic properties regardless of the number of layers. It is of interest to note that their number is equal to the number of independent physical characteristics of the three-layer shell (sandwich) in the case when each layer is isotropic. As can be seen from Eqs. (5.74) for the axially symmetric modes, the quantity of these parameters may be reduced to five

$$\eta_3,\ \theta,\ E,\ K,\ \nu. \tag{5.80}$$

When assuming Eqs. (5.65) of the technical shell theory, the number of independent variable parameters is reduced to four, s. Eqs. (5.78),

$$\eta,\ \theta,\ E,\ K, \tag{5.81}$$

where $\eta$ is expressed in terms of $\eta_3$ and $\nu$.

Applying a magnetic or electric field (depending on whether a shell assembled form MR or ER smart material), one can vary the parameters (5.80) or (5.81) and, in such a way, to change the frequency characteristics and damping properties of a smart structure. It is obvious that the influence of the magnetic/electric field on the above tunable parameters is different. This effect depends on the correlation between layer thicknesses and their viscoelastic properties. To analyse this effect in detail, we consider several cylindrical sandwiches of the same radius $R = 0.5$ m with the face sheets of the thickness $h_1 = h_2 = 0.5$ mm made of ABS-plastic SD-0170 (see properties in Example 5.8). Other dimensions of the sandwiches are not specified here. The viscoelastic cores of these sandwiches are made of different smart materials (MRE-1, MRE-2, MRE-3, MRE-4, MRE-5, ERC) listed with their properties in Chapt. 2. The core thickness is also varied. Figures 5.22-5.25 show the behavior of the real and imaginary parts of parameters (5.81) versus the magnetic field induction $B$ for different thicknesses $h_2$ of the viscoelastic smart core made of the MRE-1. Here $\eta_{\rm r} = \Re\eta, \eta_{\rm i} = \Im\eta$, $\theta_{\rm r} = \Re\theta, \theta_{\rm i} = \Im\theta$, $E_{\rm r} = \Re E, E_{\rm i} = \Im E$, $K_{\rm r} = \Re K$ and $K_{\rm i} = \Im K$.

As follows from equations given in Chapt. 2, parameters $\eta, \theta, E$ are expressed in terms of Young's moduli of all layers and independent of the shear moduli $G_k$, while the reduced shear parameter $K$ is a function of $G_k$. However, if a smart viscoelastic material is treated as an isotropic one, then $\eta, \theta, E$ should be considered as functions of the variable shear modulus $G_2$ for the smart core. We remind that MRE-1 was assumed as the isotropic material (s. Chapt. 2). Therefore, $\eta_{\rm r}$, $\eta_{\rm i}$, $\theta_{\rm r}, \theta_{\rm i}$, $E_{\rm r}$ and $E_{\rm i}$ reveal some dependence on the magnetic field induction $B$, these dependencies being linear. It is seen from Fig. 5.23 that parameters $\theta_{\rm r}$ and $\theta_{\rm i}$ are very small and cannot be taken into account when calculating the eigenfrequencies. The real part of the reduced Young's modulus, $E_{\rm r}$ may be considered as a constant magnitude for the fixed value of $h_2$, while $E_{\rm i}$ is a monotonically increasing function of $B$. The shear parameters $K_{\rm r}$ and $K_{\rm i}$ are the main adaptive parameters affected by

the applied magnetic field. Figure 5.25 demonstrates the nonlinear behavior of the principal dissipative parameter $K_{\rm i}$ when the magnetic field induction is varying, this nonlinearity is becoming more noticeable when increasing the thickness $h_2$ in comparison with the total thickness $h$. At a fixed value of $h_2$, the function $|K_{\rm i}(B)|$ has a maximum which increases together with $h_2$ but it is reached at more low level of the magnetic field.

The outcomes of calculations of parameters (5.81) for sandwich structures with a core made of other VSMs (MRE-3, MRE-4, MRE-5 and ERC) treated as isotropic materials are presented in Figs. 5.26-5.41. Their analysis allows concluding that the qualitative behavior of all tunable parameters versus the magnetic field induction (for the MRE-3, MRE-4 and MRE-5 based cores) or the electric field strength (for the ERC based core) is the same as for the MRE-1 based sandwich: the influence of the magnetic or electric field on $\eta_{\rm r}$, $\eta_{\rm i}$, $\theta_{\rm r}$, $\theta_{\rm i}$, $E_{\rm r}$ and $E_{\rm i}$ turns out to be minor or very small, while the shear parameters $K_{\rm r}$ and $K_{\rm i}$ reveal the nonlinear behavior and strong dependence on the intensity of applied magnetic or electric field.

Let us compare parameters (5.78) calculated for sandwiches containing isotropic smart cores with similar parameters for the MRE-2 based sandwich. MRE-2 is a

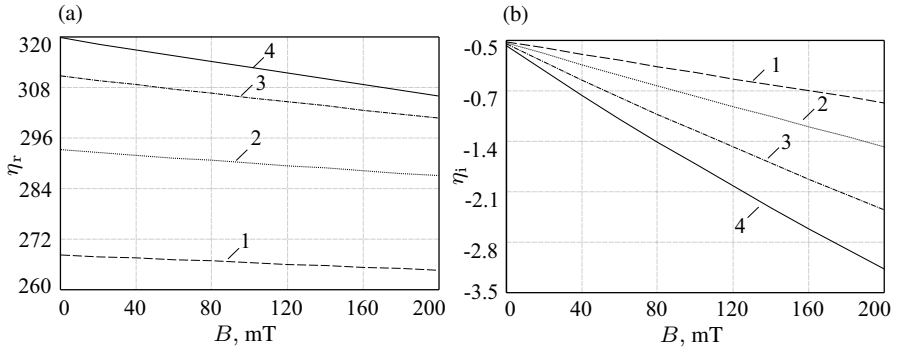


**Fig. 5.22** Parameters $\eta_{\rm r}$ (a) and $\eta_{\rm i}$ (b) for sandwich with MRE-1 core vs. induction $B$ at different values of thickness $h_2$: 1 - $h_2 = 3$ mm, 2 - $h_2 = 5$ mm, 3 - $h_2 = 8$ mm, 5 - $h_2 = 11$ mm.

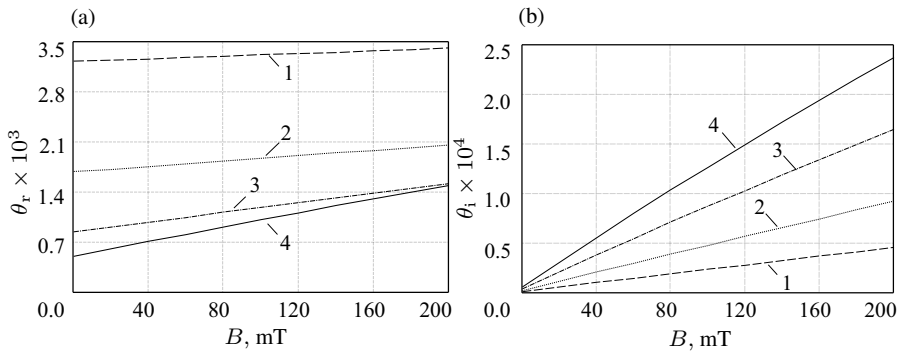


**Fig. 5.23** Parameters $\theta_{\rm r}$ (a) and $\theta_{\rm i}$ (b) for sandwich with MRE-1 core vs. induction $B$ at different values of thickness $h_2$: 1 - $h_2 = 3$ mm, 2 - $h_2 = 5$ mm, 3 - $h_2 = 8$ mm, 5 - $h_2 = 11$ mm.

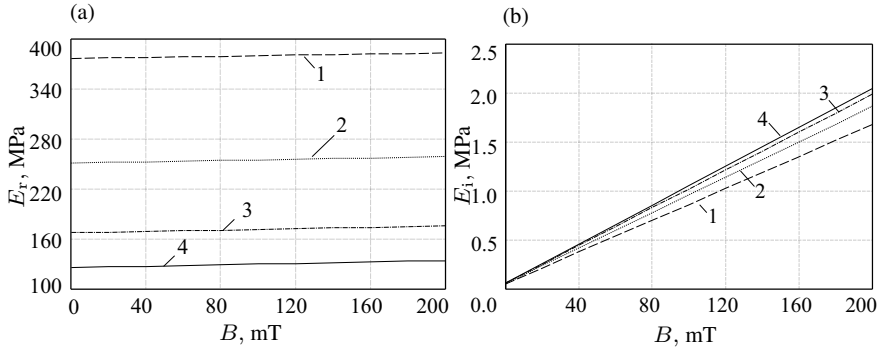


**Fig. 5.24** Parameters $E_{\rm r}$ (a) and $E_i$ (b) for sandwich with MRE-1 core vs. induction $B$ at different values of thickness $h_2$: 1 - $h_2 = 3$ mm, 2 - $h_2 = 5$ mm, 3 - $h_2 = 8$ mm, 5 - $h_2 = 11$ mm.

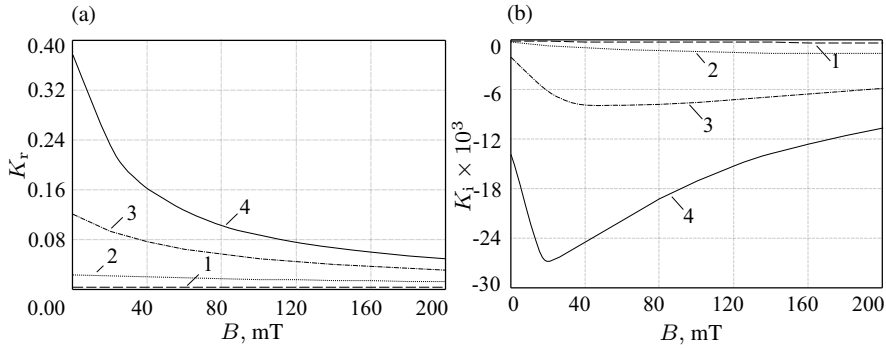


**Fig. 5.25** Parameters $K_{\rm r}$ (a) and $K_{\rm i}$ (b) for sandwich with MRE-1 core vs. induction $B$ at different values of thickness $h_2$: 1 - $h_2 = 3$ mm, 2 - $h_2 = 5$ mm, 3 - $h_2 = 8$ mm, 5 - $h_2 = 11$ mm.

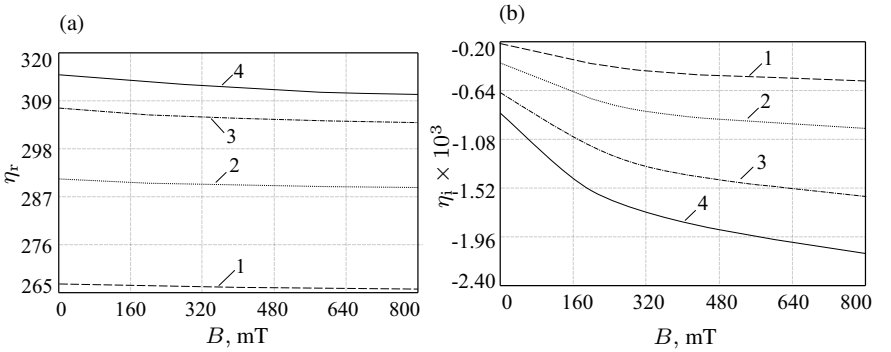


**Fig. 5.26** Parameters $\eta_{\rm r}$ (a) and $\eta_{\rm i}$ (b) for sandwich with MRE-3 core vs. induction $B$ at different values of thickness $h_2$: 1 - $h_2 = 3$ mm, 2 - $h_2 = 5$ mm, 3 - $h_2 = 8$ mm, 4 - $h_2 = 11$ mm.

isotropic material with the Young's modulus independent of the magnetic field induction $B$ (Aguib et al, 2014). Table 5.1 shows that $\eta, \theta$ and the reduced Young's modulus $E$ are real magnitudes depending only on the thickness $h_2$ of the transversally isotropic smart core made of MRE-2. Figure 5.42 demonstrates the strong

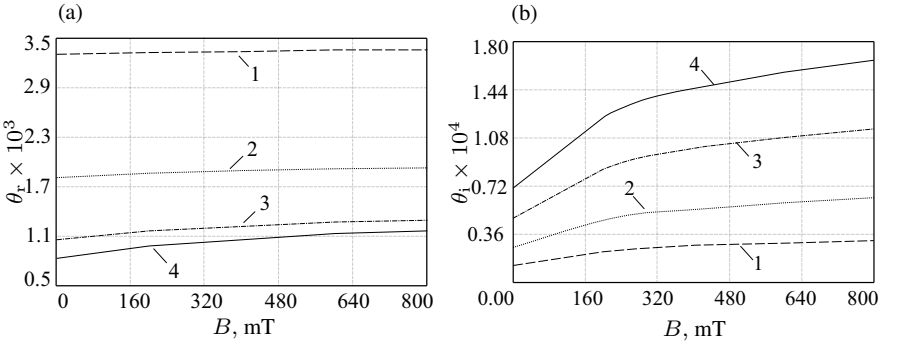


**Fig. 5.27** Parameters $\theta_r$ (a) and $\theta_i$ (b) for sandwich with MRE-3 core vs. induction $B$ at different values of thickness $h_2$: 1 - $h_2 = 3$ mm, 2 - $h_2 = 5$ mm, 3 - $h_2 = 8$ mm, 4 - $h_2 = 11$ mm.

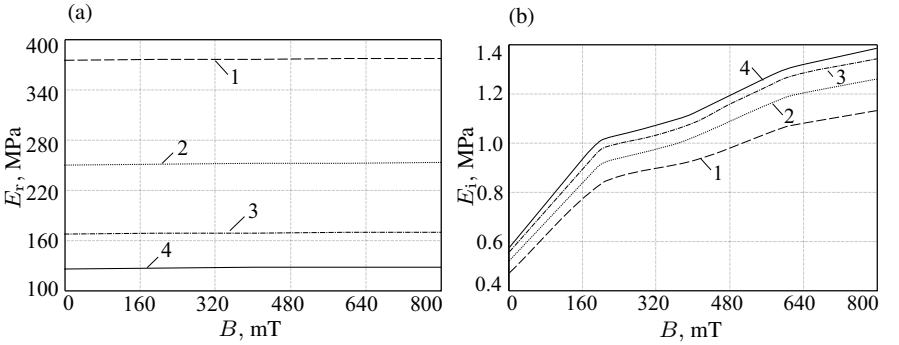


**Fig. 5.28** Parameters $E_r$ (a) and $E_i$ (b) for sandwich with MRE-3 core vs. induction $B$ at different values of thickness $h_2$: 1 - $h_2 = 3$ mm, 2 - $h_2 = 5$ mm, 3 - $h_2 = 8$ mm, 4 - $h_2 = 11$ mm.

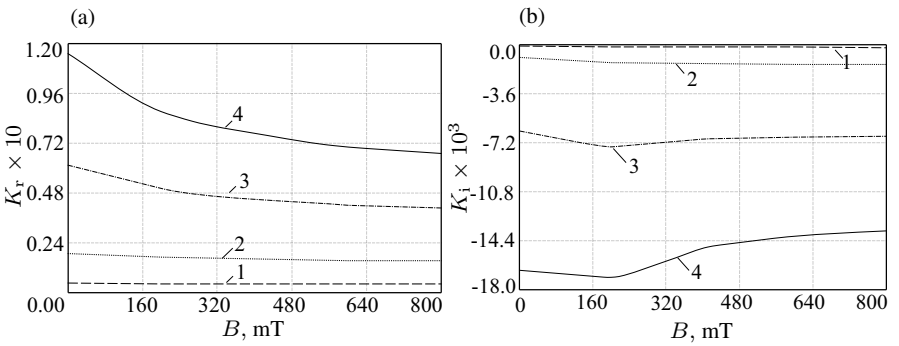


**Fig. 5.29** Parameters $K_r$ (a) and $K_i$ (b) for sandwich with MRE-3 core vs. induction $B$ at different values of thickness $h_2$: 1 - $h_2 = 3$ mm, 2 - $h_2 = 5$ mm, 3 - $h_2 = 8$ mm, 4 - $h_2 = 11$ mm.

influence of induction $B$ on the shear parameters $K_r$ and $K_i$. When comparing the plots $K_r(B)$ and $K_i(B)$ for MRE-1 with the same curves for other smart materials listed in Chapt. 2, s. Figs. 5.26-5.41, one can conclude that MRE-1 reveals the highest sensitiveness to a signal of an external physical field.

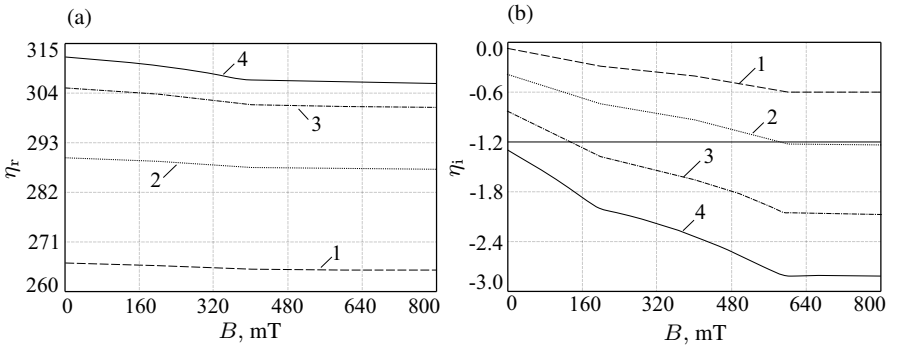


**Fig. 5.30** Parameters $\eta_r$ (a) and $\eta_i$ (b) for sandwich with MRE-4 core vs. induction $B$ at different values of thickness $h_2$: 1 - $h_2 = 3$ mm, 2 - $h_2 = 5$ mm, 3 - $h_2 = 8$ mm, 4 - $h_2 = 11$ mm.

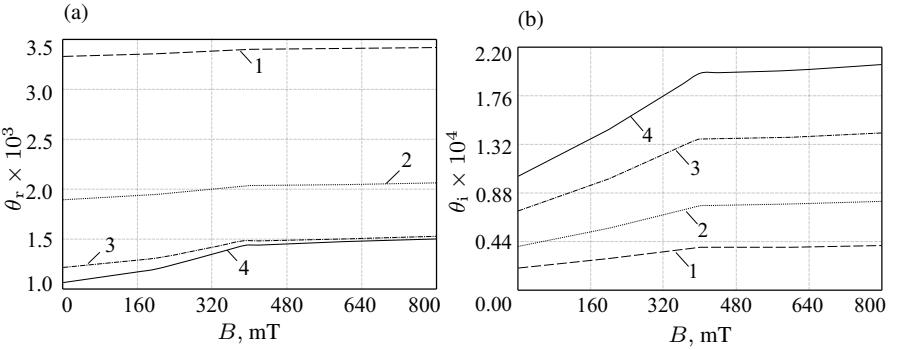


**Fig. 5.31** Parameters $\theta_r$ (a) and $\theta_i$ (b) for sandwich with MRE-4 core vs. induction $B$ at different values of thickness $h_2$: 1 - $h_2 = 3$ mm, 2 - $h_2 = 5$ mm, 3 - $h_2 = 8$ mm, 4 - $h_2 = 11$ mm.

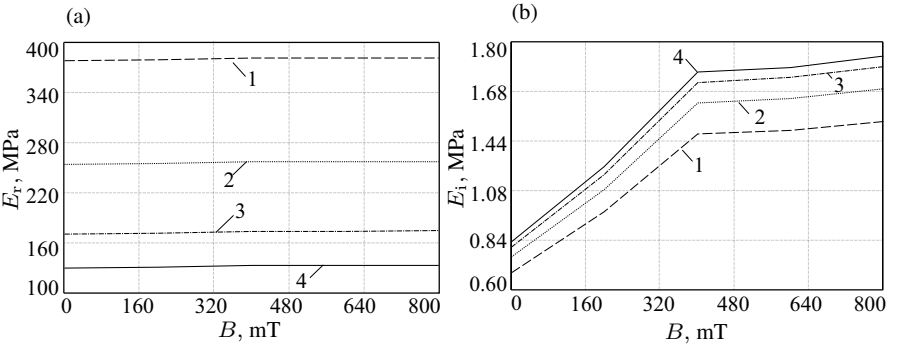


**Fig. 5.32** Parameters $E_r$ (a) and $E_i$ (b) for sandwich with MRE-4 core vs. induction $B$ at different values of thickness $h_2$: 1 - $h_2 = 3$ mm, 2 - $h_2 = 5$ mm, 3 - $h_2 = 8$ mm, 4 - $h_2 = 11$ mm.

#### 5.4.2.2 Free Low-frequency Vibrations of Medium-length Cylindrical Sandwich Panels

To display the real damping capability of aforementioned VSMs, we study free low-frequency vibrations of thin cylindrical sandwiches with different viscoelastic cores.

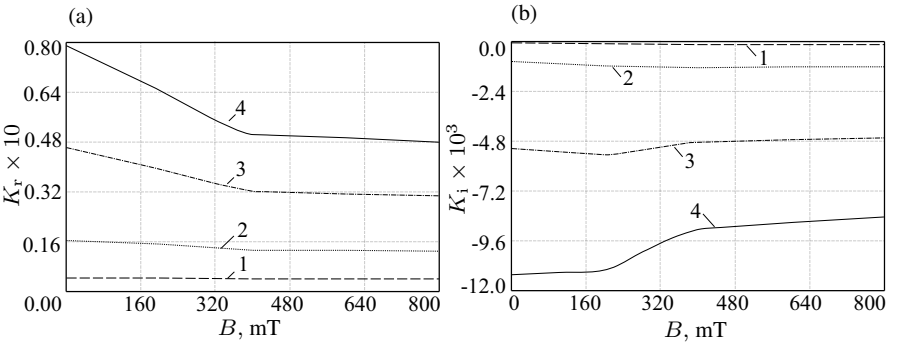


**Fig. 5.33** Parameters $K_r$ (a) and $K_i$ (b) for sandwich with MRE-4 core vs. induction $B$ at different values of thickness $h_2$: 1 - $h_2 = 3$ mm, 2 - $h_2 = 5$ mm, 3 - $h_2 = 8$ mm, 4 - $h_2 = 11$ mm.

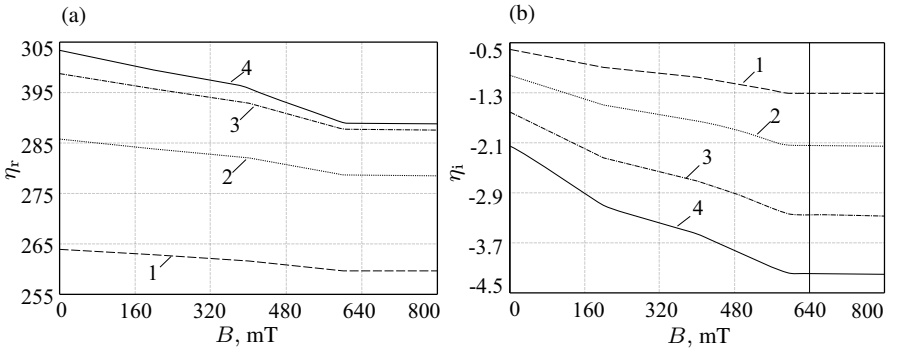


**Fig. 5.34** Parameters $\eta_r$ (a) and $\eta_i$ (b) for sandwich with MRE-5 core vs. induction $B$ at different values of thickness $h_2$: 1 - $h_2 = 3$ mm, 2 - $h_2 = 5$ mm, 3 - $h_2 = 8$ mm, 4 - $h_2 = 11$ mm.

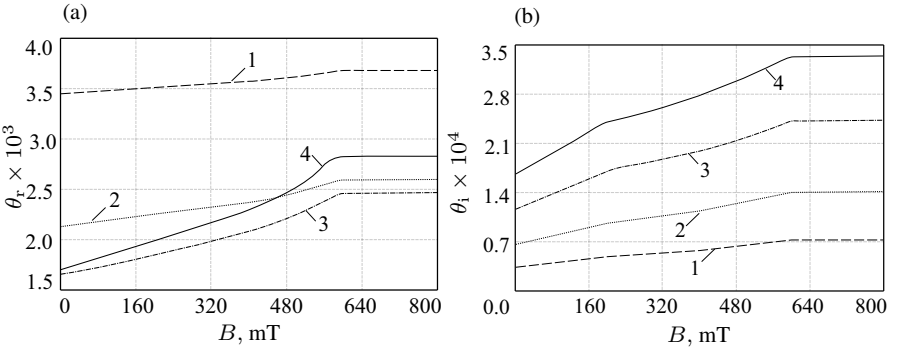


**Fig. 5.35** Parameters $\theta_r$ (a) and $\theta_i$ (b) for sandwich with MRE-5 core vs. induction $B$ at different values of thickness $h_2$: 1 - $h_2 = 3$ mm, 2 - $h_2 = 5$ mm, 3 - $h_2 = 8$ mm, 4 - $h_2 = 11$ mm.

**Example 5.9.** The sandwich has the length $L_2 = 1$ m, the radius of the reference surface $R = 0.5$ m and the apex angle $\varphi_2 = \pi$. The face sheets (thickness $h_1 = h_2 = 0.5$ mm) are made of ABS-plastic SD-0170. The smart core of the thickness $h_2 = 8$ mm is MRE-1. The natural modes of low-frequency vibrations of a thin

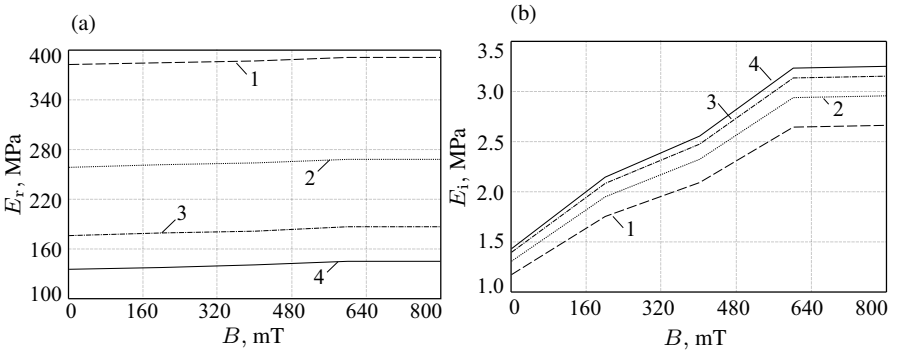


**Fig. 5.36** Parameters $E_r$ (a) and $E_i$ (b) for sandwich with MRE-5 core vs. induction $B$ at different values of thickness $h_2$: 1 - $h_2 = 3$ mm, 2 - $h_2 = 5$ mm, 3 - $h_2 = 8$ mm, 4 - $h_2 = 11$ mm.

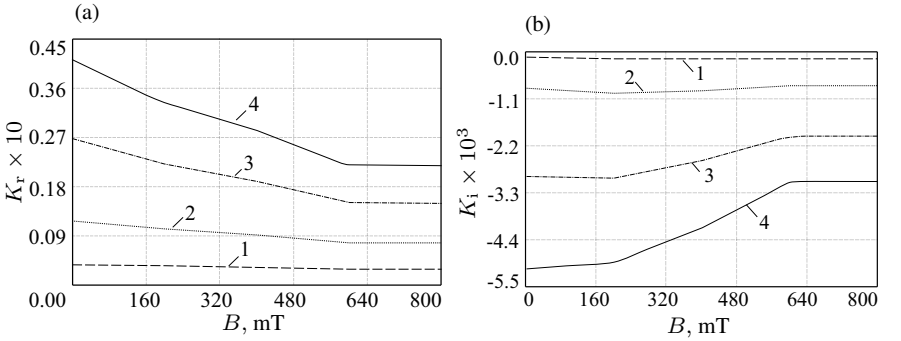


**Fig. 5.37** Parameters $K_r$ (a) and $K_i$ (b) for sandwich with MRE-5 core vs. induction $B$ at different values of thickness $h_2$: 1 - $h_2 = 3$ mm, 2 - $h_2 = 5$ mm, 3 - $h_2 = 8$ mm, 4 - $h_2 = 11$ mm.

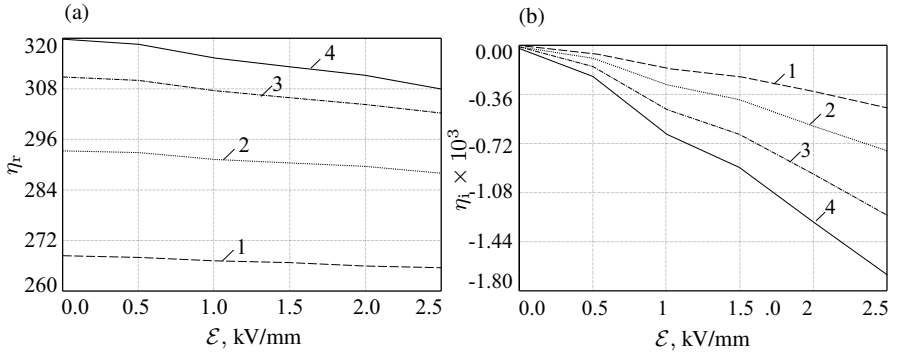


**Fig. 5.38** Parameters $\eta_r$ (a) and $\eta_i$ (b) for sandwich with ERC core vs. electric field strength $\mathcal{E}$ at different values of thickness $h_2$: 1 - $h_2 = 3$ mm, 2 - $h_2 = 5$ mm, 3 - $h_2 = 8$ mm, 4 - $h_2 = 11$ mm.

medium-length cylindrical shell are characterized by one semi-wave in the axial direction and a large number of waves in the circumferential direction. To find the lowest eigenfrequencies $\omega = \Re\Omega$, we apply Eq. (5.78) for $n = 1$ and different numbers $m$ of semi-waves in the circumferential direction. Figure 5.43 shows that

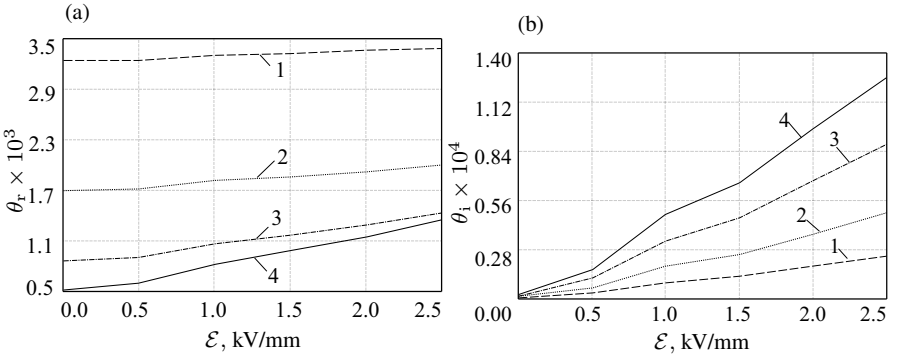


**Fig. 5.39** Parameters $\theta_\mathrm{r}$ (a) and $\theta_\mathrm{i}$ (b) for sandwich with ERC core vs. electric field strength $\mathcal{E}$ at different values of thickness $h_2$: 1 - $h_2 = 3$ mm, 2 - $h_2 = 5$ mm, 3 - $h_2 = 8$ mm, 4 - $h_2 = 11$ mm.

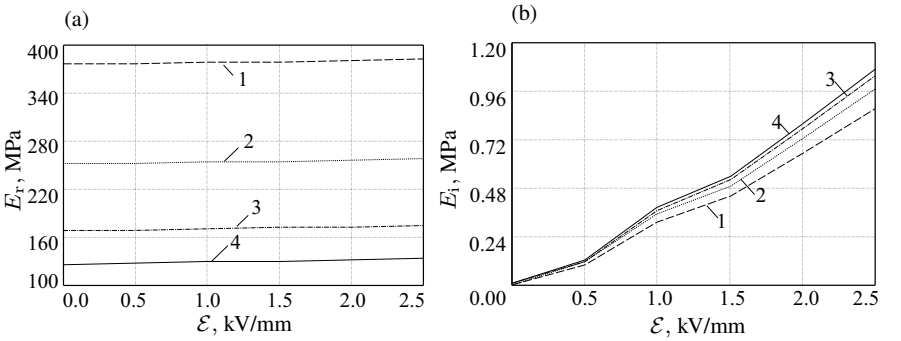


**Fig. 5.40** Parameters $E_\mathrm{r}$ (a) and $E_\mathrm{i}$ (b) for sandwich with ERC core vs. electric field strength $\mathcal{E}$ at different values of thickness $h_2$: 1 - $h_2 = 3$ mm, 2 - $h_2 = 5$ mm, 3 - $h_2 = 8$ mm, 4 - $h_2 = 11$ mm.

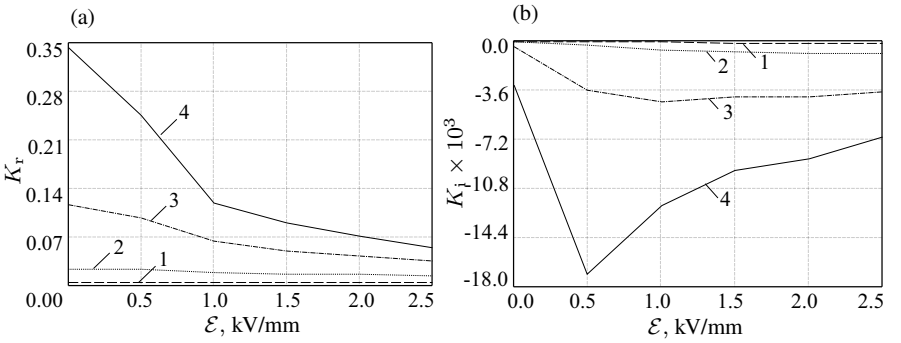


**Fig. 5.41** Parameters $K_\mathrm{r}$ (a) and $K_\mathrm{i}$ (b) for sandwich with ERC core vs. electric field strength $\mathcal{E}$ at different values of thickness $h_2$: 1 - $h_2 = 3$ mm, 2 - $h_2 = 5$ mm, 3 - $h_2 = 8$ mm, 4 - $h_2 = 11$ mm.

for any $B$ the lowest eigenfrequency refers to the mode with $m = 4$ semi-waves. The effect of magnetic field on natural frequencies turns out to be minor for modes with $m = 1, 2, 3$ semi-waves and becomes significant for a large number $m$ beginning from $m = 5$. This effect depends on the core thickness and the type of VSM.

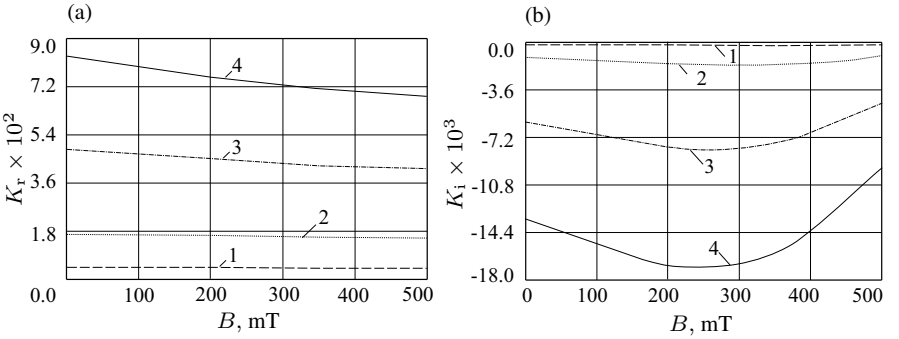


**Fig. 5.42** Parameters $K_r$ (a) and $K_i$ (b) for sandwich with MRE-2 core vs. induction $B$ at different values of thickness $h_2$: 1 - $h_2 = 3$ mm, 2 - $h_2 = 5$ mm, 3 - $h_2 = 8$ mm, 5 - $h_2 = 11$ mm.

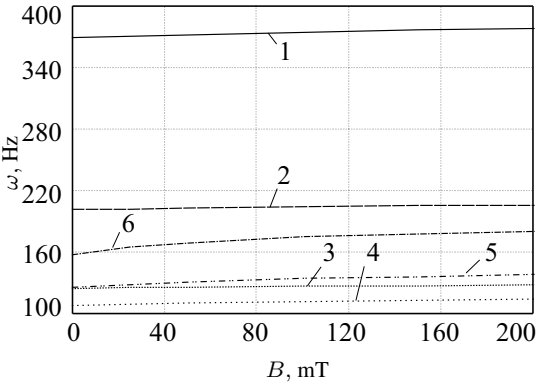


**Fig. 5.43** Natural frequencies of the MRE-1 based sandwich corresponding to $n = 1$ semi-waves in the axial direction and different number $m$ of semi-waves in the circumferential direction vs. induction $B$. The plot number corresponds to a number $m$.

The next series of calculations is aimed to examine the effect of a thickness $h_2$ and available smart materials on the lowest natural frequencies and corresponding damping ratios at different levels of applied magnetic or electric field.

**Example 5.10.** We consider six different sandwiches, S-1, S-2, S-3, S-4, S-5 and S-6, with cores made of MRE-1, MRE-2, MRE-3, MRE-4, MRE-5 or ERC, respectively. The viscoelastic properties of these smart composite materials are given in Chapt. 2. The behavior of the principal complex parameters $\eta, \theta, E$ and $K$ versus the magnetic induction (or electric strength) was shown above. The geometrical dimensions of all sandwiches are the same as in the previous example. In Figs. 5.44-5.49 the

**Table 5.1** Parameters $\eta, \theta$ and reduced Young's modulus $E$ vs. the core thickness $h_2$.

| $h_2$, mm | $\eta$ | $\theta \times 10^3$ | $E$, MPa |
|---|---|---|---|
| 3 | 267 | 3.265 | 376 |
| 5 | 292 | 1.751 | 251 |
| 8 | 308 | 0.963 | 168 |
| 11 | 317 | 0.693 | 127 |

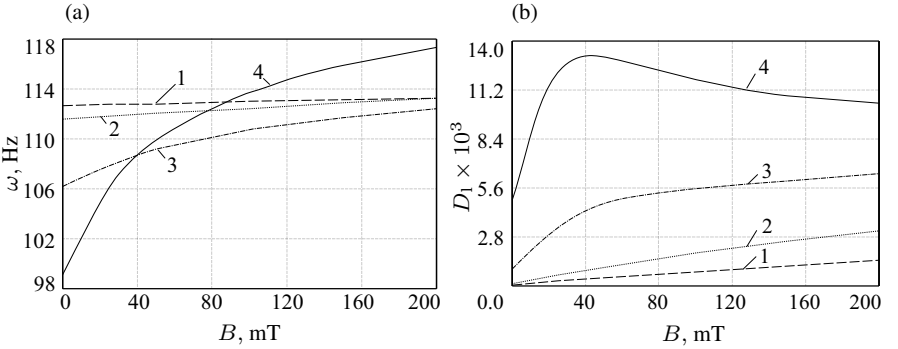


**Fig. 5.44** Natural frequency $\omega$ (a) and logarithmic decrement $D_1$ (b) for sandwiches S-1 with MRE-1 core and different values of thickness $h_2$ vs. induction $B$: 1 - $h_2 = 3$ mm, 2 - $h_2 = 5$ mm, 3 - $h_2 = 8$ mm, 4 - $h_2 = 11$ mm.

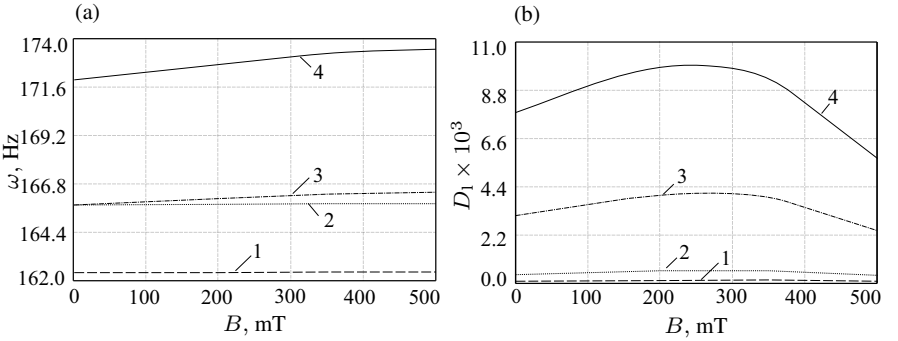


**Fig. 5.45** Natural frequency $\omega$ (a) and logarithmic decrement $D_1$ (b) for sandwiches S-2 with MRE-2 core and different values of thickness $h_2$ vs. induction $B$: 1 - $h_2 = 3$ mm, 2 - $h_2 = 5$ mm, 3 - $h_2 = 8$ mm, 4 - $h_2 = 11$ mm.

lowest natural frequencies $\omega = \Re\Omega$ and corresponding logarithmic decrements $D_1$ calculated by Eq. (5.7) are plotted as functions of the magnetic field induction $B$ (for sandwiches with MRE-core) or the electric field strength $\mathcal{E}$ (for S-6 sandwich with ERC-core) at different values of $h_2$. For any fixed $h_2$, the lowest eigenfrequencies are monotonically increasing functions of the intensity of the external physical field, the frequency gain being higher for sandwiches with more thick smart viscoelastic core. However, the behavior of $\omega$ vs. $h_2$ at a fixed $B$ (or $\mathcal{E}$) is very complicated and strongly depends on the VSM embedded between elastic layers. For the sandwiches S-2 and S-5 assembled from MRE-2 and MRE-5 smart materials, respectively, the lowest eigenfrequencies increase together with the core thickness at any $B$, while for other sandwiches the monotonic growth of $\omega(h_2)$ is not detected. Note that MRE-2 is considered as a material with the Young's modulus independent of $B$, and MRE-5 with the highest content of carbon black and treated here as a material possesses a very large shear modulus. Interesting results are shown in Figs. 5.44 (a) and 5.49 (a) related to S-1 and S-6 sandwiches: if a magnetic (or electric) field is weak, then increasing the thickness of soft MRE-1 or ERC cores leads to some softening of

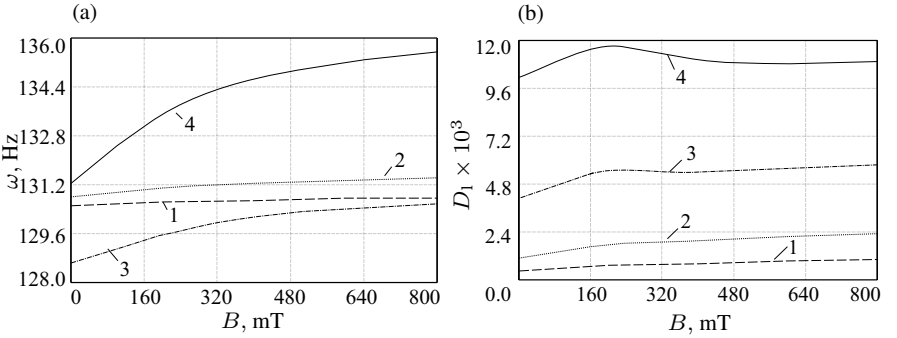


**Fig. 5.46** Natural frequency $\omega$ (a) and logarithmic decrement $D_1$ (b) for sandwiches S-3 with MRE-3 core and different values of thickness $h_2$ vs. induction $B$: 1 - $h_2 = 3$ mm, 2 - $h_2 = 5$ mm, 3 - $h_2 = 8$ mm, 4 - $h_2 = 11$ mm.

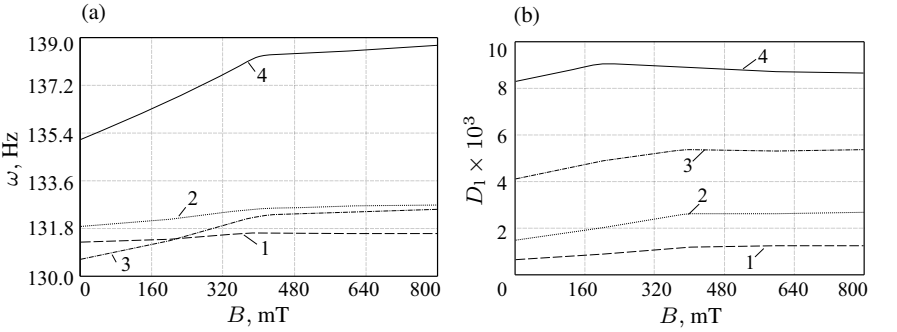


**Fig. 5.47** Natural frequency $\omega$ (a) and logarithmic decrement $D_1$ (b) for sandwiches S-4 with MRE-4 core and different values of thickness $h_2$ vs. induction $B$: 1 - $h_2 = 3$ mm, 2 - $h_2 = 5$ mm, 3 - $h_2 = 8$ mm, 4 - $h_2 = 11$ mm.

entire packet and, in such a way, to decreasing eigenfrequencies. The application of a strong physical field violent increases the core stiffness and, finally, results in growing natural frequencies.

As expected, the damping capabilities of all VSMs under consideration are different and strongly affected by the level of an applied physical field and thickness of a smart core as well. For the S-5 sandwich with the MRE-5 core possessing the highest shear modulus and lowest loss factor, the logarithmic decrement $D_{\mathrm{L}}$ monotonically increases at all range of varying the induction $B$, from 0 to 800 mT. The same behavior of $D_{\mathrm{L}}$ is observed for all other sandwiches (excluding S-2) with medium and very thin viscoelastic cores. For the S-2 sandwich with the transversally isotropic MRE-2 core as well as for other sandwiches but with thick viscoelastic cores (at about $h_2 = 11$ mm), there are value $B = B^*$ (or $\mathcal{E} = \mathcal{E}^*$ ) corresponding to the yielding point for a rheological material and resulting in the maximum value of the decrement $D_{\mathrm{L}}$. Finally, when comparing damping capabilities of all VSMs at the same geometrical dimensions for sandwiches, the MRE-1 and MRE-3 reveal the best damping properties.

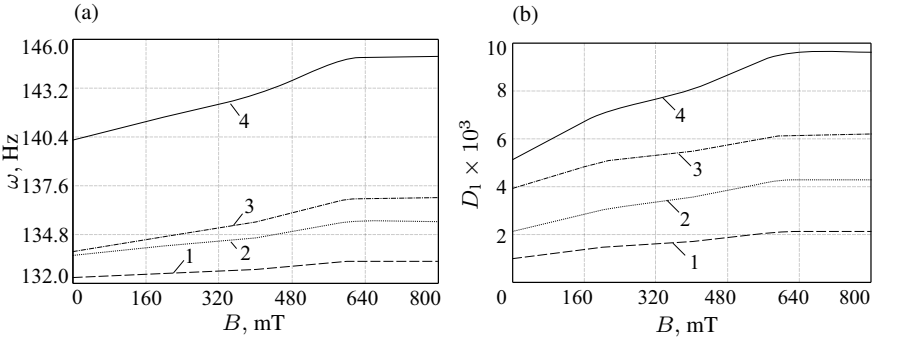


**Fig. 5.48** Natural frequency $\omega$ (a) and logarithmic decrement $D_1$ (b) for sandwiches S-5 with MRE-5 core and different values of thickness $h_2$ vs. induction $B$: 1 - $h_2 = 3$ mm, 2 - $h_2 = 5$ mm, 3 - $h_2 = 8$ mm, 4 - $h_2 = 11$ mm.

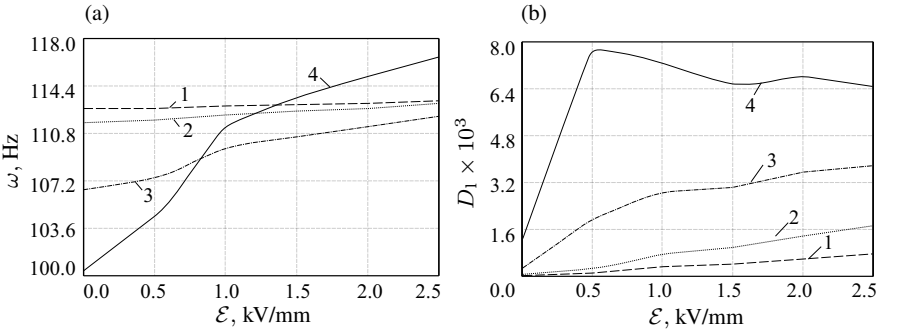


**Fig. 5.49** Natural frequency $\omega$ (a) and logarithmic decrement $D_1$ (b) for sandwiches S-6 with ERC core and different values of thickness $h_2$ vs. the electric strength $\mathcal{E}$: 1 - $h_2 = 3$ mm, 2 - $h_2 = 5$ mm, 3 - $h_2 = 8$ mm, 4 - $h_2 = 11$ mm.

The example considered allows concluding:

- using VSMs and correctly choosing a thickness for smart core or layers, one can assemble a smart thin-walled medium-length cylindrical laminated (in particular, sandwich) panels with tunable viscoelastic properties;
- the application of an external physical field permits to shift right the spectrum of natural frequencies of a panel and greatly improve damping capacity of smart viscoelastic core or layers composing a laminated structure.

### *5.4.3 Steady-state Forced Vibrations and Their Suppression*

Let us consider the nonhomogeneous coupled Eqs. (5.61) with the boundary conditions (5.64) for

$$q_{\rm n}(\alpha_1, \alpha_2, t) = q_3(\alpha_1, \alpha_2)\mathrm{e}^{\mathrm{i}\omega_{\rm e} t}, \tag{5.82}$$

where $\omega_{\mathrm{e}}$ is the frequency of excitation and $q_3$ is some complex dimensionless amplitude function. Intending to study predominantly bending vibrations, we shall omit the inertia terms in the first two equations from (5.61). To satisfy the boundary conditions (5.64), we seek a solution of Eqs. (5.61) in the form of double series

$$\begin{aligned}
\hat{u}_1 &= R\sum_{n=1}^{\infty}\sum_{m=1}^{\infty} U_{nm}^{(1)}(t)\cos\frac{\pi n\alpha_1}{L_1}\sin\frac{\pi m\alpha_2}{L_2},\\
\hat{u}_2 &= R\sum_{n=1}^{\infty}\sum_{m=1}^{\infty} U_{nm}^{(2)}(t)\sin\frac{\pi n\alpha_1}{L_1}\cos\frac{\pi m\alpha_2}{L_2},\\
w &= R\sum_{n=1}^{\infty}\sum_{m=1}^{\infty} W_{nm}(t)\sin\frac{\pi n\alpha_1}{L_1}\sin\frac{\pi m\alpha_2}{L_2},\\
\psi_1 &= \sum_{n=1}^{\infty}\sum_{m=1}^{\infty} \Psi_{nm}^{(1)}(t)\cos\frac{\pi n\alpha_1}{L_1}\sin\frac{\pi m\alpha_2}{L_2},\\
\psi_2 &= \sum_{n=1}^{\infty}\sum_{m=1}^{\infty} \Psi_{nm}^{(2)}(t)\sin\frac{\pi n\alpha_1}{L_1}\cos\frac{\pi m\alpha_2}{L_2},
\end{aligned} \tag{5.83}$$

where $U_{nm}^{(j)}(t), W_{nm}(t), \Psi_{nm}^{(j)}(t)(j=1,2)$ are the required functions of $t$ called the generalized co-ordinates of the mechanical system.

The function $q_3(\alpha_1,\alpha_2)$ is also expended into the series

$$q_3 = \sum_{n=1}^{\infty}\sum_{m=1}^{\infty} q_{nm}\sin\frac{\pi n\alpha_1}{L_1}\sin\frac{\pi m\alpha_1}{L_2}, \tag{5.84}$$

where

$$q_{nm} = \frac{4}{L_1L_2}\int_0^{L_1}\int_0^{L_2} q_3(\alpha_1,\alpha_2)\sin\frac{\pi n\alpha_1}{L_1}\sin\frac{\pi m\alpha_1}{L_2}\mathrm{d}\alpha_1\mathrm{d}\alpha_2. \tag{5.85}$$

We substitute Eqs. (5.83) and (5.84) into the governing equations (5.61), multiplying the equations by the following terms

$$\begin{aligned}
&\cos\frac{\pi i\alpha_1}{L_1}\sin\frac{\pi j\alpha_2}{L_2}, \quad \sin\frac{\pi i\alpha_1}{L_1}\cos\frac{\pi j\alpha_2}{L_2}, \quad \sin\frac{\pi i\alpha_1}{L_1}\sin\frac{\pi j\alpha_2}{L_2},\\
&\cos\frac{\pi i\alpha_1}{L_1}\sin\frac{\pi j\alpha_2}{L_2}, \quad \sin\frac{\pi i\alpha_1}{L_1}\cos\frac{\pi j\alpha_2}{L_2},
\end{aligned}$$

respectively, where $i, j$ are fixed natural numbers, and integrate them over the panel surface. Then, eliminating $U_{nm}^{(\varsigma)}(t)$ and $\Psi_{nm}^{(\varsigma)}(t), \varsigma = 1,2$, from the first four equations, we arrive at the differential equation

$$\ddot{W}_{ij} + \Omega_{ij}^2 W_{ij} = \frac{q_{ij}}{\rho_0 hR}\mathrm{e}^{\mathrm{i}\omega_{\mathrm{e}}t}, \quad i,j = 1,2,\ldots, \tag{5.86}$$

with respect to the functions $W_{ij}(t)$, where $\Omega_{ij} = \pm(\omega_{ij} + \mathrm{i}\alpha_{ij})$ are two complex eigenvalues determined from Eq. (5.71). Note that the in-plane inertia forces in (5.61) are neglected.

The partial solution of Eq. (5.86) is the function

$$W_{ij}(t) = \frac{q_{ij}}{\rho_0 hR(\Omega_{ij}^2 - \omega_{\mathrm{e}}^2)} \mathrm{e}^{\mathrm{i}\,\omega_{\mathrm{e}} t}. \tag{5.87}$$

Then the amplitude of forced steady-state vibrations at any point on the shell surface will be defined by the formula

$$w = R \sum_{n=1}^{\infty} \sum_{m=1}^{\infty} \frac{q_{nm} \mathrm{e}^{\mathrm{i}\,\omega_{\mathrm{e}} t}}{\rho_0 hR(\Omega_{nm}^2 - \omega_{\mathrm{e}}^2)} \sin \frac{\pi n \alpha_1}{R} \sin \frac{\pi m \alpha_2}{R}, \tag{5.88}$$

and the associated displacements $\hat{u}^{(1)}, \hat{u}^{(2)}, \psi^{(1)}, \psi^{(2)}$ are calculated by Eqs. (5.73), where

$$U_{nm}^{(\varsigma)}(t) = b_{\varsigma}(n,m)\tilde{W}_{nm}(t), \quad \Psi_{nm}^{(\varsigma)}(t) = d_{\varsigma}(n,m)\tilde{W}_{nm}(t), \quad \varsigma = 1,2.$$

Equation (5.88) determines the amplitude-frequency response which depends on the distribution of harmonic force over the shell surface. Because the complex eigenvalue $\Omega_{nm}$ depends upon the effective complex shear modulus $G$ being a function of the induction $B$, the amplitude of sustained forced vibration becomes to some extent a controlled quantity. To detect this effect, we consider the following example.

**Example 5.11.** Let two S-1 cylindrical sandwich panels (the notations of sandwiches are the same as in Example 5.10) with the opening angles $\varphi_2 = \pi/3$ and $\varphi_2 = \pi$ be subjected to the concentrated harmonic force

$$F = F_0 \sin \omega_{\mathrm{e}} t \tag{5.89}$$

applied in the point $\alpha_1 = \alpha_1^{\circ} = L_1/2, \alpha_2 = \alpha_2^{\circ} = L_2/2$, where $F_0$ is the amplitude of concentrated force which is not specified in view of the linearity of the problem. All other geometrical dimensions and physical characteristics are the same as in Example 5.10.

The normal pressure $q_{\mathrm{n}}$ per unit area can be expressed as follows

$$\begin{aligned} q_{\mathrm{n}} = \lim_{\substack{x_1 \to 0 \\ x_2 \to 0}} \frac{F_0}{4x_1 x_2} [H_0(\alpha_1^{\circ} - x_1 - \alpha_1) - H_0(\alpha_1^{\circ} + x_1 - \alpha_1)] \\ \times [H_0(\alpha_2^{\circ} - x_2 - \alpha_2) - H_0(\alpha_2^{\circ} + x_2 - \alpha_2)] \sin \omega_{\mathrm{e}} t, \end{aligned} \tag{5.90}$$

where $H_0(x)$ is the Heaviside function. Then

$$q_{ij} = -\frac{2\mathrm{i}F_0}{L_1 L_2} \sin \frac{\delta_i \alpha_1^{\circ}}{R} \sin \frac{\delta_j \alpha_2^{\circ}}{R}, \tag{5.91}$$

where $\delta_i, \delta_j$ are determined by Eqs. (5.70).

We consider the real part of an amplitude of forced stationary vibrations calculated by Eq. (5.88) in the point of the force application

$$w_{\mathrm{r}}^{\circ} = \frac{4F_0}{\rho_0 h L_1 L_2} \sum_{n=1}^{\infty} \sum_{m=1}^{\infty} \frac{\omega_{nm}^2 - \alpha_{nm}^2 - \omega_{\mathrm{e}}^2}{(\omega_{nm}^2 - \alpha_{nm}^2 - \omega_{\mathrm{e}}^2)^2 + 4\alpha_{nm}^2 \omega_{nm}^2} \times \sin^2 \frac{\delta_n L_1}{2R} \sin^2 \frac{\delta_m L_2}{2R}. \tag{5.92}$$

Figures 5.50 and 5.51 show the scaled amplitude $w_{\mathrm{r}}^{\circ}$, denoted by $A_{\mathrm{m}}$, versus the frequency of excitation $\omega_{\mathrm{e}}$ varying from 0 to 400 Hz. The amplitude-frequency plots for both sandwiches are displayed for three different cases, for $B = 0$ (magnetic field is absent), $B = 40$ and 200 mT. It may be seen that the application of a magnetic field results in significant reduction of the amplitude of resonance vibrations. So, for the first sandwich cylindrical panel with the opening angle $\varphi_2 = \pi/3$, one has about two- and three-fold reductions at $B = 40$ and $B = 200$ mT, respectively.

It is also seen that in all cases, with and without magnetic field, for the panel with the opening angle $\varphi_2 = \pi/3$, more intensive resonance vibrations occur on the lowest (first) eigenfrequency with one semi-wave in both the axial and circumferential

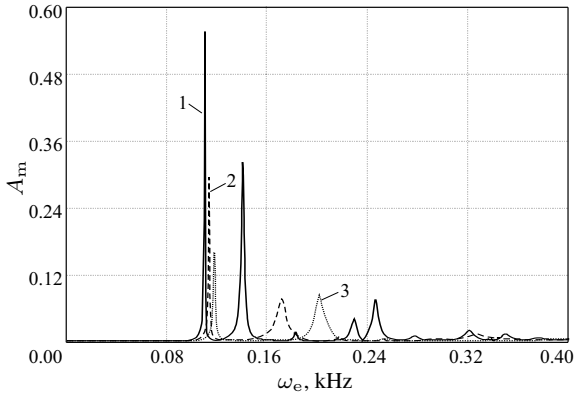


**Fig. 5.50** Amplitude-frequency characteristic for the sandwich S-1 with the opening angle $\varphi_2 = \pi/3$ at different levels of applied magnetic field: 1 - $B = 0$ mT, 2 - $B = 40$ mT, 3 - $B = 200$ mT.

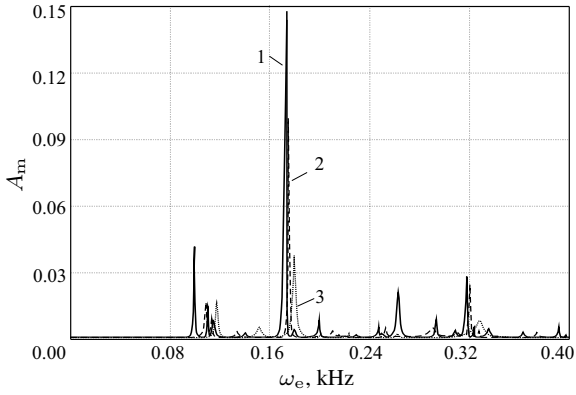


**Fig. 5.51** Amplitude-frequency characteristic for the sandwich S-1 with the opening angle $\varphi_2 = \pi$ at different levels of applied magnetic field: 1 - $B = 0$ mT, 2 - $B = 40$ mT, 3 - $B = 200$ mT.

directions ($n = 1, m = 1$), while for the panel with $\varphi_2 = \pi$, the maximum amplitude of resonance vibrations is observed due to superposition of the fifth and sixth modes with the wave numbers $n = 2, m = 5$ and $n = 2, m = 6$, respectively, which have very close natural frequencies. Our additional accurate calculations (their outcomes are omitted here) detected that for cylindrical panels with a small opening angle as well as for plates, the amplitude of resonance vibrations is a monotonically decreasing function of the resonance frequency (at least at the low part of the spectrum), while for panels with a large $\varphi_2$ as well as for cylindrical shells closed in the circumferential direction, the peak of maximum amplitude shifts to the right (at the frequency axis) and corresponds to the superposition of two or more modes with very close associated eigenfrequencies.

It should be noticed that the *mechanisms* of suppression of resonance vibrations at the first eigenmode are different for sandwiches with small and large opening angles. So, Fig. 5.50 shows that applying magnetic field results in slight shifting of the first resonance frequency, and the suppression occurs mainly due to the increase the damping capability of the smart material (here, MRE-1). As for panels with large opening angle $\varphi_2$ (s. Fig. 5.51) and cylindrical shells closed in the circumferential direction, the action of magnetic field leads to very noticeable shifting the first resonance region to the right and about two-fold decreasing the resonance peak.

It is obvious that different VSMs incorporated with a sandwich panel possess different capability to suppress resonance vibrations. For instance, we choose here the MRE-3 because the logarithmic decrement corresponding to the lowest eigenfrequency for the sandwich S-3 (here, the sandwich notation is the same as in Subsect. 5.4.2) is larger (in the average for any induction $B$) than for other smart materials under consideration (compare Figs. (b) of 5.44-5.49). To estimate the damping power of MRE-3, we shall consider one more example.

**Example 5.12.** Let the sandwich cylindrical panel S-3 with MRE-3 based core (see the property of this smart material in Subsect. 2.3.3) has the opening angle $\varphi = \pi$ and all other geometrical and physical characteristics are the same as in Example 5.11. The panel experiences the same periodic load (5.89) and (5.90) applied at the point $\alpha_1 = \alpha_1^\circ = L_1/2, \alpha_2 = \alpha_2^\circ = L_2/2$. Figure 5.52 demonstrates the amplitude-frequency response of the panel without magnetic field and under its action with the induction $B = 800$ mT. The plots show that the application of very strong magnetic field leads to only shifting the first and second resonance regions to the right, while the reduction of amplitudes corresponding to these regions is very weak. The noticeable lowering of the amplitude (about twofold reduction) is observed for the resonance vibrations on the third natural frequency, however this reduction is reached by the application of very strong magnetic field in comparison with the sandwich S-2 (see the fifth resonance region in Fig. 5.51) subjected to more weak magnetic field. Similar calculations for other sandwiches (S-3, S-4 and S-5) and their comparison with outcomes for the S-1 sandwich revealed that the smart material MRE-1 possesses the best damping capability to suppress resonance vibrations. This suppression being provided by applying relatively weak magnetic field.

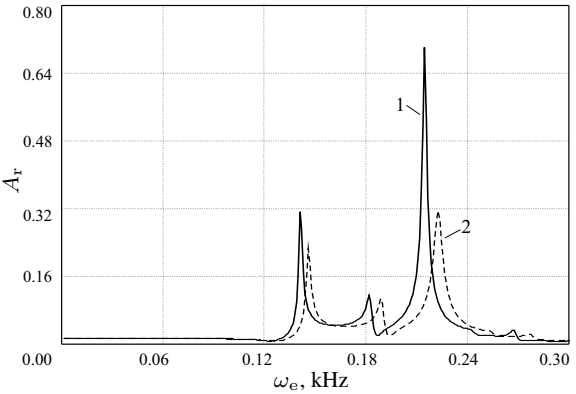


**Fig. 5.52** Amplitude-frequency characteristic for the sandwich S-3 with the opening angle $\varphi_2 = \pi$ without and with magnetic field: 1 - $B = 0$ mT, 2 - $B = 800$ mT.

## 5.5 Influence of Stationary Magnetic Field on Localized Modes of Free Vibrations

In this section, we shall study localized modes of free vibrations of medium-length MRE-based laminated cylindrical shells. Using the asymptotic approach (Mikhasev and Tovstik, 2009) displayed in Chapt. 4, the effect of magnetic field on the natural frequencies, damping ratios and associated localized modes will be analyzed (Mikhasev et al, 2014). As an example, a sandwich cylinder with highly polarized MRE-1 embedded between two elastic face layers will be examined.

### *5.5.1 Setting the Problem*

Let a medium-length laminated cylindrical shell with at least one layer made of a MRE be in a stationary magnetic field. The MRE is assumed to be inhomogeneous so that its complex shear and Young's moduli are functions of an angle $\varphi$. The reasons resulting in nonhomogeneity of viscoelastic properties of MRE layer may be different. The heterogeneous magnetic field may leads to not uniform distribution of magneto-sensitive particles in a MRE. But even if the magnetic field is uniform, their impact on various parts of a polarized MRE may be unequal because of different angles between the magnetic force lines and the alignment of magnetic particles (s. Fig. 5.53). This assumption is confirmed by experimental results presented in Boczkowska et al (2012). Studying the urethane MRE consisting of carbonyl-iron particles in a polyurethane matrix, it was found out that the maximum value of the modulus $G' = 0.5$ MPa was observed for samples with particles orientated at $30^\circ$ with respect to the lines of magnetic field, whereas the minimum magnitude $G' = 0.1$ MPa corresponded to samples with angle $90^\circ$ between the magnetic force lines and the particle alignment.

In what follows, not specifying the reason causing inhomogeneity of viscoelastic properties of a MRE, we assume that all magneto-sensitive complex magnitudes

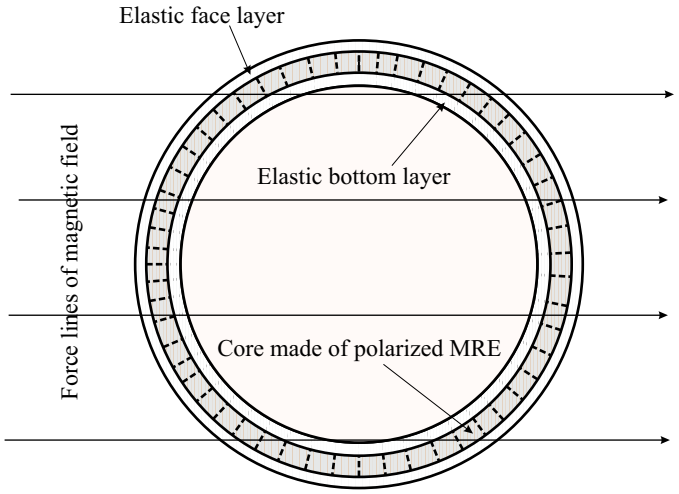


**Fig. 5.53** Cross-section of sandwich cylindrical shell with the core made of polarized MRE in magnetic field with parallel force lines (after Mikhasev et al, 2014).

$\nu, \eta_3, E, \theta, \beta$ and $K$ appearing in Eq. (5.65) are functions of the circumferential co-ordinate $\alpha_2$. We introduce a small parameter

$$\varepsilon^8 = \frac{h_*^2 \eta_{3\mathrm{r}}^{(0)}}{12[1-(\nu_{\mathrm{r}}^{(0)})^2]}, \tag{5.93}$$

and consider sufficiently thin shells for which parameter $h_*$ is a quantity of the order $\sim 0.01$ or less. In Eq. (5.93) and below, the superscript $(0)$ means that an appropriate parameter is calculated at $B = 0$. Here, $\eta_{3\mathrm{r}} = \Re\,\eta_3$, $\nu_{\mathrm{r}} = \Re\,\nu$, $\nu_{\mathrm{r}}^{(0)} \approx 0.4$. We assume also the following asymptotic estimations for the basic tunable parameters

$$\begin{aligned}
\nu \quad &= \nu_{\mathrm{r}}^{(0)}[1+\varepsilon^4\delta\nu(\varphi)], \quad \theta_{\mathrm{r}} \sim \varepsilon^3, \quad \theta_{\mathrm{i}} \sim \varepsilon^4, \\
\eta_3 \quad &= \eta_{3\mathrm{r}}^{(0)}[1+\varepsilon^2\delta\eta_3(\varphi)], \quad \eta_{3\mathrm{r}}^{(0)} = \pi^{-4}\eta_{\mathrm{r}}^{(0)}[1-(\nu_{\mathrm{r}}^{(0)})^2], \\
E_{\mathrm{r}} \quad &= E_{\mathrm{r}}^{(0)} d(\varphi) = E_{\mathrm{r}}^{(0)}[1+\varepsilon d_1(\varphi)], \quad E_{\mathrm{i}}/E_{\mathrm{r}}^{(0)} \sim \varepsilon^4, \\
\pi^{-2}K &= \varepsilon^2\kappa(\varphi) = \varepsilon^2[\kappa_0(\varphi) + \mathrm{i}\varepsilon\kappa_1(\varphi)] \quad \text{for} \quad \varepsilon \to 0.
\end{aligned} \tag{5.94}$$

In Eqs. (5.94), $\delta\nu, \delta\eta_3$ and $d_1, \kappa_0, \kappa_1$ are complex and real functions of angle $\varphi = \alpha_2/R$, respectively, so that their absolute magnitudes are quantities of the order $O(1)$ at $\varepsilon \to 0$. Estimates (5.94) hold for laminated cylindrical panels and shells containing any MRE specified in Chapt. 2 with the summary thickness of a smart material not less then $70\%$ from the total thickness $h$ of a shell. In particular, these conditions are valid for the considered above S-1 sandwiches with the MRE-1 based core. In the general case, the shell is non-circular with the radius of curvature

$R_2 = Rk(\varphi)$. At the shell edges, the boundary conditions (5.66) are assumed. The solution of Eqs. (5.65) describing free vibrations (at $q_{\rm n} = 0$) are assumed to be of the form

$$\chi = \varepsilon^{-4} R\chi^*(s,\varphi)\exp(\mathrm{i}\Omega t), \quad F = E_{\rm r}^{(0)} hR^2\Phi^*(s,\varphi)\exp(\mathrm{i}\Omega t), \quad \phi = 0, \tag{5.95}$$

where $s = \alpha_1/R$ is a dimensionless axial co-ordinate, $\Omega$ is a required complex eigenvalue, and $\chi^*, F^*$ are dimensionless displacement and stress functions.

The substitution of Eqs. (5.95) into Eqs. (5.65) results in the differential equations

$$\begin{gathered}\varepsilon^4 d(\varphi)\Delta^2\chi^* + k(\varphi)\frac{\partial^2\Phi^*}{\partial s^2} - \Lambda[1-\varepsilon^2\kappa(\varphi)\Delta]\chi^* = 0,\\ \varepsilon^4\Delta^2\Phi^* - k(\varphi)\frac{\partial^2}{\partial s^2}[1-\varepsilon^2\kappa(\varphi)\Delta]\chi^* = 0\end{gathered} \tag{5.96}$$

written in the dimensionless form, where $\Lambda = \rho R^2\Omega^2/(\varepsilon^4 E_{\rm r}^{(0)})$ is the dimensionless frequency parameter. When deriving Eqs. (5.96) from Eqs. (5.65), we have omitted the operator $\Delta^3\chi$ because of smallness of the coefficient $K\theta$, s. Eqs. (5.76) for $K$ and (5.94), and disregarded by very small dimensionless parameters $\varepsilon^4\delta\nu, \varepsilon^2\delta\eta_3, E_{\rm i}/E_{\rm r}^{(0)}$. It should be noticed that when studying low-frequency eigenmodes this simplification leads to the error of the order $h_*$ which is comparable with the error of Eqs. (5.65). In Eqs. (5.96),

$$\kappa = \kappa_0(\varphi) + \varepsilon\mathrm{i}\kappa_1(\varphi) \tag{5.97}$$

is the principal complex shear parameter depending on both the co-ordinate $\varphi$ and the magnetic field induction $B$. The appropriate boundary conditions are as follows

$$\chi^* = \Delta\chi^* = \Delta^2\chi^* = \frac{\partial^2\Phi^*}{\partial s^2} = \frac{\partial^2\Phi^*}{\partial\varphi^2} = 0 \quad \text{at} \quad s = 0,\, l, \tag{5.98}$$

where $l = L/R$.

### 5.5.2 Localized Natural Modes

The boundary-value problem (5.96), (5.98) is identical to the problem considered in Sect. 4.4. The difference lies in the fact that now the coefficients $d, \kappa$ are complex functions those depend not only on the angle $\varphi$, but also on the induction of magnetic field. Varying the magnetic field, one can affect the localized natural modes. Furthermore, applying a nonuniform magnetic field, it is possible to disturb the uniform natural modes and result in localization of some modes corresponding to low-frequency vibrations.

Let $y$ be any of the foregoing parameters depending on $\varphi$. It is assumed that $\mathrm{d}y/\mathrm{d}\varphi \sim y$ at $\varepsilon \to 0$. Then, under some additional conditions for the functions

$\kappa_0(\varphi), k(\varphi)$ (which will be specified below), the boundary value problem (5.96), (5.98) may have a solution localized in the neighborhood of some generator $\varphi = \varphi_0$ called the weakest one (Mikhasev and Tovstik, 2009). The required solution is seeking in the form identical to (4.111)

$$\begin{aligned}
\chi^* &= \sin\frac{\pi n s}{l}\sum_{j=0}^{\infty}\varepsilon^{j/2}\chi_j(\zeta)\exp\left\{\mathrm{i}\left(\varepsilon^{-1/2}p\zeta + 1/2b\zeta^2\right)\right\},\\
\Phi^* &= \sin\frac{\pi n s}{l}\sum_{j=0}^{\infty}\varepsilon^{j/2}\Phi_j(\zeta)\exp\left\{\mathrm{i}\left(\varepsilon^{-1/2}p\zeta + 1/2b\zeta^2\right)\right\},\\
\Lambda &= \Lambda_0 + \varepsilon\Lambda_1 + \ldots,
\end{aligned} \tag{5.99}$$

where $\zeta = \varepsilon^{-1/2}(\varphi - \varphi_0)$, $p$ is a real wave parameter, $b$ is a complex parameter so that $\Im\, b > 0$, and $\chi_j, \Phi_j$ are polynomials in $\zeta$.

The functions $\kappa_0(\varphi), \kappa_1(\varphi), k(\varphi), d_1(\varphi)$ are expanded into series in the neighborhood of the generatrix $\varphi = \varphi_0$. In particular,

$$\kappa_0(\varphi) = \kappa_0(\varphi_0) + \varepsilon^{1/2}\kappa_0'(\varphi_0)\zeta + \frac{1}{2}\varepsilon\kappa_0''(\varphi_0)\zeta^2 + \ldots \tag{5.100}$$

Because the procedure of seeking all required parameters and functions in series (5.99) are the same as in Sect. 4.4, we omit it and give only the resulting formulas and equations for two particular cases.

#### 5.5.2.1 Non-circular Cylinder

Let only the dimensionless curvature $k(\varphi)$ be a function of the angle $\varphi$, and parameters $\kappa_0(B)$, $\kappa_1(B)$, $d_1(B)$ dependent only on the induction $B$. Here the weakest line is the generatrix with the minimum curvature which can found from the conditions

$$k'(\varphi_0^\circ) = 0, \quad k''(\varphi_0^\circ) > 0, \tag{5.101}$$

and the natural frequency and damping ratio are determined by equations

$$\begin{aligned}
&\omega = \Re\,\Omega = \omega_{\mathrm{c}}\omega^*, \quad \alpha = \Im\,\Omega = \omega_{\mathrm{c}}\alpha^*,\\
&\omega^* = (f^\circ)^{1/2} + \frac{\varepsilon}{2(f^\circ)^{1/2}}\left[\frac{(1+2m)\pi^2 n^2\sqrt{f^\circ_{pp}k''(\varphi_0^\circ)}}{2l^2(p^\circ)^2} + d_1(p^\circ)^4\right],\\
&\alpha^* = -\frac{\varepsilon(f^\circ)^{1/2}\kappa_1(p^\circ)^2}{2[1+\kappa_0(p^\circ)^2]},
\end{aligned} \tag{5.102}$$

where $\omega_{\mathrm{c}} = \varepsilon^2 R^{-1}(E_{\mathrm{r}}^{(0)}/\rho)^{1/2}$ is the characteristic frequency, and $\omega^*, \alpha^*$ are dimensionless parameters. The parameter $b^\circ$ is the same as for the elastic shell - to compare s. Eq. (4.128)

$$b^\circ = \frac{\mathrm{i}\pi^2 n^2}{l^2 (p^\circ)^2} \sqrt{\frac{k''(\varphi_0^\circ)}{f_{pp}^\circ}}. \tag{5.103}$$

Here, $f_{pp}^\circ$ is the second derivative of the function (s. Eq. (4.118))

$$f(p, \varphi_0) = \frac{\pi^4 n^4 k^2(\varphi_0)}{l^4 p^4} + \frac{p^4}{1 + \kappa_0(\varphi_0) p^2} \tag{5.104}$$

with respect to $p$ calculated at constant $\kappa_0$ (not dependent of $\varphi_0$) and $p = p^\circ$, $\varphi_0 = \varphi_0^\circ$, and the parameter $p^\circ$ is found from Eq. (4.121)

$$\kappa_0 p^{10} + 2p^8 - 2\pi^4 n^4 k^2(\varphi_0^\circ) l^{-4} (\kappa_0^2 p^4 + 4\kappa_0 p^2 + 2) = 0. \tag{5.105}$$

Equations (5.102), (5.103) show that increasing the parameter $k''(\varphi_0^\circ)$ results in increasing the correction $\omega^* - \omega_0^*$ for the natural frequency, where $\omega_0^* = (f^\circ)^{1/2}$, and leads to growing power of localization of eigenmodes. To analysis the effect of a magnetic field on these modes we consider the following example.

**Example 5.13.** The sandwich cylindrical shell is assembled from the face sheets made of the ABS-plastic SD-0170 and MRE-1 core. The cross-section of the shell is an ellipse with semi-axes $e_1, e_2 (e_1 \le e_2)$. Here

$$k = \frac{r^2 + 2r'^2 - rr''}{(r^2 + r'^2)^{3/2}}, \tag{5.106}$$

where

$$r(\varphi) = \sqrt{\frac{e_1^2}{1 - \delta^2 \sin^2 \varphi}}, \quad -\pi < \varphi \le \pi, \quad \delta = \sqrt{1 - \frac{e_1^2}{e_2^2}}. \tag{5.107}$$

Then, one has two the weakest generatrix $\varphi = \varphi_0^\circ = 0$ and $\varphi = \varphi_0^\circ = \pi$. Table 5.2 shows the parameters $p^\circ$, $\omega_0^*$, $\omega^*$, $\alpha^*$, $\Im\, b^\circ$, $D_1 = 2\pi\alpha^*/\omega^*$ versus the induction $B$ for the shells with the following geometrical parameters: $R = 1$ m, $L = 1.5$ m, $e_1 = 1, e_2 = 2, h_1 = h_3 = 0.5$ mm, $h_2 = 11$ mm. The calculations were performed at $n = 1, m = 0$ in Eqs. (5.102), (5.103). The parameters $\kappa_0(\varphi_0^\circ), \kappa_1(\varphi_0^\circ), d_1(\varphi_0^\circ)$ were calculated by using Eqs. (5.94) and Figs. 5.24 and 5.25. To define the natural frequency $\omega$ and damping ratio $\alpha$, the corresponding dimensionless parameters $\omega^*, \alpha^*$ from Table 5.2 should be multiplied by the characteristic frequency $\omega_\mathrm{c}$ dependent on the thickness $h_2$ for the MR layer. Table 5.2 reveals a weak dependence of the wave parameter $p^\circ$ on the induction $B$. As for the behavior of residual parameters, one can conclude that increasing the magnetic field induction results in some increase in the natural frequency (up to 7%) and minor decrease of the parameter $\Im\, b^\circ$ specifying the width of the area where intensive vibrations occur. The effect of a magnetic field on the damping capability of the MRE-1 is found to be more appreciable. In particular, in the presence of magnetic field with the induction from 25 to 75 mT, the damping ratio $\alpha^*$ is about three times than that at $B = 0$. Thus, the localized natural modes of the non-circular sandwich cylindrical shell with MRE-1 core are insignif-

**Table 5.2** Parameters $p^\circ$, $\omega^*$, $\alpha^*$, $\Im\, b^\circ$, $D_1$ for a thin sandwich cylinder with ellipse-type cross-section vs. the magnetic induction $B$ at $h_1 = h_3 = 0.5$ mm, $h_2 = 11$ mm, $\varepsilon = 0.248$ and $\omega_c = 13.704$ Hz (after Mikhasev et al, 2014).

| $B$, mT | $p^\circ$ | $\omega^*$ | $\alpha^*$ | $\Im\, b^\circ$ | $D_1$ |
|---|---|---|---|---|---|
| 0 | 1.054 | 2.749 | 0.0040 | 0.2903 | 0.0136 |
| 25 | 1.040 | 2.846 | 0.0123 | 0.2678 | 0.0272 |
| 50 | 1.035 | 2.886 | 0.0110 | 0.2592 | 0.0240 |
| 75 | 1.032 | 2.907 | 0.0095 | 0.2546 | 0.0205 |
| 100 | 1.031 | 2.921 | 0.0082 | 0.2518 | 0.0176 |
| 125 | 1.029 | 2.930 | 0.0072 | 0.2499 | 0.0154 |
| 150 | 1.029 | 2.937 | 0.0064 | 0.2486 | 0.0136 |

icantly influenced by the magnetic field, but the associated decrement demonstrates the significant dependence on induction $B$ for the MRE-1.

#### 5.5.2.2 Circular Magnetorhelogical Elastomer-based Cylinder with Nonuniform Physical Properties

Let all geometrical parameters of a cylindrical shell be constant. The viscoelastic properties of a MRE composing layer(s) are nonuniform in the circumferential direction. Here $k \equiv 1$, and $\kappa_0, \kappa_1, d_1$ are functions of $\varphi$. Similar inhomogeneity of elastic and shear parameters may be observed if a magnetic field is spatially nonuniform or/and a MRE embedded between elastic layers is polarized and the angle between the magnetic force lines and the alignment of magnetic particles depends on a co-ordinate $\varphi$ (Fig. 5.53).

Here, the weakest generatrix $\varphi = \varphi_0^\circ$ is the line at which the reduced shear parameter $K_r$ introduced by (5.94) approaches the maximum:

$$\kappa_0'(\varphi_0^\circ) = 0, \quad \kappa_0''(\varphi_0^\circ) < 0. \tag{5.108}$$

In this case, the asymptotic approach stated in Sect. 4.4 results in the following new equations for the dimensionless frequency $\omega^*$, damping ratio $\alpha^*$ and parameter $b^\circ$

$$\omega^* = \frac{1}{(f^\circ)^{1/2}} \left\{ f^\circ + \frac{\varepsilon}{2} \left[ \frac{(1+2m)(p^\circ)^3 \sqrt{-f_{pp}^\circ \kappa_0''(\varphi_0^\circ)}}{2[1+(p^\circ)^2 \kappa_0(\varphi_0^\circ)]} + d_1(\varphi_0^\circ)(p^\circ)^4 \right] \right\},$$

$$\alpha^* = -\frac{\varepsilon (f^\circ)^{1/2} \kappa_1(\varphi_0^\circ)(p^\circ)^2}{2[1+\kappa_0(\varphi_0^\circ)(p^\circ)^2]}, \qquad b^\circ = \frac{\mathrm{i}\,(p^\circ)^3}{1+(p^\circ)^2 \kappa_0(\varphi_0^\circ)} \sqrt{-\frac{\kappa_0''(\varphi_0^\circ)}{f_{pp}^\circ}}.$$

Tables 5.3 and 5.4 reveal the effect of the applied magnetic field on parameters $p^\circ$, $\omega^*, \alpha^*, \Im\, b^\circ$, $D_1$ for two circular sandwich cylinders with nonuniform elastic and shear moduli of the same radius $R = 1$ m and length $L = 1.5$ m but having different thickness of the MRE-1 core ($h_2 = 8$ mm and $h_2 = 11$ mm, respectively). The face

sheets are the same as in the previous example. The calculations were performed at $n = 1, m = 0$, $h_1 = h_3 = 0.5$ mm. The parameter $\kappa_0''(\varphi_0^\circ)$ characterizing the variability of the reduced shear modulus in the neighborhood of the weakest generator $\varphi = \varphi_0^\circ$ has been taken as $\kappa_0'' = -1.5$ for both cases. This is the approximate value estimated proceeding from the experimental data from Boczkowska et al (2012). The parameters $\kappa_0(\varphi_0^\circ), \kappa_1(\varphi_0^\circ), d_1(\varphi_0^\circ)$ were found from Eqs. (5.94) and Figs. 5.24, 5.25. Calculations shown that for both shells accounting inhomogeneity of the reduced shear parameter $K$ results in increasing the natural frequency up to 20 %. For the second sandwich, increasing the level of magnetic field from $B = 0$ to $B = 150$ mT leads to increasing the natural frequency $\omega^*$ up to 8.4 % (from $3.304\omega_c$ at $B = 0$ mT to $3.582\omega_c$ at $B = 150$ mT) and minor decreasing the number of waves in the circumferential direction (the parameter $p^\circ$). The effect of magnetic field on the damping ratio $\alpha^*$ and logarithmic decrement $D_1$ is more complicated and appreciable. It is also influenced by the thickness $h_2$ of the MRE-1 core. For $h_2 = 8$ mm and $h_2 = 11$ mm, the best passive suppression of the eigenmodes takes place at $B = 75$ mT and $B = 25$ mT respectively. In particular, applying the magnetic field of the intensity $B = 75$ mT (at $h_2 = 8$ mm) gives three-fold increase in the damping ratio. Decreasing the parameter $\Im\, b^\circ$ under increasing the induction $B$ indicates that applying strong magnetic field results in some spreading of localized modes over the shell surface.

**Table 5.3** Parameters $p^\circ$, $\omega^*$, $\alpha^*$, $\Im\, b^\circ$, $D_1$ for a cylinder vs. induction $B$ at $h_2 = 8$ mm, $\varepsilon = 0.231, \omega_c = 13.828$ Hz (after Mikhasev et al, 2014).

| $B$, mT | $p^\circ$ | $\omega^*$ | $\alpha^*$ | $\Im\, b^\circ$ | $D_1$ |
|---|---|---|---|---|---|
| 0 | 1.479 | 3.438 | 0.0025 | 0.498 | 0.0046 |
| 25 | 1.471 | 3.472 | 0.0091 | 0.487 | 0.0165 |
| 50 | 1.466 | 3.494 | 0.0107 | 0.480 | 0.0193 |
| 75 | 1.463 | 3.511 | 0.0108 | 0.475 | 0.0193 |
| 100 | 1.461 | 3.523 | 0.0104 | 0.472 | 0.0186 |
| 125 | 1.459 | 3.534 | 0.0098 | 0.470 | 0.0175 |
| 150 | 1.458 | 3.543 | 0.0093 | 0.468 | 0.0164 |

**Table 5.4** Parameters $p^\circ$, $\omega^*$, $\alpha^*$, $\Im\, b^\circ$, $D_1$ for a cylinder vs. induction $B$ at $h_2 = 11$ mm, $\varepsilon = 0.248, \omega_c = 13.704$ Hz (after Mikhasev et al, 2014).

| $B$, mT | $p^\circ$ | $\omega^*$ | $\alpha^*$ | $\Im\, b^\circ$ | $D_1$ |
|---|---|---|---|---|---|
| 0 | 1.532 | 3.304 | 0.0133 | 0.573 | 0.0253 |
| 25 | 1.494 | 3.436 | 0.0291 | 0.519 | 0.0532 |
| 50 | 1.480 | 3.493 | 0.0266 | 0.499 | 0.0479 |
| 75 | 1.472 | 3.527 | 0.0231 | 0.488 | 0.0411 |
| 100 | 1.467 | 3.550 | 0.0201 | 0.481 | 0.0355 |
| 125 | 1.464 | 3.568 | 0.0177 | 0.477 | 0.0311 |
| 150 | 1.462 | 3.582 | 0.0157 | 0.474 | 0.0276 |

## 5.6 Suppression of Travelling Vibrations in Magnetorhelogical Elastomer-based Shells

Below we consider the special class of vibrations, localized bending waves running in the circumferential direction in MRE-based cylindrical shells of medium length. Localized non-stationary vibrations may be generated in a shell by some static (Lukasiewicz, 1979) or transient forces (Skudrzyk, 1968) applied along a line or point on the shell surface. Similar vibrations may also appear as a result of parametric excitation of a shell with variable geometric parameters (e.g., curvature, thickness or generatrix length) and/or experiencing non-uniform loading (Mikhasev, 1997; Mikhasev and Kuntsevich, 1999) and/or situated in non-stationary temperature field (Botogova and Mikhasev, 1996; Mikhasev and Kuntsevich, 1997).

If some natural modes of a shell are localized in the neighbourhood of so-called weakest line or point, then dynamic loading may result in unsteady localized vibrations running over the shell surface. In particular, growing axial force (Avdoshka and Mikhasev, 2001) or external pressure (Mikhasev, 2002) leads to splitting natural modes localized near the weakest generatrix and, as a result, generate a family of bending waves (wave packets) travelling in the circumferential direction of an isotropic elastic cylindrical shell. A similar problem on packets of bending, tangential and torsional waves in an infinite thin elastic isotropic cylindrical pipe under non-uniform internal pressure was studied in Mikhasev (1998). The above-mentioned and other papers (e.g., s. Mikhasev, 1996a,b) have detected that unsteady localized vibrations may be accompanied by such complicated effects as multiple reflection of wave packets (WPs) from more stiffen regions, focusing WPs and growth of amplitudes, which are extremely undesirable and destructive because they are the cause of the noise radiation and results in concentration of dangerous stresses in a thin-walled structure.

The main purpose of this section is to show that the application of a magnetic field allows suppressing unsteady (running) localized vibrations in laminated shells containing layers or core made of a MRE (Mikhasev et al, 2016). Using the asymptotic approach (Mikhasev and Tovstik, 2009), a solution of equations governing motion of a medium-length cylindrical MRE-based laminated shell will be constructed in the form of travelling WPs with dynamic characteristics (current frequency, amplitude, width of WPs) being tunable by means of an applied magnetic field.

### *5.6.1 Setting of the Initial Boundary Value Problem*

We consider a medium-length cylindrical laminated MRE-based shell as was stated in Sect. 5.5. The shell is sufficiently thin so that $h_* = h/R$ is a quantity of the order $\sim 0.01$ or less.

Let $\varepsilon$ be a small parameter introduced by Eq. (5.93), where all notations are the same as were assumed in Sect. 5.5. Equations (5.65) are considered as the governing

ones with the boundary conditions (5.66) at not plane edges $\alpha_j = L_2(\alpha_2)\,(j = 1, 2)$. We assume also that the geometrical dimensions and viscoelastic properties of the layers composing the shell are such that the asymptotic estimations (5.94) hold. In our case, $\delta\nu(B), \delta\eta_3(B), d_1(B), \kappa_0(B), \kappa_1(B)$ are functions of induction $B$.

We introduce the dimensionless magnitudes $\chi^*, \Phi^*$ and time $\tau$ as follows

$$\chi = \varepsilon^{-4} R\chi^*(s, \varphi, t), \quad F = E_{\mathrm{r}}^{(0)} hR^2 \Phi^*(s, \varphi, t), \quad t = \varepsilon^{-3} t_{\mathrm{c}} \tau, \tag{5.109}$$

where $t_{\mathrm{c}} = \sqrt{\rho R^2 / E_{\mathrm{r}}^{(0)}}$ is the characteristic time. Then Eqs. (5.65) may be rewritten in the dimensionless form

$$\begin{aligned} &\varepsilon^4 d(B) \Delta^2 \chi^* + k(\varphi) \frac{\partial^2 \Phi^*}{\partial s^2} + \varepsilon^2 \frac{\partial^2}{\partial \tau^2} [1 - \varepsilon^2 \kappa(B) \Delta] \chi^* = 0, \\ &\varepsilon^4 \Delta^2 \Phi^* - d(B) k(\varphi) \frac{\partial^2}{\partial s^2} [1 - \varepsilon^2 \kappa(B) \Delta] \chi^* = 0, \end{aligned} \tag{5.110}$$

and the corresponding boundary conditions are

$$\chi^* = \Delta\chi^* = \Delta^2 \chi^* = \Phi^* = \Delta\Phi^* = 0 \quad \text{at} \quad s = s_1(\varphi),\ s_2(\varphi), \tag{5.111}$$

where $s_j(\varphi) = L_j(R\varphi)/R$.

Let us consider the following initial conditions for the displacement function $\chi^*$

$$\begin{aligned} &\chi^*|_{\tau=0} = \hat{\chi}_0 \exp\left[\mathrm{i}\varepsilon^{-1} S_0(\varepsilon)\right], \\ &\dot{\chi}^*|_{\tau=0} = \mathrm{i}\varepsilon^{-1} \hat{v}_0 \exp\left[\mathrm{i}\varepsilon^{-1} S_0(\varepsilon)\right], \\ &S_0(\varphi) = a^\circ \varphi + \frac{1}{2} b^\circ \varphi^2, \quad a^\circ > 0, \quad \Im b^\circ > 0, \end{aligned} \tag{5.112}$$

$$a^\circ,\ |b^\circ|,\ |\hat{\chi}_0|,\ |\hat{v}_0|,\ \left|\frac{\partial \hat{\chi}_0}{\partial s}\right|,\ \left|\frac{\partial \hat{v}_0}{\partial s}\right| = O(1) \quad \text{when} \quad \varepsilon \to 0, \tag{5.113}$$

where $\hat{\chi}_0(s, \varphi, \varepsilon), \hat{v}_0(s, \varphi, \varepsilon)$ are complex-valued functions satisfying (5.111).

The real and imaginary parts of functions (5.112) define the two initial wave packets localized near the generatrix $\varphi = 0$ on the shell surface. These functions may be considered as approximations of the initial perturbations being the result of some transient forces applied along the line $\varphi = 0$. It should be also noted that under some conditions for parameters $a_0, b_0$, functions (5.112) coincide with the eigenmodes (5.99) localized in a vicinity of the weakest generatrix. The problem is to construct a solution of the initial-boundary-value problem (5.110)-(5.112) and to analyze the effect of applied magnetic field on the dynamic characteristics of running WPs, including amplitudes.

### 5.6.2 Asymptotic Approach

Let

$$y_j(s,\varphi)=\sin\frac{\pi j[s-s_1(\varphi)]}{l(\varphi)}\quad\text{and}\quad\lambda_j=\frac{\pi^4 j^4}{l^4(\varphi)},\quad j=1,2,3,\dots \tag{5.114}$$

be an infinite system of eigenfunctions and associated eigenvalues of the boundary-value problem

$$\frac{\mathrm{d}^4 y}{\mathrm{d}s^4}-\lambda y=0, \tag{5.115}$$

$$y=y''=0\quad\text{at}\quad s=s_1(\varphi),\ s=s_2(\varphi), \tag{5.116}$$

where $l(\varphi)=s_2(\varphi)-s_1(\varphi)$.

Because the functions $\chi_0(s,\varphi), v_0(s,\varphi)$ appearing in (5.112) satisfy the boundary conditions (5.111), they can be expanded in terms of the eigenfunctions $y_j(s,\varphi)$ into uniformly convergent series in some section $\varphi_1\le\varphi\le\varphi_2$

$$\begin{aligned}\hat\chi_0&=\sum_{j=1}^{\infty}\chi_j^\circ(\varphi,\varepsilon)y_j(s,\varphi),\quad \chi_j^\circ=\int\limits_{s_1(\varphi)}^{s_2(\varphi)}\hat\chi_0(s,\varphi,\varepsilon)y_j(s,\varphi)\mathrm{d}s,\\ \hat v_0&=\sum_{j=1}^{\infty}v_j^\circ(\varphi,\varepsilon)y_j(s,\varphi),\quad v_j^\circ=\int\limits_{s_1(\varphi)}^{s_2(\varphi)}\hat v_0(s,\varphi,\varepsilon)y_j(s,\varphi)\mathrm{d}s.\end{aligned} \tag{5.117}$$

It is assumed that $\chi_j^\circ, v_j^\circ$ are polynomials of $\varepsilon^{-1/2}$ whose coefficients are regular functions of $\varepsilon$. Then they may be represented by the series

$$\chi_j^\circ=\sum_{i=0}^{\infty}\varepsilon^{i/2}\chi_{ji}^\circ(\zeta),\ \chi_{ji}^\circ(\zeta)=\sum_{\iota=0}^{M_{ji}}c_{ji\iota}^\circ\zeta^\iota,\ v_j^\circ=\sum_{i=0}^{\infty}\varepsilon^{i/2}v_{ji}^\circ(\zeta),\ v_{ji}^\circ(\zeta)=\sum_{\iota=0}^{M_{ji}}d_{ji\iota}^\circ\zeta^\iota \tag{5.118}$$

where $\zeta=\varepsilon^{-1/2}\varphi$, and $c_{j\,i\,\iota}^\circ, d_{j\,i\,\iota}^\circ=O(1)$.

Due to linearity of the initial-boundary-value problem (5.110)-(5.112), its solution may be presented in the form

$$\chi^*=\sum_{j=1}^{\infty}\chi_j^*(s,\varphi,\tau,\varepsilon),\quad \Phi^*=\sum_{j=1}^{\infty}\Phi_j^*(s,\varphi,\tau,\varepsilon), \tag{5.119}$$

where $\chi_j^*,\Phi_j^*$ are the required functions localized in a neighborhood of moving generatrix $\varphi=q_j(\tau)$. Here $q_j(t)$ is a twice differentiable function such that $q_j(0)=0$. The pair of functions $\chi_j^*,\Phi_j^*$ is called the $j^{\text{th}}$ wave packet (WP) with the center at $\varphi=q_j(\tau)$ (Mikhasev, 2002).

#### 5.6.2.1 Initial Boundary Value Problem for the $j^{\text{th}}$ Wave Packet

Let us hold any natural number $j$ fixed and study the behavior of the $j^{\text{th}}$ WP. It is convenient to go over to a local co-ordinate system $\varphi = q_j(\tau) + \varepsilon^{1/2}\xi_j$ associated with the moving center $\varphi = q_j(\tau)$. In the new co-ordinate system, equations (5.110) read

$$
\begin{aligned}
&d(B)\left(\varepsilon^2\frac{\partial^4\chi_j^*}{\partial\xi_j^4} + 2\varepsilon^3\frac{\partial^4\chi_j^*}{\partial\xi_j^2\partial s^2} + \varepsilon^4\frac{\partial^4\chi_j^*}{\partial s^4}\right) + k(\varphi)\frac{\partial^2\Phi_j^*}{\partial s^2} \; + \left(\varepsilon^2\frac{\partial^2}{\partial\tau^2}\right.\\
&\left.-2\varepsilon^{3/2}\dot q_j\frac{\partial^2}{\partial\xi_j\partial\tau} + \varepsilon\dot q_j^2\frac{\partial^2}{\partial\xi_j^2} - \varepsilon^{3/2}\ddot q_j\frac{\partial}{\partial\xi_j}\right)\left[\chi_j^* - \kappa(B)\left(\varepsilon\frac{\partial^2\chi_j^*}{\partial\xi_j^2} + \varepsilon^2\frac{\partial^2\chi_j^*}{\partial s_j^2}\right)\right] = 0,\\
&\varepsilon^2\frac{\partial^4\Phi_j^*}{\partial\xi_j^4} + 2\varepsilon^3\frac{\partial^4\Phi_j^*}{\partial\xi_j^2\partial s^2} + \varepsilon^4\frac{\partial^4\Phi_j^*}{\partial s^4}\\
&-d(B)k(\varphi)\frac{\partial^2}{\partial s^2}\left[\chi_j^* - \kappa(B)\left(\varepsilon\frac{\partial^2\chi_j^*}{\partial\xi_j^2} + \varepsilon^2\frac{\partial^2\chi_j^*}{\partial s_j^2}\right)\right] = 0,
\end{aligned}
\tag{5.120}
$$

where $\kappa = \kappa_0(B) + \mathrm{i}\kappa_1(B)$, and the function $k(\varphi)$, $s_1(\varphi)$, $s_2(\varphi)$ are expanded into a series in the neighborhood of the center $\varphi = q_j(\tau)$. For instance,

$$
k(\varphi) = k[q(t)] + \varepsilon^{1/2}k'[q(t)]\xi_j + \frac{1}{2}\varepsilon k''[q(\tau)]q_j^2 + \ldots \tag{5.121}
$$

Here and in what follows, the dot $(\cdot)$ and prime $(\prime)$ denote differentiation with respect to dimensionless time $\tau$ and angle $\varphi$, respectively.

The initial conditions for $j^{\text{th}}$ WP take the form

$$
\begin{aligned}
&\chi_j^*|_{\tau=0} = \chi_j^\circ(\varphi,\varepsilon)y_j(s,\varphi)\exp\left[\mathrm{i}\varepsilon^{-1}S_0(\varphi)\right],\\
&\dot\chi_j^*|_{\tau=0} = \mathrm{i}\varepsilon^{-1}v_j^\circ(\varphi,\varepsilon)y_j(s,\varphi)\exp\left[\mathrm{i}\varepsilon^{-1}S_0(\varphi)\right].
\end{aligned}
\tag{5.122}
$$

The dynamic stress state of the shell consists of the basic stress state and the dynamic edge-effect integrals describing the shell behavior in a small neighborhood of each edge. To study the basic state on each edge, we have to satisfy two basic conditions only. Apart from terms of the order $\varepsilon^2$, these conditions for the $j^{\text{th}}$ WP have the form

$$
\chi_j^* = \Phi_j^* = 0 \quad \text{at} \quad s = s_1(\varphi), s_2(\varphi). \tag{5.123}
$$

We note that the functions $y_j(s,\varphi)$ should be also expended into series in a vicinity of the center $\varphi = q_j(\tau)$. In what follows, we omit the subscript $j$. For instance, the notations $\chi_j^*, \chi_j^\circ, y_j, \chi_{ji}^\circ, \xi_j, c_{ji\iota}^\circ$ are replaced by $\chi^*, \chi^\circ, y, \chi_i^\circ, \xi, c_{i\iota}^\circ$, respectively.

When following to the asymptotic approach developed in Mikhasev and Tovstik (2009), the solution of the initial-boundary-value problem (5.120), (5.122), (5.123) may be constructed in the form of complex WKB-approximations

$$\chi^* = \sum_{\varsigma=0}^{\infty} \varepsilon^{\varsigma/2} \chi_\varsigma \exp\left(\mathrm{i}\varepsilon^{-1} S\right),\ \Phi^* = \sum_{\varsigma=0}^{\infty} \varepsilon^{\varsigma/2} \Phi_\varsigma \exp\left(\mathrm{i}\varepsilon^{-1} S\right),$$
$$S(\xi,\tau) = \int_0^\tau \omega(\tilde{\tau})\mathrm{d}\tilde{\tau} + \varepsilon^{1/2} p(\tau)\xi + \frac{1}{2}\varepsilon b(\tau)\xi^2. \tag{5.124}$$

In anzatz (5.124), $\Im b(\tau) > 0$ for any time $\tau > 0$, $\chi_\varsigma(s,\xi,\tau), \Phi_\varsigma(s,\xi,\tau)$ are polynomials in $\xi$ with complex coefficients depending on $\tau$ and $s$, $|\omega(\tau)|$ is the current frequency of vibrations in the neighborhood of the moving center $\varphi = q(t)$, $p(\tau)$ is the variable wave parameter, and $b(\tau)$ defines the width of the $j^{\text{th}}$ WP, the inequality $\Im b(\tau) > 0$ guaranteeing attenuation of wave amplitudes within the WP.

As seen, functions (5.124) approximate running unsteady localized vibrations in the shell. In the case when $q = 0$, and $\omega, p, b, \chi_\varsigma$ and $\Phi_\varsigma$ are independent of time $\tau$, expansions (5.124) are degenerated into the stationary WP, like (5.99), describing free localized vibrations in a vicinity of the fixed (weakest) generatrix.

#### 5.6.2.2 Sequence of One-dimensional Boundary Value Problems on *Moving Generatrix*

To define all required functions appearing in ansatz (5.124), one needs to substitute them into governing equations and boundary conditions as well. The substitution of expansions (5.124) into Eqs. (5.120) results in a sequence of 1D differential equations

$$\sum_{j=0}^{\varsigma} \mathbf{L}_j \chi_{\varsigma-j} = 0, \quad \varsigma = 0, 1, 2, \ldots \tag{5.125}$$

where

$$\mathbf{L}_0 z = \frac{k^2(q) d(B)[1+\kappa_0(B)p^2]}{p^4} \frac{\partial^4 z}{\partial s^4} + \left\{p^4 - [1+\kappa_0(B)p^2](\omega - \dot{q}p)^2\right\} z,$$

$$\begin{aligned}
\mathbf{L}_1 &= (b\mathbf{L}_p + \mathbf{L}_q + \dot{p}\mathbf{L}_\omega)\,\xi - \mathrm{i}\mathbf{L}_p \frac{\partial}{\partial \xi},\\
\mathbf{L}_2 &= \left(b^2\mathbf{L}_{pp} + 2b\mathbf{L}_{pq} + \mathbf{L}_{qq} + \dot{p}^2\mathbf{L}_{\omega\omega} + 2\dot{p}\mathbf{L}_{\omega q}\right.\\
&\quad \left. +\ 2\dot{p}b\mathbf{L}_{\omega p} + \dot{b}\mathbf{L}_\omega\right)\xi^2 - \frac{1}{2}\mathbf{L}_{pp}\frac{\partial^2}{\partial \xi^2} - \mathrm{i}\,(b\mathbf{L}_{pp} + \mathbf{L}_{pq} + \dot{p}\mathbf{L}_{\omega p})\,\xi\frac{\partial}{\partial \xi}\\
&\quad - \mathrm{i}\mathbf{L}_\omega \frac{\partial}{\partial t} - \mathrm{i}\left(\frac{1}{2}b\mathbf{L}_{pp} + \frac{1}{2}\dot{\omega}\mathbf{L}_{\omega\omega} + \dot{p}\mathbf{L}_{\omega p} + \frac{1}{2}\mathbf{L}_{pq} + \ddot{q}p + \mathbf{N}\right), \ldots,
\end{aligned} \tag{5.126}$$

$$\mathbf{N} = \frac{\mathrm{i}\kappa_1(B) d(B) p^6(\tau)}{1+\kappa_0(B)p^2(\tau)}.$$

In Eqs. (5.126), the subscripts $p, q, \omega$ denote the differentiation with respect to the corresponding variables $p, q, \omega$. Operators $L_\varsigma$ for $\varsigma \geq 3$ are not written out here because of its awkwardness.

The functions $\Phi_\varsigma$ may be found step by step from a sequence of inhomogeneous equations and expressed in terms of the functions $\chi_\varsigma$. The substitution of (5.124) into the basic boundary conditions lead to the sequence of boundary conditions at the moving center of the $j^{\text{th}}$ WP

$$\chi_0 = 0, \qquad \frac{\mathrm{d}^2\chi_0}{\mathrm{d}s^2} = 0 \quad \text{at} \quad s = s_i[q(t)]; \tag{5.127}$$

$$\chi_1 + \xi s_i' \frac{\partial \chi_0}{\partial s} = 0, \quad \frac{\partial^2 \chi_1}{\partial s^2} + \xi s_i' \frac{\partial^3 \chi_0}{\partial s^3} = 0 \quad \text{at} \quad s = s_i[q(t)]; \quad \ldots \tag{5.128}$$

The sequence of the 1D boundary-value-problems (5.125)-(5.128) serves for determination of required functions appearing in (5.124). The procedure for their seeking is given in Mikhasev and Tovstik (2009); Mikhasev (2002). Omitting its details, we shall give here only the principal equations.

#### 5.6.2.3 Zeroth-order Approximation

In the leading approximation ($\varsigma = 0$), one has the homogeneous ordinary differential equation (5.125) with the homogeneous boundary conditions (5.127). Its solution may be presented in the form

$$\chi_0(s, \xi) = P_0(\xi, \tau) y[s, q(\tau)], \tag{5.129}$$

where $P_0(\xi, \tau)$ is an unknown polynomial in $\xi$. Substituting Eq. (5.129) into Eq. (5.125) at $\varsigma = 0$ yields the relation

$$\omega = \dot{q}(\tau) p(\tau) \mp H[p(\tau), q(\tau), \tau] \tag{5.130}$$

coupling the current frequency $\omega(\tau)$ to the wave parameter $p(\tau)$ and the group velocity $v(\tau) = \dot{q}(\tau)$ of the $j^{th}$ WP, where

$$H(p, q, \tau) = \sqrt{d[B(\tau)] \left\{ \frac{p^4}{1 + \kappa_0[B(\tau)] p^2} + \frac{\lambda(q) k^2(q)}{p^4} \right\}} \tag{5.131}$$

is the Hamilton function. In Eqs. (5.130), the signs $\pm$ indicate the availability of positive and negative branches of the required solution.

#### 5.6.2.4 First-order Approximation

In the first-order approximation (at $\varsigma = 1$), we arrive at the non-homogeneous differential equation (5.125) with the non-homogeneous boundary conditions (5.128). The

compatibility condition for this non-homogeneous boundary-value problem results in the two Hamiltonian systems

$$\dot{q} = \frac{\partial H}{\partial p}, \quad \dot{p} = -\frac{\partial H}{\partial q} \qquad \text{and} \qquad \dot{q} = -\frac{\partial H}{\partial p}, \quad \dot{p} = \frac{\partial H}{\partial q} \tag{5.132}$$

corresponding to the positive and negative branches of the solution, respectively. These solutions are associated with two WPs moving in the opposite directions. In what follows, all calculations are given for the positive $j^{\text{th}}$ WP governed by Eqs. $(5.132)_1$. Comparing anzatz (5.124) with the initial condition (5.122) for the $j^{\text{th}}$ WP, we readily obtain the initial conditions for the Hamiltonian system

$$p(0) = a^{\circ}, \quad q(0) = 0. \tag{5.133}$$

#### 5.6.2.5 Second-order Approximation

The compatibility condition for the non-homogeneous boundary-value problem (5.125), (5.128) arising in the second-order approximation ($\varsigma = 2$) yields

$$(\xi^2 \mathbf{D}_b - 2\mathbf{D}_{\xi t}) P_0 = 0, \tag{5.134}$$

where

$$\mathbf{D}_b = \dot{b} + H_{pp} b^2 + 2H_{pq} b + H_{qq}, \quad \mathbf{D}_{\xi t} = \hat{h}_0 \frac{\partial^2}{\partial \xi^2} + \hat{h}_1 \xi \frac{\partial}{\partial \xi} + \hat{h}_2 \frac{\partial}{\partial t} + \hat{h}_3,$$

$$\hat{h}_0(t) = \frac{1}{2} H_{pp}, \quad \hat{h}_1(t) = \mathrm{i}(bH_{pp} + H_{pq}), \quad \hat{h}_2 = \mathrm{i},$$

$$\hat{h}_3(t) = \frac{\mathrm{i}}{2H} \left\{ bHH_{pp} - \dot{\omega} - 2H_q H_p + \ddot{q}p + \frac{1}{\eta} \int_{s_1}^{s_2} \mathbf{L}_{\omega} \dot{y} y \mathrm{d}s + \Gamma \right\},$$

$$\Gamma(t) = -\frac{2k(\tau)k'(\tau)d(B)[2 + \kappa_0(B)p^2(\tau)]\lambda[q(\tau)]}{p^5(\tau)} - \frac{d(B)\kappa_1(B)p^6(\tau)}{1 + \kappa_0(B)p^2(\tau)}.$$

Equation (5.134) has a solution of polynomial form if and only if the function $b(\tau)$ satisfies the Riccati equation

$$\dot{b} + H_{pp} b^2 + 2H_{pq} b + H_{qq} = 0. \tag{5.135}$$

The repeated comparison of Eqs. (5.124) and (5.122) gives the initial condition

$$b(0) = b^{\circ} \tag{5.136}$$

for the above equation.

Taking into account the Riccati equation, Eq. (5.134) is reduced to the following equation

$$\mathbf{D}_{\xi t}P_0 \equiv \hat{h}_0\frac{\partial^2 P_0}{\partial \xi^2} + \hat{h}_1\xi\frac{\partial P_0}{\partial \xi} + \hat{h}_2\frac{\partial P_0}{\partial \tau} + \hat{h}_3 P_0 = 0 \tag{5.137}$$

called the amplitude one. Its solution in two different forms has been given in Mikhasev (2002). We adduce here the solution expressed in terms of the Hermite polynomials. Such presentation will be suitable in two special cases:

1. to compare expansion (5.124) with the localized natural mode (5.99);
2. to study the effect of non-stationary magnetic field on eigenmode (5.99).

The required polynomial $P_0(\xi,\tau)$ in $\xi$ with coefficients depending on dimensionless time $\tau$ may be represented in the form:

$$P_0 = \Theta_m(\tau)\mathcal{H}_m(x), \tag{5.138}$$

where $\mathcal{H}_m(x)$ is the Hermite polynomials in $x$ of the $m$th degree, and

$$\begin{gathered} x = \hat{\varrho}(\tau)\xi, \quad \hat{\varrho}(\tau) = \frac{\exp\left[-\int \dfrac{\hat{h}_1(\tau)\mathrm{d}\tau}{\hat{h}_2(\tau)}\right]}{\sqrt{4\int \dfrac{\hat{h}_0(\tau)}{\hat{h}_2(\tau)}\exp\left[-2\int \dfrac{\hat{h}_1(\tau)\mathrm{d}\tau}{\hat{h}_2(\tau)}\right]\mathrm{d}\tau}}, \\ \Theta_m(\tau) = \frac{\left\{4\int (\hat{h}_0/\hat{h}_2)\exp\left[-2\int (\hat{h}_1/\hat{h}_2)\mathrm{d}\tau\right]\mathrm{d}\tau\right\}^{m/2}}{\exp\left[\int (\hat{h}_3/\hat{h}_2)\mathrm{d}\tau\right]}. \end{gathered} \tag{5.139}$$

It is evident that the polynomial

$$P_0(\xi,\tau;c_m) = \sum_{m=0}^{M} c_m\Theta_m(\tau)\mathcal{H}_m[\hat{\varrho}(\tau)\xi] \tag{5.140}$$

of the $M$th degree is also the solution of the amplitude equation (5.137), where $c_m$ are arbitrary constants found from the initial conditions.

#### 5.6.2.6 Higher-order Approximations

To find $\chi_\varsigma, \Phi_\varsigma$ for $\varsigma \geq 1$, one need to consider corresponding boundary-value problem (5.125), (5.128) in the $\varsigma + 2$nd approximation. The existence of a solution of this problem results in the non-homogeneous differential equation

$$\mathbf{D}_{\xi t}P_\varsigma = P_\varsigma^* \tag{5.141}$$

for a polynomial $P_\varsigma(\chi,\tau)$, where $P^*_\varsigma(\chi,\tau)$ is some polynomial expressed by means of polynomials $P_0,\dots,,P_{\varsigma-1}$. However, we interrupt the formal procedure of seeking $\chi_1,\chi_2,\dots$ because the accuracy of governing equations (5.110) is not sufficient.

### 5.6.3 Solution of the Initial Boundary Value Problem in the Leading Approximation

We note that there exist two branches of solutions of the initial boundary-value problem. Let $p^+(\tau),q^+(\tau)$ and $p^-(\tau),q^-(\tau)$ be solutions of the Hamiltonian systems $(5.132)_1$ and $(5.132)_2$, respectively. Here, $\varphi=q^+(\tau)$ and $\varphi=q^-(\tau)$ are centers of the positive and negative WPs moving in the opposite directions. We introduce also the local coordinates

$$\xi^\pm=\varepsilon^{-1/2}[\varphi-q^\pm(\tau)]. \tag{5.142}$$

in the scaled coordinate systems with centers at the moving generatrix $\varphi=q^\pm(\tau)$. Then

$$\omega^\pm,\quad b^\pm,\quad P_0^\pm,\quad \chi_0^\pm,\quad \Phi_0^\pm \tag{5.143}$$

are found above functions corresponding to the positive and negative WPs, respectively. Consider the following functions:

$$\chi=\chi^+ +\chi^-,\quad \Phi=\Phi^+ +\Phi^-, \tag{5.144}$$

where

$$\begin{aligned}
&\chi^\pm=\left[\chi_0^\pm+O\left(\varepsilon^{1/2}\right)\right]\exp\left(\mathrm{i}\varepsilon^{-1}S^\pm\right),\\
&\Phi^\pm=\left[\Phi_0^\pm+O\left(\varepsilon^{1/2}\right)\right]\exp\left(\mathrm{i}\varepsilon^{-1}S^\pm\right),\\
&\chi_0^\pm=P_0^\pm(\xi^\pm,\tau;\,c_m^\pm)y[s,q^\pm(\tau)],\quad P_0^\pm=\sum_{m=0}^{M}c_m^\pm\Theta_m(\tau)\mathcal{H}_m[\hat{\varrho}(\tau)\xi^\pm],\\
&\Phi_0^\pm=\frac{d(B)k[q^\pm(\tau)]P_0^\pm(\xi^\pm;\tau;\,c_m^\pm)}{[p^\pm(\tau)]^4}\left[\frac{\partial^2y(s,\varphi)}{\partial s^2}+\kappa(B)[p^\pm(\tau)]^2y(s,\varphi)\right]_{\varphi=q^\pm(\tau)},\\
&S^\pm=\int_0^\tau\omega^\pm(\tilde{\tau})\mathrm{d}\tilde{\tau}+\varepsilon^{1/2}p^\pm(\tau)\xi^\pm+\frac{1}{2}\varepsilon b^\pm(\tau)(\xi^\pm).
\end{aligned} \tag{5.145}$$

The composed functions (5.144) are the leading approximation of the required solution of the initial-boundary-value problem (5.110)-(5.112) for the fixed $j$. They contain undefined constants $c_m^\pm$ which are found from the initial conditions for the WPs with the fixed number $j$ (we remind that a number $j$ is associated with the number of eigenvalue $\lambda$ of the boundary-value problem (5.115), (5.116)). If the polynomials $P_0^\pm$ are expressed in terms of the Hermite polynomials, then as shown in Mikhasev (2002), these constants calculated by the equation

$$c_m^{\pm} = \frac{1}{2^{m+1} m! \sqrt{\pi} \Theta_m(0)} \int\limits_{-\infty}^{+\infty} \mathrm{e}^{-\zeta^2} \mathcal{H}_m[\hat{\varrho}(0)\zeta] \left[ \chi_0^{\circ}(\zeta) \mp \frac{v_0^{\circ}(\zeta)}{H^{\circ}} \right] \mathrm{d}\zeta, \qquad (5.146)$$

where $\chi_0^{\circ} \equiv \chi_{j0}^{\circ}, v_0^{\circ} \equiv v_{j0}^{\circ}$ are polynomials evaluated by Eqs. (5.118), and $H^{\circ} = H(a^{\circ}, 0, 0)$ is the initial value of the Hamiltonian function.

**Remark 5.3.** Let the parameters $q = 0, p = a^{\circ}$ satisfy equations

$$H_p = 0, \quad H_q = 0, \qquad (5.147)$$

and $b = b^{\circ}$ is the solution of the quadratic equation

$$H_{pp} b^2 + 2H_{pq} b + H_{qq} = 0 \qquad (5.148)$$

in the absence of magnetic field ($B = 0$). Then $p^{\pm}(\tau) \equiv a^{\circ}, q^{\pm}(\tau) \equiv 0$ and $b^{\pm}(\tau) \equiv b^{\circ}$ are the solutions of the Hamiltonian systems and Riccati equations, respectively, at $B = 0$. In this case, the constructed solution (5.144)-(5.146) gives the stationary WP with the center $\varphi = 0$, which coincide with the localized natural mode (5.99).

In what follows, we shall study the effect of growing magnetic field on the localized eigenmodes (5.99) being characteristics of a shell without magnetic field.

## *5.6.4 Running Localized Vibrations in Magnetorhelogical Elastomer-based Cylindrical Shells vs. Magnetic Field*

The constructed asymptotic solution (5.144)-(5.146) may be used to predict the response of a laminated MRE-based shell to the initial localized perturbations at the shell surface taking into account an applied magnetic field. We note that the principal tunable parameters $d(B), \kappa(B)$ and $\kappa_1(B)$ appearing in the Hamiltonian function and amplitude equation depend on the magnetic field induction $B$. Varying the intensity of magnetic field, one can affect the behavior of running WPs and softly suppress vibrations as well.

### 5.6.4.1 Wave Packets in Shells with Constant Parameters

At first, we consider the simplest case when all geometrical parameters, including the curvature and the generatrix length, are constants, and the applied magnetic field is non-stationary. Here $k \equiv 1$, $s_1 = 0$, $s_2 = l$ and the induction $B(\tau)$ is a function of the dimensionless time $\tau$. In this case, the Hamilton function for the $j^{\text{th}}$ WP is simplified

$$H(p, \tau) = \sqrt{d[B(t)] \left\{ \frac{p^4}{1 + \kappa_0[B(t)] p^2} + \frac{\pi^4 j^4}{l^4 p^4} \right\}}, \qquad (5.149)$$

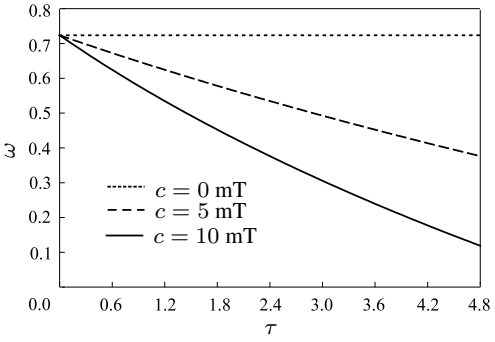


**Fig. 5.54** Dimensionless current frequency $\omega = |\omega^{\pm}(\tau)|$ versus dimensionless time for different $c = 0, 5, 10$ mT (after Mikhasev et al, 2016).

and the Hamiltonian systems and Riccati equations admit solutions in the explicit form

$$p^{\pm} = a^{\circ}, \quad q^{\pm}(\tau) = \pm \int_0^{\tau} H_p \mathrm{d}\tau, \quad \omega^{\pm}(\tau) = \pm a^{\circ} H_p \mp H,$$
$$b^{\pm}(\tau) = \frac{b_0}{1 + b_0 \int_0^{\tau} H_{pp} \mathrm{d}\tau}. \tag{5.150}$$

If the magnetic field is constant, then the current frequencies $|\omega^{\pm}|$ for both WPs are constants; if not, then $|\omega^{\pm}(\tau)|$ are time-dependent. The functions $\Im b^{\pm}(\tau)$ characterize the size of the shell area spanned by vibrations and $\chi_0^{\pm}(\tau)$ define the amplitudes of these unsteady vibrations. To analyze the effect of magnetic field on travelling WPs in detail, we consider the following example.

**Example 5.14.** A sandwich cylindrical shell is assembled from two face sheets made of ABS-plastic SD-0170 and MRE-1 core. The geometrical parameters are the following: $R = 0.4$ m, $L = 1.5$ m, $h_1 = h_3 = 0.5$ mm, $h_2 = 11$ mm. The numerical computations of magnitudes $\omega = |\omega^{\pm}(\tau)|, \Im b = \Im b^{\pm}(\tau), |\chi_0| = |\chi_0^{\pm}(\tau)|$ versus dimensionless time were performed for two different cases: (a) $B = 0$; (b) the magnetic induction $B(\tau) = c\tau$ is the linear function of dimensionless time at $c = 5, 10$ mT. The following parameters were considered as the initial ones: $a_0 = 2.5$, $b_0 = \mathrm{i}$, $\chi_1^{\circ} = 1$, $v_1^{\circ} = 0$ and $\chi_j^{\circ} = v_j^{\circ} = 0$ at $j > 1$. Figure 5.54 shows that for the accepted parameters and case (b) the current frequency $\omega(\tau)|$ is the decreasing function of time. As seen from Fig. 5.55, the width of the $1^{\mathrm{st}}$ running WP increases in time for both cases, (a) and (b), that means that the WP spreads in the circumferential direction. But the speed of this spreading depends weakly on whether the magnetic field is stationary or time-dependent. As concerns the wave amplitudes (s. Fig. 5.56), they demonstrate a very strong dependence on the visco-elastic properties of MREs which are affected by the applied magnetic field. The curve corresponding to $c = 0$ mT shows the capability of the MRE to damp travelling vibrations in the sandwich without magnetic field. The other two curves

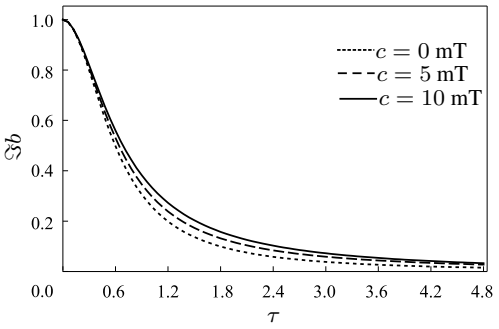


**Fig. 5.55** Parameter $\Im b = \Im b^{\pm}(\tau)$ vs. dimensionless time for different $c = 0, 5, 10$ mT (after Mikhasev et al, 2016).

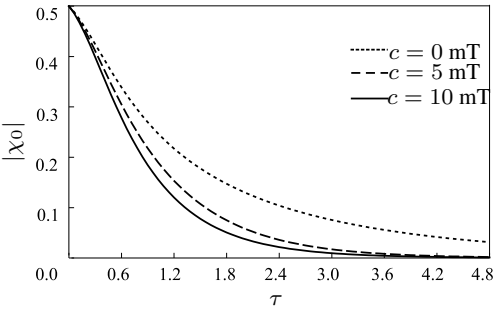


**Fig. 5.56** Maximum amplitude $|\chi_0|$ versus dimensionless time for different $c = 0, 5, 10$ mT (after Mikhasev et al, 2016).

bring out clearly that this capability becomes stronger under the action of growing magnetic field. So, when comparing amplitudes at the fixed moment $\tau = 2.4$, one can see that the maximum amplitude $|\chi_0|$ for $c = 5$ mT and $c = 10$ mT are 3-and 6-times less, respectively, than that for $c = 0$ mT.

### 5.6.4.2 Wave Packets in Shells with Variable Geometrical Parameters

The numerical calculations performed by Mikhasev and Tovstik (1990) for single-layer isotropic shells revealed that behavior of excited WPs in shells with variable curvature or/and generatrix length may be very complicated and characterized by reflection of WPs possessing a small initial energy from some generatrix. As a rule, these reflections are accompanied by strong focusing of WPs and growing amplitudes. Additionally, if a shell is subjected to an external dynamic load (Avdoshka and Mikhasev, 2001; Mikhasev, 2002), then increasing amplitudes in running WPs may be dramatic and lead to possible dynamic instability of a structure. To study similar effects in MRE-based shell with variable geometrical parameters, we apply to the next example

**Example 5.15.** Consider a circular sandwich cylindrical shell with an oblique edge as shown in Fig. 5.57. Here

$$k = 1, \quad s_1 = 0, \quad s_2(\varphi) = l_0 + (\cos\varphi - 1)\tan\alpha, \tag{5.151}$$

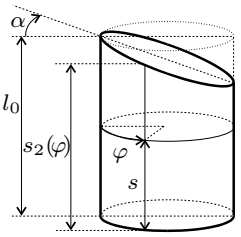


**Fig. 5.57** Medium surface of a circular cylindrical shell with oblique edge. (after Mikhasev et al, 2016).

where $Rl_0$ is the longest generatrix length and $\alpha$ is the slope angle of the oblique edge. The viscoelastic properties of two elastic layers and MRE core are the same as in Example 5.14 and the geometrical parameters are the following: $h_1 = h_3 = 0.5$ mm, $h_2 = 11$ mm, $R = 0.4$ m, $l_0 = 2$.

For this shell, the longest generatrix $\varphi = \varphi_0^\circ = 0$ is the weakest one. The natural modes (5.99) localized in the neighbourhood of this line are characterized by parameters $p = a^\circ$, $b = b^\circ$ which jointly with $q = 0$ are determined as the solutions of Eqs. (5.138), (5.148) for $j = 1$ (s. Remark 5.3). As the initial conditions for Hamiltonian systems $(5.132)_1$, $(5.132)_2$ and Riccati equation (5.135), we assume the above parameters $p = a^\circ$, $q = 0$, $b = b^\circ$. In other words, up to amplitudes $\chi_j^\circ, \mathrm{i}\varepsilon^{-1}v_j^\circ$, one of the localized eigenmodes (5.99) with $j = 1$ semi-waves in the axial direction to be considered as the initial WP. It is of interest to study its behavior when apply non-stationary magnetic field with the induction $B = c\tau$.

Figures 5.58 to 5.62 show parameters $p^+, q^+, \omega^+, \Im b^+, |\Re\chi_0^+|, |\Im\chi_0^+|$ vs. dimensionless time $\tau$ for different $c = 0, 5$ and $10$ mT. The calculations were performed for the $1^{\mathrm{st}}$ positive WP (at $j = 1$) with the initial amplitudes $\chi_1^\circ = 1$, $v_1^\circ = 0$ in (5.122). Due to the symmetry of the shell and the initial WP with regard to the plane $\varphi = 0$, the curves for all functions corresponding to the negative WP are the same as in Figs. 5.58-5.62. In all figures the straight dotted lines correspond to the eigenform localized in the neighborhood of the longest generatrix $\varphi = 0$. Thus, if a magnetic field is absent ($c = 0$ mT), the initial WP coinciding with one of eigenmodes stays motionless, with the wave number $p^+$, eigenfrequency $\omega^+$ and parameter $b^+$ being constants for any point of time. The maximum amplitude of free

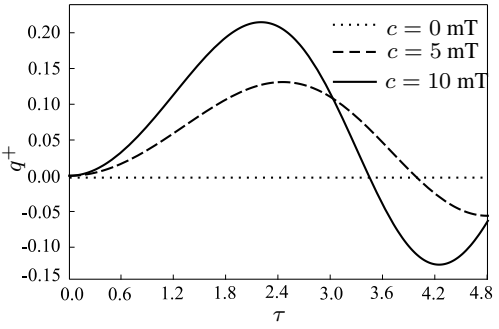


**Fig. 5.58** Center $\varphi = q^+ = 0$ of the initial WP (at $c = 0$ mT) and the center $\varphi = q^+$ of the $1^{\mathrm{st}}$ positive WP versus dimensionless time $\tau$ at different rates of growing of the magnetic field induction, $c = 5, 10$ mT (after Mikhasev et al, 2016).

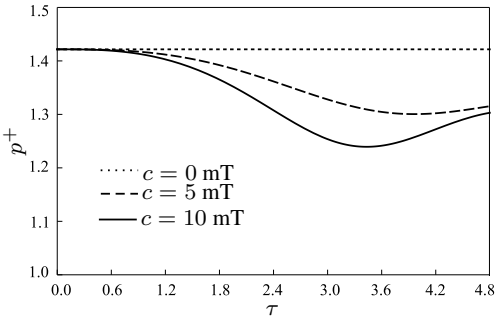


**Fig. 5.59** Wave parameter $p^+ = a_0 \approx 1.41$ of the initial WP (at $c = 0$ mT) and parameter $p^+$ of the 1st positive WP versus dimensionless time $\tau$ at different rates of growing of the magnetic field induction, $c = 5, 10$ mT (after Mikhasev et al, 2016).

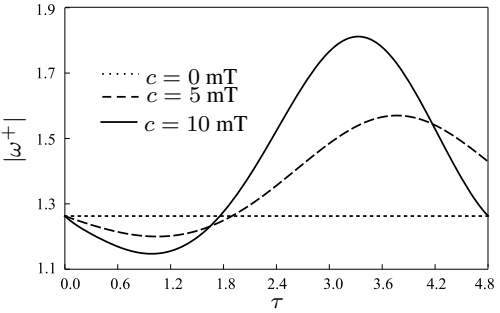


**Fig. 5.60** Natural frequency $|\omega^+| = \omega_0 \approx 1.25$ of the initial WP (at $c = 0$ mT) and the current frequency $|\omega^+|$ of the 1st positive WP versus dimensionless time $\tau$ at different rates of growing of the magnetic field induction, $c = 5, 10$ mT (after Mikhasev et al, 2016).

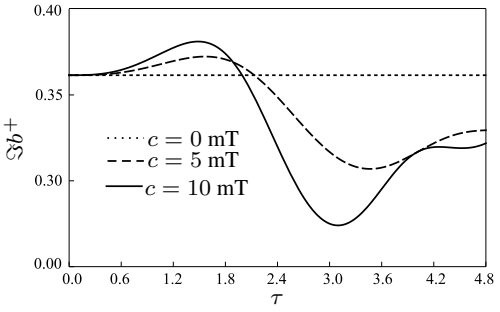


**Fig. 5.61** Parameter $\Im b^+ = \Im b_0 \approx 0.36$ for the initial WP and parameter $\Im b^+$ for the 1st positive WP versus dimensionless time at different rates of growing of the magnetic field induction, $c = 5, 10$ mT (after Mikhasev et al, 2016).

vibrations (s. Fig. 5.62) is the decreasing function of the dimensionless time $\tau$ due to viscoelastic properties of the MRE core regardless of whether the magnetic field is applied or not.

Interesting effects are observed when the magnetic field is applied. After its turning on, the eigenmode (initial WP) is spitted into two WPs, positive and negative ones, travelling in the opposite directions (s. Fig. 5.58). Figure 5.58 shows also that the increase of the magnetic field results in the multiple refections of the WP from the certain generatrices $\varphi = \varphi_{\rm r} = q^+(\tau_{\rm r})$, these refections being accompanied by slight focusing (s. Fig. 5.61). Herewith, the larger the growth rate of the induction (parameter $c$, mT) is, the earlier the reflection occurs. So, for $c = 5$ mT the first reflection occurs from the generatrix $\varphi \approx 0.13$ at the point of time $\tau = \tau_{\rm r} \approx 2.45$, and for $c = 10$ mT, one has $\varphi \approx 0.21$, $\tau_{\rm r} \approx 2.1$. At $\tau = \tau_0$, the WP center goes back

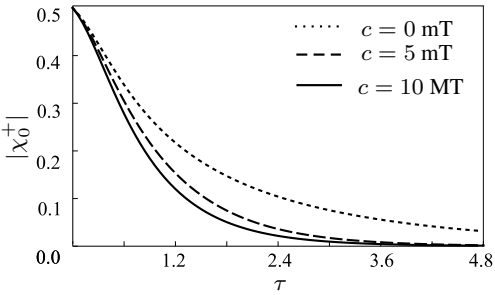


**Fig. 5.62** $|\chi_0^+|$ for the 1st positive WP versus dimensionless time at $c = 0$ and different rates of growing of the magnetic field induction, $c = 5, 10$ mT (after Mikhasev et al, 2016).

to the initial position at the longest generatrix ($\varphi = 0$). Here, $\tau_0 \approx 4.0$ and $\tau_0 \approx 3.58$ for $c = 5$ mT and $c = 10$ mT, respectively. Figures 5.59 and 5.60 demonstrate how the wave parameter $p^+$ and the dimensionless current frequency $|\omega^+|$ vary with time. In the beginning, the frequency $|\omega^+|$ drops slightly, but then it runs up together with the induction $B(\tau)$. The strong growth of the frequency is explained by increasing the total stiffness for the sandwich at high level of the applied magnetic field.

From the analysis of Fig. 5.62 follows that the increase of the magnetic field induction leads to a soft suppression of running vibrations. For instance, at $c = 10$ mT, the damping decrement is about two times than that without magnetic field (at $c = 0$ mT): the larger the growth rate of the magnetic field is, the faster the damping of running vibrations occurs.

## References

Aguib S, Noura A, Zahloul H, Bossis G, Chevalier Y, Lançon P (2014) Dynamic behavior analysis of a magnetorheological elastomer sandwich plate. Int J Mech Sc 87:118–136

Aguib S, Nour A, Djedid T, Bossis G, Chikh N (2016) Forced transverse vibration of composite sandwich beam with magnetorheological elastomer core. J Mech Sc Techn 30(1):15–24

Allahverdizadeh A, Mahjoob M, Eshraghi I, Nasrollahzadeh N (2013) On the vibration behavior of functionally graded electrorheological sandwich beams. Int J Mech Sc 70:130–139

Avdoshka I, Mikhasev G (2001) Wave packets in a thin cylindrical shell under a non-uniform axial load. J Appl Maths Mechs 65(2):301–309

Berg CD, Evans LF, Kermode PR (1996) Composite structure analysis of a hollow cantilever beam filled with electro-rheological fluid. J Intell Mater Syst Struct 7(5):494–502

Boczkowska A, Awietjan SF, Pietrzko S, Kurzydlowski KJ (2012) Mechanical properties of magnetorheological elastomers under shear deformation. Comp: Part B 43:636–640

Botogova M, Mikhasev G (1996) Free vibrations of non-uniformly heated viscoelastic cylindrical shell. Technische Mechanik 16(3):251–256

Chikh N, Nour A, Aguib S, Tawfiq I (2016) Dynamic analysis of the non-linear behavior of a composite sandwich beam with a magnetorheological elastomer core. Acta Mechanica Solida Sinica 29(3):271–283

Choi W, Xiong Y, Shenoi R (2010) Vibration characteristics of sandwich beams with steel skins and magnetorheological elastomer cores. Advances in Structural Engineering 13(5):837–847

Choi Y, Sprecher AF, Conrad H (1990) Vibration characteristics of a composite beam containing an electrorheological fluid. J Intell Mater Syst Struct 1(1):91–104

DiTaranto RA (1965) Theory of vibratory bending for elastic and viscoelastic layered finite-length beams. Trans ASME J Appl Mech 32(4):881–886

Dwivedy SK, Mahendra N, Sahu KC (2009) Parametric instability regions of a soft and magnetorheological elastomer cored sandwich beam. J Sound Vibr 325(4–5):686–704

Eshaghi M, Sedaghati R, Rakheja S (2015) The effect of magneto-rheological fluid on vibration suppression capability of adaptive sandwich plates: experimental and finite element analysis. Journal of Intelligent Material Systems and Structures 26(14):1920–1935

Eshaghi M, Sedaghati R, Rakheja S (2016) Dynamic characteristics and control of magnetorheological/electrorheological sandwich structures: a state-of-the-art review. Journal of Intelligent Material Systems and Structures 27(15):2003–2037

Gandhi MV, Thompson BS (1992) Smart Materials and Structures. Chapman&Hall, London

Gandhi MV, Thompson BS, Choi SB (1989) A new generation of innovative ultraadvanced intelligent composite materials featuring electro-rheological fluids: an experimental investigation. J Comp Mater 23(12):1232–1255

Hu B, Wang D, Xia P, Shi Q (2006) Investigation on the vibration characteristics of a sandwich beam with smart composites - MRF. World Journal of Modelling and Simulation 2(3):201–206

Hu G, Guo M, Li W, Du H, Alici G (2011) Experimental investigation of the vibration characteristics of a magnetorheological elastomer sandwich beam under non-homogeneous small magnetic fields. Smart Materials and Structures 20(12):127,001–1–127,001–7

Hu G, Guo M, Li W (2012) Analysis of vibration characteristics of magnetorheological elastomer sandwich beam under non-homogeneous magnetic field. Appl Mech Mat 101–102:202–206

Irazu L, Elejabarrieta M (2017) Magneto-dynamic analysis of sandwiches composed of a thin viscoelastic-magnetorheological layer. J Intel Mat Syst Struct 28(20):3106–3114

Kang Y, Kim J, Choi S (2001) Passive and active damping characteristics of smart electrorheological composite beams. Smart Materials and Structures 10:724–729

Korobko EV, Mikhasev GI, Novikova ZA, Zurauski MA (2012) On damping vibrations of three-layered beam containing magnetorheological elastomer. J Intel Mat Syst Struct 23(9):1019–1023

Kozlowska J, Boczkowska A, Czulak A, Przybyszewski B, Holeczek K, Stanik R, Gude M (2016) Novel MRE/CFRP sandwich structures for adaptive vibration control. Smart Mater Struct 25(3):035,025

Lai J, Wang K (1996) Parametric contral of structural vibrations via adaptable stiffness dynamic absorbers. Journal of Vibration and Acoustics 118:41–47

Lara-Prieto V, Parkin R, Jackson M, Silberschmidt V, Kęsy Z (2010) Vibration characteristics of MR cantilever sandwich beams: experimental study. Smart Mater Struct 19(1):015,005

Lee CY (1995) Finite element formulation of a sandwich beam with embedded electrorheological fluids. J Intell Mater Syst Struct 6(5):718–728

Li Y, Li J, Li W (2014) A state-of-the-art review on magnetorheological elastomer devices. Smart Materials and Structures 23(12):123,001–1–123,001–24

Long M, Hu G, Wang S (2013) Vibration response analysis of MRE cantilever sandwich beam under non-homogeneous magnetic fields. Applied Mechanics and Materials 303–306:49–52

Lukasiewicz S (1979) Local loads in plates and shells. Springer Netherlands

Mead DJ, Markus S (1970) Loss factors and resonant frequencies of encastrè damped sandwich beams. J Sound Vibr 12(1):99–112

Megha S, Kumar N, D'Silva R (2016) Vibration analysis of magnetorheological elastomer sandwich beam under different magnetic fields. J Mech Engng Automat 6:75–80

Mikhasev G (1996a) Localized families of bending waves in a non-circular cylindrical shell with sloping edges. Journal of Applied Mathematics and Mechanics 60(4):629–637

Mikhasev G (1996b) Localized wave forms of motion of an infinite shell of revolution. Journal of Applied Mathematics and Mechanics 60(5):813–820

Mikhasev G (1997) Free and parametric vibrations of cylindrical shells under static and periodic axial loads. Technische Mechanik 17(3):209–216

Mikhasev G (1998) Travelling wave packets in an infinite thin cylindrical shell under internal pressure. Journal of Sound and Vibrations 209(4):543–559

Mikhasev G (2002) Localized families of bending waves in a thin medium-lenght cylindrical shell under pressure. Journal of Sound and Vibrations 253(4):833–857

Mikhasev G (2017) Some problems on localized vibrations and waves in thin shells. In: Altenbach H, Eremeev V (eds) Shell-like Structures. Advanced Theories and Applications, Courses and Lectures, vol 572, Springer, CISM International Center for Mechanical Sciences, pp 259–262

Mikhasev G (2018) Thin laminated cylindrical shells containing magnetorheological elastomers: Buckling and vibrations. In: Pietraszkiewicz W, Witkowski W (eds) Shell Structures: Theory and Applications, vol 4, Taylor&Francis Group, London, pp 259–262

Mikhasev G, Kuntsevich S (1997) Thermoparametric vibrations of noncircular cylindrical shell in nonstationary temperature field. Technische Mechanik 17(2):113–120

Mikhasev G, Kuntsevich S (1999) Parametric vibrations of viscoelastic cylindrical shell under static and periodic axial loads. Technische Mechanik 19(3):187–195

Mikhasev G, Botogova M, Korobko E (2011) Theory of thin adaptive laminated shells based on magnetorheological materials and its application in problems on vibration suppression. In: Altenbach H, Eremeyev V (eds) Shell-like Structures, Springer, Heidelberg, Advanced Structured Materials, vol 15, pp 727–750

Mikhasev G, Mlechka I, Altenbach H (2016) Soft suppression of travalling localized vibrations in medium-length thin sandwich-like cylindrical shells containing magnetorheological layers via nonstationary magnetic field. In: Awrejcewicz J (ed) Dynamical Systems: Theoretical and Experimental Ananlysis, Springer Proceedings in Mathematics&Statistics, vol 182, Springer, Singapore, pp 241–260

Mikhasev GI, Tovstik PE (1990) Stability of conical shells under external pressure. Mech Solids 25(4):106–119

Mikhasev GI, Tovstik PE (2009) Localized Vibrations and Waves in Thin Shells. Asymptotic Methods (in Russ.). FIZMATLIT, Moscow

Mikhasev GI, Korobko EV, Novikova ZA (2010) On suppression of vibrations of three-layered beam containing magnetorheological composite (in Russ.). Mechanics of Machines, Mechanisms and Materials 4:49–53

Mikhasev GI, Altenbach H, Korchevskaya EA (2014) On the influence of the magnetic field on the eigenmodes of thin laminated cylindrical shells containing magnetorheological elastomer. Composite Structures 113:186 – 196

Mohammadi F, Sedaghati R (2012) Nonlinear free vibration analysis of sandwich shell structures with a constrained electrorheological fluid layer. Smart Materials and Structures 21(7):075,035

Nayak B, Dwivedy SK, Murthy KSRK (2011) Dynamic analysis of magnetorheological elastomer-based sandwich beam with conductive skins under various boundary conditions. J Sound Vibr 325(9):1837–1859

Nayak B, Dwivedy SK, Murthy KSRK (2012) Multi-frequency excitation of magnetorheological elastomer-based sandwich beam with conductive skins. Int J Non-Linear Mech 47(5):448–460

Nayak B, Dwivedy SK, Murthy KSRK (2014) Dynamic stability of a rotating sandwich beam with magnetorheological elastomer core. Eur J Mech A/Solids 47:143–155

Oyadiji SO (1996) Applications of electro-rheological fluids for constrained layer damping treatment of structures. J Intell Mater Syst Struct 7(5):541–549

Phani AS, Venkatraman K (2003) Vibration control of sandwich beams using electrorheological fluids. Mech Syst and Signal Processing 17(5):1083–1095

Qatu MS, Sullivan RW, Wang W (2010) Recent research advances on the dynamic analysis of composite shells: 2000-2009. Composite Structures 93(1):14–31

Rajamohan V, Sedaghati R, Rakheja S (2010) Vibration analysis of a multi-layer beam containing magnetorheological fluid. Smart Materials and Structures 19(1):015,013–1–015,013–12

Shaw J (2000) Hybrid control of cantilevered er sandwich beam for vibration suppression. J Intell Material Systems and Struct, 11(1):26–31

Skudrzyk E (1968) Simple and Complex Vibratory Systems. Pennsylvania State Univ Pr (Trd), Pennsylvania

de Souza Eloy F, Gomes G, Ancelotti A, da Cunha S, Bombard A, Junqueira D (2018) Experimental dynamic analysis of composite sandwich beams with magnetorheological honeycomb core. Engineering Structures 176(1):231–242

de Souza Eloy F, Gomes G, Ancelotti A, da Cunha S, Bombard A, Junqueira D (2019) A numerical-experimental dynamic analysis of composite sandwich beam with magnetorheological elastomer honeycomb core. Composite Structures 209(1):242–257

Sun Q, Zhou JX, Zhang L (2003) An adaptive beam model and dynamic characteristics of magnetorheological materials. J Sound Vibr 261(3):465–481

Vemuluri R, Rajamohan V (2016) Dynamic analysis of tapered laminated composite magnetorheological elastomer (MRE) sandwich plates. Smart Materials and Structures 25(3):035,006

Vemuluri R, Rajamohan V, Arumugam A (2018) Dynamic characterization of tapered laminated composite sandwich plates partially treated with magnetorheological elastomer. Journal of Sandwich Structures & Materials 20(3):308–350

Wei K, Meng G, Zhang W (2008) Experimental investigation on vibration characteristics of sandwich beams with magnetorheological elastomers cores. Journal of Central South University of Technology 15(1):239–242

Yalcintas M, Coulter J (1995) Electrorheological material based adaptive beams subjected to various boundary conditionss. Journal of Intelligent Material Systems and Structures 6:700–717

Yalcintas M, Coulter JP (1998) Electrorheological material based non-homogeneous adaptive beams. Smart Mater Struct 7(1):128–143

Yalcintas M, Dai H (1999) Magnetorheological and electrorheological materials in adaptive structures and their performance comparison. Smart Mater Struct 8(5):560–573

Yalcintas M, Dai H (2004) Vibration suppression capabilities of magnetorheological materials based adaptive structures. Smart Mater Struct 13(1):1–11

Yeh JY (2011) Vibration and damping analysis of orthotropic cylindrical shells with electrorheological core layer. Aerospace Sc Technology 15(4):293–303

Yeh JY (2013) Vibration analysis of sandwich rectangular plates with magnetorheological elastomer damping treatment. Smart Mater Struct 22:035,010–035,018

Yeh JY (2014) Vibration characteristics analysis of orthotropic rectangular sandwich plate with magnetorheological elastomer. Procedia Engng 79:378–385

Yildirim T, Ghayesh M, Li W, Alici G (2016) Experimental nonlinear dynamics of a geometrically imperfect magneto-rheological elastomer sandwich beam. Composite Structures 138:381–390

Zeerouni N, Aguib S, Nour A, Djedid T, Nedjar A (2018) Active control of the nonlinear bending behavior of magnetorheological elastomer sandwich beam with magnetic field. Vibroengineering Procedia 18:73–78

Zhang J, Yildirim T, Alici G, Zhang S, Li W (2018) Experimental nonlinear vibrations of an mre sandwich plate. Smart Structures and Systems 22(1):71–79

Zhou GY, Wang Q (2005) Magnetorheological elastomer-based smart sandwich beams with nonconductive skins. Smart Mater Struct 14(5):1001–1009

Zhou GY, Wang Q (2006a) Study on the adjustable rigidity of magnetorheological-elastomer-based sandwich beams. Smart Mater Struct 15(1):59–74

Zhou GY, Wang Q (2006b) Use of magnetorheological elastomer in an adaptive sandwich beam with conductive skins. Part I: magnetoelastic loads in conductive skins. Int J Solids Struct 43(17):5386–5402

Zhou GY, Wang Q (2006c) Use of magnetorheological elastomer in an adaptive sandwich beam with conductive skins. Part II: dynamic properties. Int J Solids Struct 43(17):5403–5420